ACS Biomaterials SCIENCE & ENGINEERING

APRIL 2021 | VOLUME 7 | NUMBER 4

PUBS.ACS.ORG/ACSBIOMATERIALS

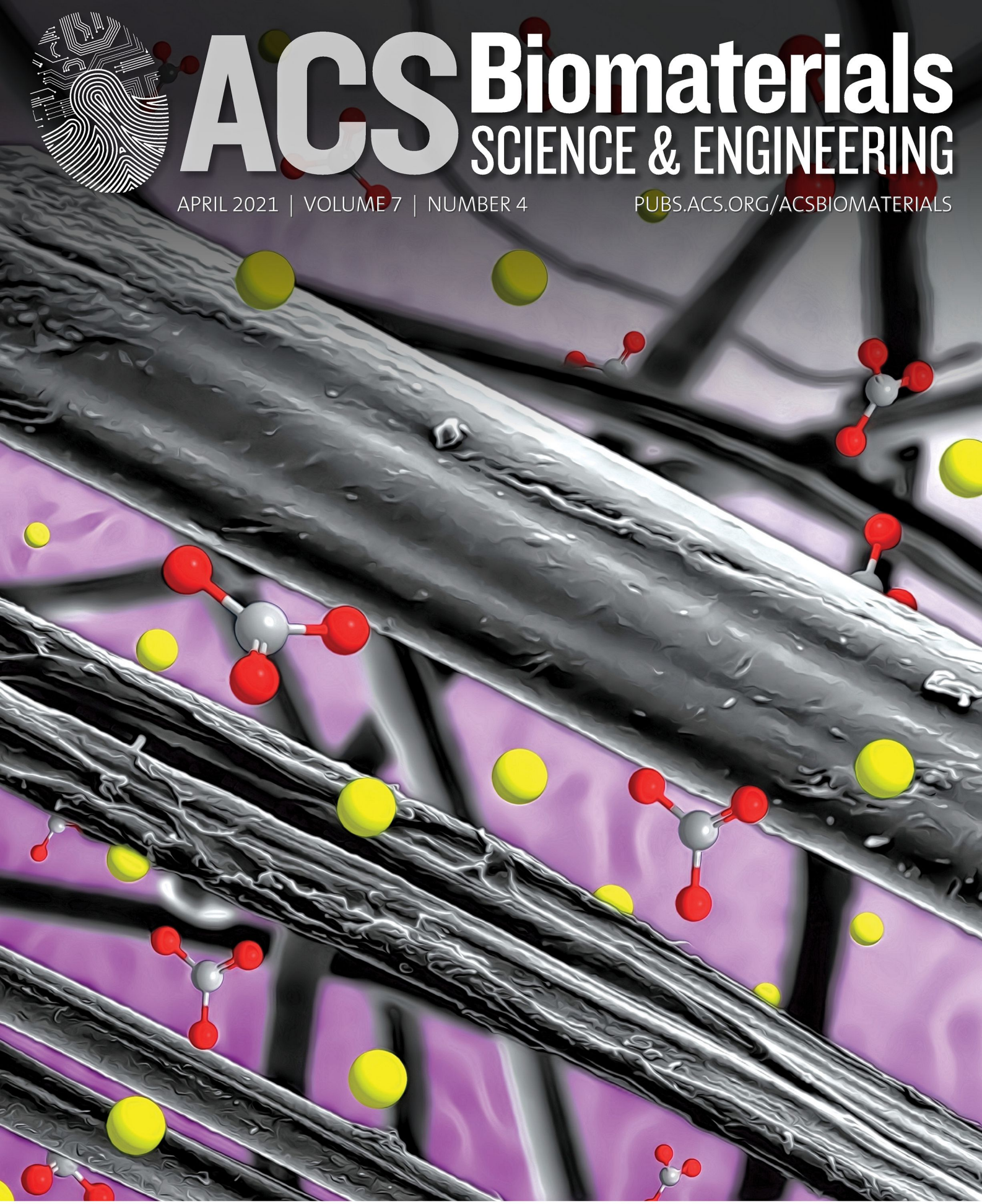

ACS Publications
Most Trusted. Most Cited. Most Read.

www.acs.org

ACS Biomaterials SCIENCE & ENGINEERING

pubs.acs.org/journal/abseba

Article

A Design of Experiment Rational Optimization of the Degumming Process and Its Impact on the Silk Fibroin Properties

Alessio Bucciarelli,* Gabriele Greco, Ilaria Corridori, Nicola M. Pugno, and Antonella Motta

Cite This: *ACS Biomater. Sci. Eng.* 2021, 7, 1374−1393

Read Online

ACCESS | Metrics & More | Article Recommendations | Supporting Information

ABSTRACT: Silk fibroin is a protein with a unique combination of properties and is widely studied for biomedical applications. The extraction of fibroin (degumming) from the silk filament impacts the properties of the outcoming material. The degumming can be conducted with different procedures. Among them, the most used and studied procedure in the research field is the alkali degumming with sodium carbonate (Na_2CO_3). In this study, by the use of a statistical method, namely, design of experiment (DOE), we characterized the Na_2CO_3 degumming, taking into consideration the main process factors involved and changing them within a selected range of values. We considered the process temperature and time, the salt concentration, and the number of baths used, testing the impact of these variables on the fibroin properties by building empirical models. These models not only took into consideration the direct effect of the process factors but also their combined effect, which are not conventionally detectable with other methods. The weight loss and the amount of sericin removed in the process were determined and used as a measure of the effectiveness of the process. The secondary structure, the molecular weight, the diameter of fibers, and their morphology and mechanical properties were studied with the intent to correlate the macroscopical properties with the structural changes. We report, for the first time, the possibility to effectively remove all sericin from the silk fibroin using Na_2CO_3, using a process that requires less salt, water, and energy, in comparison with the standard alkali protocol, making this technique overall more environmentally sustainable; in addition, we have demonstrated the possibility to tune the material properties by varying the degumming conditions and even to optimize them with empirical statistically based equations that allow one to directly set the optimal process parameters. The major effect on the macroscopical properties (such as the ultimate strength and Young's modulus) has been proved to be correlated with the removal of sericin instead of the microstructural variations. Finally, a ready-to-use table with a set of optimized degumming procedures to maximize or minimize the studied properties was provided.

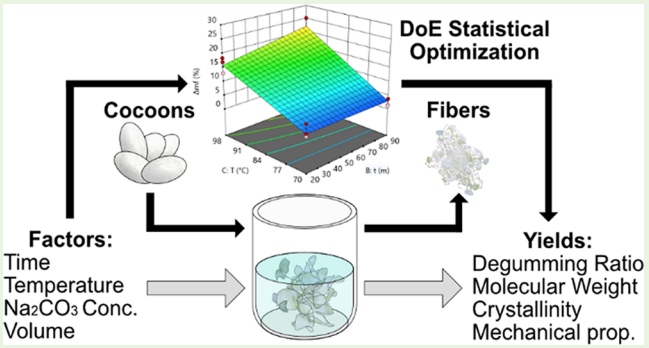

KEYWORDS: *silkworm silk, design of experiment, statistical methods, mechanical properties, secondary structure, molecular weight*

INTRODUCTION

Silk is a proteinic fiber produced by several arthropods and is known since the ancient time for the production of textiles. Over the centuries, the coerced evolution from the wild moth to the domestic silkworm, namely, *Bombyx mori*, had led to the development of sericulture and the wide abundance of the raw silk cocoons.[1] Each cocoon is made of a continuous silk filament with a length between 700 and 1500 m, which is known as bave. The silk bave is composed of two proteins disposed in a core−shell structure in which two fibers (known as brin) of the internal protein, called fibroin, are glued together by an external layer of a globular protein called sericin.[2−4] These two proteins have different functions: the purpose of fibroin is mainly structural and confers to the silk its unique mechanical properties; meanwhile, sericin acts like a glue, which helps in the formation of the cocoon. Depending on the typology of silk, sericin impacts 25−30% of the cocoon weight, while the rest of the weight is due to fibroin. The separation of these two proteins can be accomplished with a procedure called degumming in which sericin is solubilized in a chemical bath while fibroin remains as fibers. The aim of the separation of these two proteins is to improve the mechanical properties, to standardize the outcoming material, and to improve the overall biocompatibility. In fact, early studies reported some compatibility issues of the raw silk because of the presence of residual sericin[5,6] and further research demonstrated that sericin in combination with fibroin can

Received: November 25, 2020
Accepted: February 5, 2021
Published: February 17, 2021

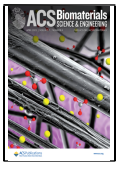

https://dx.doi.org/10.1021/acsbiomaterials.0c01657
ACS Biomater. Sci. Eng. 2021, 7, 1374−1393

cause a serious allergic reaction.[7,8] For this reason, the removal of sericin is vital if silk is intended as a material for biomedical applications. Upon degumming, fibroin becomes an excellent material for biomedical purposes because of the positive responses of biological tissues.[4] Nowadays, the use of silk fibroin is of particular interest in all the fields in which the interaction with living tissues is crucial. The combinations of properties such as high mechanical strength, easy processability, and resorbability make this material unique among the other available biopolymers[9] because of its exceptional versatility.[2] In particular, in tissue engineering, silk fibroin in different structural forms is widely studied as a material for bone,[10−14] cartilage,[15−17] tendon,[18−20] skin,[21−23] and cornea regeneration[24−27] and, in minor part, for nerve, muscle, spinal cord, and liver regeneration.[5] In addition, the possibility to produce different structures and to chemically modify the regenerated protein allows the use of silk fibroin in an increasing number of frontier applications in which traditional fields like electronics and optics encounter the integration with biology (bio-electronics[28−30] and bio-optics[31−34]). This wide range of usage had led to the development of an entire plethora of protocols to produce different materials starting from the fibroin extracted from the silk cocoon.[35] The properties of all the outcoming materials are affected by the very fundamental operation of separating fibroin and sericin; during this process, the properties of silk fibroin are changed accordingly on which method is used and how the different variables are set.[36−38] Several methods were developed to conduct this process: from the simple immersion of the cut cocoons in boiling water[39] to the use of soaps,[40] acid solutions,[41] ionic liquids,[42] enzymes,[43−46] and amine[47] and the more recent use of physical methods such as sonication,[46] microwave,[48] steam treatment,[49] and CO_2 critical fluid.[39] Most of these processes were developed with two purposes: as an enviromentally sustainable alternative to the commonly used alkaline degumming and as methods to preserve the fibers against degradation.[48,50] However, none of these alternatives could effectively substitute the far more used alkali degumming method because of the incapacity to remove most of sericin from the fiber in a suitable amount of time. The most common degumming method consists of the dissolution of sericin in a boiling bath of sodium carbonate (Na_2CO_3) in water. This process is well established in a series of protocols known as the Rockwood protocol[35] and its impact on the properties of the resultant fibroin fibers has been extensively studied in the literature, giving results that are, in their complexity, not self-consistent. Both the molecular weight and the secondary structure tend to be modified by the effect of the degumming procedure. It is known that the increase in the degumming time decreases the molecular weight of the protein and consequently decreases also the tensile strength.[48,51] This is usually used to modulate also the mechanical response of the materials produced starting from the degummed fibers.[51,52] Several efforts have been made to maintain a high-molecular-weight protein with the lowest possible degradation after degumming.[36,53−56] However, even for a low degumming time and also using different degumming methods, the highest molecular weight obtained was around 400 kDa, corresponding to the weight of the H-L unit.[36,51] In the specific case of the Rockwood protocol, 30 min in a boiling solution gives a molecular weight centered around 100 kDa.[35] It is also known that during the degumming time, the fibers tend to crystallize proportionally with the increase of the degumming agent.[36,51] Most of the studies present in the literature take into consideration only single-process variables, demonstrating how it is possible to modify specific material properties (e.g., degumming time versus molecular weight or elastic modulus and the effect of the salt concentration) by varying them one by one. This procedure is known as one factor at a time (OFAT); it does not take into consideration the process in its complexity, neither the interaction that could be present among the different process variables. Instead, the application of statistical methods may be effectively used to optimize a process even in the case of silk fibroin.[57−59] In particular, a design of experiment (DOE) method allows one to distinguish the statistical relevant process factors from the irrelevant ones and to build empirical equations that relate the factors and their interaction with the material properties of interest (from now on called yields)[60−65] whithout engaging in a mechanistic description of the phenomena, as usually done by other disciplines. In this study, by the use of DOE, we characterized the most used alkali degumming with Na_2CO_3, taking into consideration the main process variables involved and modifying them within a selected range. Excluding the uncontrollable external variations (such the environmental temperature, pressure, and humidity), at least four controllable variables (from now on called "factors") are involved in the Na_2CO_3 degumming: the process time, the process temperature, the volume of water, and the salt concentration. For each factor, a minimum level and a maximum level were chosen in a range with a lower material (salt and water) and energy consumption (lower temperature) compared to the common protocol. The factors were taken into account to build a 2^4 full factorial experiment, resulting in 16 different degumming treatments, and for each of them, three replicas were produced to ensure reproducible results. As yields, we studied the weight loss (degumming ratio), the molecular weight, the dispersion index, and the secondary structure of the resulting fibers as well as their mechanical properties (Young's modulus, ultimate strength, strain at break, and toughness modulus) and morphology (diameter and microstructure), building predictive empirical equations (with a 95% confidence interval) as a function of the degumming factors. These equations and the contour plots provided can be used to effectively design the material properties of the end product just by changing the degumming conditions without running an additional set of trials. We also report for the first time the possibility to effectively remove all sericin from the silk fibroin using Na_2CO_3 with a process that requires less salt, water, and energy in comparison with the standard protocol, maintaining a discretely high molecular weight (with a peak center tunable between 100 and 300 kDa). The morphological analysis conducted by secondary electron microscopy in combination with the weight loss was used to discern between effective and ineffective treatments in terms of sericin removal. Gel permeation chromatography allowed us to determine both the molecular weight and the dispersion index, while Fourier transform infrared spectroscopy has been used to determine the protein secondary structure on the fiber surface. Tensile tests have been performed to seek a correlation between the secondary structure, the molecular weight, and the mechanical properties. The correlation index revealed that the mechanical properties were not affected by the secondary structure changes, which in the studied process were modest.

https://dx.doi.org/10.1021/acsbiomaterials.0c01657
ACS Biomater. Sci. Eng. 2021, 7, 1374−1393

Table 1. Factors, Corresponding Variables, and Their Levels (Positive and Negative)[a]

$$F(Y_i) = c_0 + c_1 \times A + c_2 \times B + c_3 \times C + c_4 \times D + c_5 \times A \times B + c_6 \times A \times C + c_7 \times A \times D + c_8 \times B \times C + c_9 \times B \times D + c_{10} \times C \times D + c_{11} \times A \times B \times C + c_{12} \times A \times B \times D + c_{13} \times A \times C \times D + c_{14} \times B \times C \times D + c_{15} \times A \times B \times C \times D$$

factor	variable	type	+1 level	−1 level
A	number of baths	discrete	1	2
B	time (min)	continuous	20	90
C	temperature (°C)	continuous	98	70
D	salt concentration (g/mL)	continuous	0.1	1.1
confounded factor				
factor	variable	type	+1 level	−1 level
E (confounded A)	total volume (mL)	continuous	400 (133 mL/g cocoons)	800 (266 mL/g cocoons)

[a]Four factors, each of them in two levels, were tested: the number of baths (1 or 2), the degumming total time (20 or 90 min), the temperature of the bath (80 or 98 °C), and the salt concentration (0.1 or 1.1 g/L). All the combinations of the factor's levels were considered. We can consider as a confounded factor also the total volume of water. In fact, each bath had a fixed water volume of 300 mL; it means that all the double bath processes had a total water volume of 600 mL vs 300 mL of the single bath processes.

Interestingly, we found an inverse correlation of the mechanical properties with the molecular weight. An in-depth analysis revealed the effect of a lurking variable, the sericin removal. Due to the fact that fibers with a high molecular weight had a low degumming rate, the effects of the molecular weight could not be separated from the effect of the sericin removal, giving an overall increase in the mechanical properties, due to the increase in the amount of the removed sericin, even if the molecular weight decreased. As a major accomplishment, we proved the significance not only of the single process factors but, in the case of several studied properties, of their mixed effect, while in most of the studies the effect of a single factor is detected.[36,48] We also provided a full set of empirical models that allow one to tune the degumming variables according to the desired property outcomes and, based on them, a ready-to-use set of Na_2CO_3 degumming protocols.

MATERIALS AND METHODS

Experimental Design and Statistical Methods. To verify the dependence of the silk fibroin properties on the degumming procedure, a 2^4 full factorial design has been used. Four factors have been considered in the process, each of them varying between two levels, normalized between −1 and +1. The considered variables were the number of degumming baths (−1 → 1 bath, + 1 → 2 baths), the concentration of salt (−1 → 0.1 g/L, + 1 → 1.1 g/L), the bath temperature (−1 → 70°C, + 1 → 98°C), the total time of the degumming (−1 → 20 min, + 1 → 90 min), and their respective levels and the complete empirical equations are reported in Table 1. In the model equation depending on the considered property, some terms could be missing. In fact, only the terms proved to be statistically significant by ANOVA test were included. The basic assumption for each of the further statistical analyses was the normal distribution of the data collected from each applied degumming treatment. For each sample, we studied some properties of interest (yield) and we built a predictive model based on the process variables. The considered yields are reported in Table 2, including the number of measurements conducted for each replica. The general model is reported in Table 1 including all the first-order terms that correlate the property directly with the process factors, the second-order terms that consider how couples of factors mutually interact with each other, the third-order terms that take into account the mutual interaction of triplets of factors, and one four-order term in which the interaction of all factors is considered. It is important to note that terms above the first order are not usually considered in methods that study the variation of one property vs one variable. A Pareto plot and a half-normal plot were initially used to evaluate which terms have to be included in the model. In the Pareto plot, the effects were listed in order of magnitude and only the effects higher than the critical t-value (and thus differ from normality) were chosen. The effects were reported in the half-normal plot and only the ones that resulted to be significantly out from the line (indicating the normality) were chosen. An analysis of variance (ANOVA) test was performed to evaluate the significance on the selected terms and on the resulting model; consequently, the insignificant terms were eliminated. The terms were significant if their p value was <0.1 (90% confidence interval); meanwhile, the model was considered significant only with $p < 0.05$ (95% confidence interval). This discrepancy between the single terms and the model has been chosen to consider the intrinsic nature of silk fibroin, in which, as in any natural material, the property could vary from batch to batch. So, to detect the effect of the single factors (and, eventually, their combination), a larger confidence interval was used. All the statistical tests were double-tailed. The function of the considered yield ($F(Y)$) was selected to make the residuals normally distributed and without a pattern. The entire process was then iterated again, considering the outcoming values of the function of the effects instead of the bare effects' values. On the collected data, a correlation matrix has been plotted by calculating the Pearson index r for each couple of variables by using eq 1, where x is the first variable, y is the second variable, and $\bar{x}$ and $\bar{y}$ are the corresponding mean values.

Table 2. Studied Material Properties, Method of Measurement, and the Number of Tests Conducted for Each Replica[a]

method	measured properties	unit	no. of measures/replicas
weight difference	weight loss	%	1
UV spectrophotometry	sericin removed	%	1
optical microscopy	fiber diameter	μm	5
FTIR-ATR	relative amount of secondary structures	%	1
GPC	molecular weight	kDa	1 for each treatment
	polydispersity		
tensile test	ultimate strength	MPa	at least 3
	strain at break	%	
	Young's modulus	GPa	
	toughness modulus	MJ/m^3	

[a]We performed only one measurement of the weight loss and sericin removed per trial. We also performed only one measurement/replica for FTIR and one measurement/treatment (only one measurement over the three replicas) in the case of the GPC because of the complexity of the technique. Instead, due to the variability of the tensile test, we perform it at least on 10 fibers per replica, contemporarily measuring the diameter by optical microscopy.

https://dx.doi.org/10.1021/acsbiomaterials.0c01657
ACS Biomater. Sci. Eng. 2021, 7, 1374−1393

$$r_{xy} = \frac{\sum_{i=1}^{n}(x_i - \bar{x})(y_i - \bar{y})}{\sqrt{\sum_{i=1}^{n}(x_i - \bar{x})}\sqrt{\sum_{i=1}^{n}(y_i - \bar{y})}} \quad (1)$$

Optimization. The optimization was done by a numerical method based on desirability functions.[66,67] These functions are in the [1,0] range, where 1 represents the optimum solution. Indicating Y_i, the specific yield, d_i, the corresponding desirability function, and U_i and L_i, the maximum and minimum values of the yield inside the process variable range, the equations for the maximization and minimization of Y_i can be expressed as eqs 2 and 3, respectively. Based on the willingness to minimize or maximize the specific yield, one of these two functions was chosen. To contemporarily optimize multiple yields, the overall desirability (d_{tot}) was used. d_{tot} is the geometric mean of all the desirability functions assigned to the different yields and is reported in eq 4 with k equal to the total number of yields. The maximization of d_{tot} (within the [0,1] range) gave the best compromise in the optimization of the different yields.

$$d_i = \begin{cases} 1 \text{ if } Y_i \geq U_i \\ \dfrac{Y_i - L_i}{U_i - L_i} \text{ if } L_i \geq Y_i \geq U_i \\ 0 \text{ if } Y_i \leq L_i \end{cases} \quad (2)$$

$$d_i = \begin{cases} 0 \text{ if } Y_i \geq U_i \\ \dfrac{Y_i - L_i}{U_i - L_i} \text{ if } L_i \geq Y_i \geq U_i \\ 1 \text{ if } Y_i \leq L_i \end{cases} \quad (3)$$

$$d_{tot} = (d_1 d_2 d_3 \ldots d_k)^{1/k} \quad (4)$$

Silk Fibroin Degumming. Extraction and purification of silk fibroin were conducted using an adapted version of a well-known protocol.[35] Briefly, to separate silk fibroin from silk sericin, 3 g of *B. mori* silk cocoons (imported from Chul Thai Silk Co., Phetchabun, Thailand) were cut in small pieces and placed in 400 mL of sodium carbonate (0.1 or 1.1 g/L accordingly to the trial, Na_2CO_3, Sigma-Aldrich) hot solution (70 or 98 °C accordingly to the trial) for a determined time (20 or 90 min accordingly to the trial); eventually, a second bath was performed as graphically described in Figure 1. Sixteen different degumming procedures were adopted, eight with a single bath and eight with a double bath. Each process was conducted in triplicates for a total of 48 trials. The quantity of cocoons used for each trial was about 3 g. The resultant degummed silk fibroin was progressively taken at room temperature, carefully rinsed three times using ultrapure water, and then dried for 2 days under the hood. The fibers were kept in a desiccator until their use. The 16 different degumming protocols are listed in Table 3. Three replicates of a reference sample were prepared by following the standard Rockwood protocol.[35] Briefly, 5 g of cocoons was cut and degummed in a boiling bath of 2000 mL of a Na_2CO_3 solution (2.14 g/L) for 30 min. The resulting degummed silk was then carefully taken at room temperature and rinsed three times with distilled water. Finally, the degummed silk fibroin was dried under the hood for 2 days. To avoid as much as possible the reduction of the solution volume due to the evaporation, the degumming baths were covered, and periodically, some water was added to restore the initial volume. The order of preparation of the 51 trials (17 × 3) was randomized to mediate the effect of the environmental factors (humidity and temperature) to 0. It should be noted that this study did not include other factors that may influence the silk properties (e.g., stifling method[68]), which can be dealt in a future work with the same DoE technique.

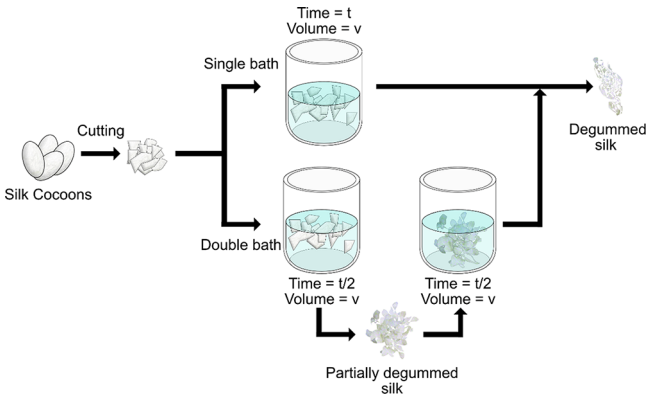

Figure 1. Scheme of the procedure followed to perform the silk fibroin degumming. The cocoons were initially cut in pieces with uniform dimensions. In the case of a single bath, the cut cocoons were placed in inside the $NaCO_3$ water solution under magnetic stirring for a determined time. In the case of the double bath, the time used for each bath was half of the time of the previous one. The volume of each bath was instead kept constant. The concentration of solution was kept constant for each bath. The partially degummed fiber was directly moved from the first bath to the second bath.

Table 3. List of the Different Process Trials; for Each Trail, Three Replicates Were Prepared[a]

sample	replicates	no. of baths	total time (min)	temperature (°C)	salt concentration (g/L)
ref	3	1	30	100	2.12
1	3	1	20	70	0.1
2	3	1	20	70	1.1
3	3	1	20	98	0.1
4	3	1	20	98	1.1
5	3	1	90	70	0.1
6	3	1	90	70	1.1
7	3	1	90	98	0.1
8	3	1	90	98	1.1
9	3	2	20	70	0.1
10	3	2	20	70	1.1
11	3	2	20	98	0.1
12	3	2	20	98	1.1
13	3	2	90	70	0.1
14	3	2	90	70	1.1
15	3	2	90	98	0.1
16	3	2	90	98	1.1

[a]To the 16 treatments, as a reference, a degumming procedure with the conventional protocol was performed (also, in this case, in triplicates).

Weight Loss and Removed Sericin. For each trial, the amount of cocoons was weighted using an analytical balance before (m_i) and after (m_f) degumming. The percentage of mass loss was then evaluated by eq 5, and the obtained quantity was used to build an empirical model. The amount of removed sericin was tested by spectroscopic analysis (NanoDrop 1000, Thermo Scientific) by collecting 5 μL from each degumming bath after the degumming procedure and using the protein absorption peak at 280 nm to evaluate the protein concentration. The concentration was estimated by comparing the absorption intensity results with a calibration curve (Figure S1) built using a set of standard solutions (with a known sericin content) prepared starting from sericin powder (Sigma-Aldrich) and ultrapure water. The amount of the removed sericin (m_s) was calculated starting from the concentration [Ser] (expressed in mg/mL) with eq 6 in the case of a single bath and with eq 7 in the case of a double bath. The percentage of removed sericin was

https://dx.doi.org/10.1021/acsbiomaterials.0c01657
ACS Biomater. Sci. Eng. 2021, 7, 1374−1393

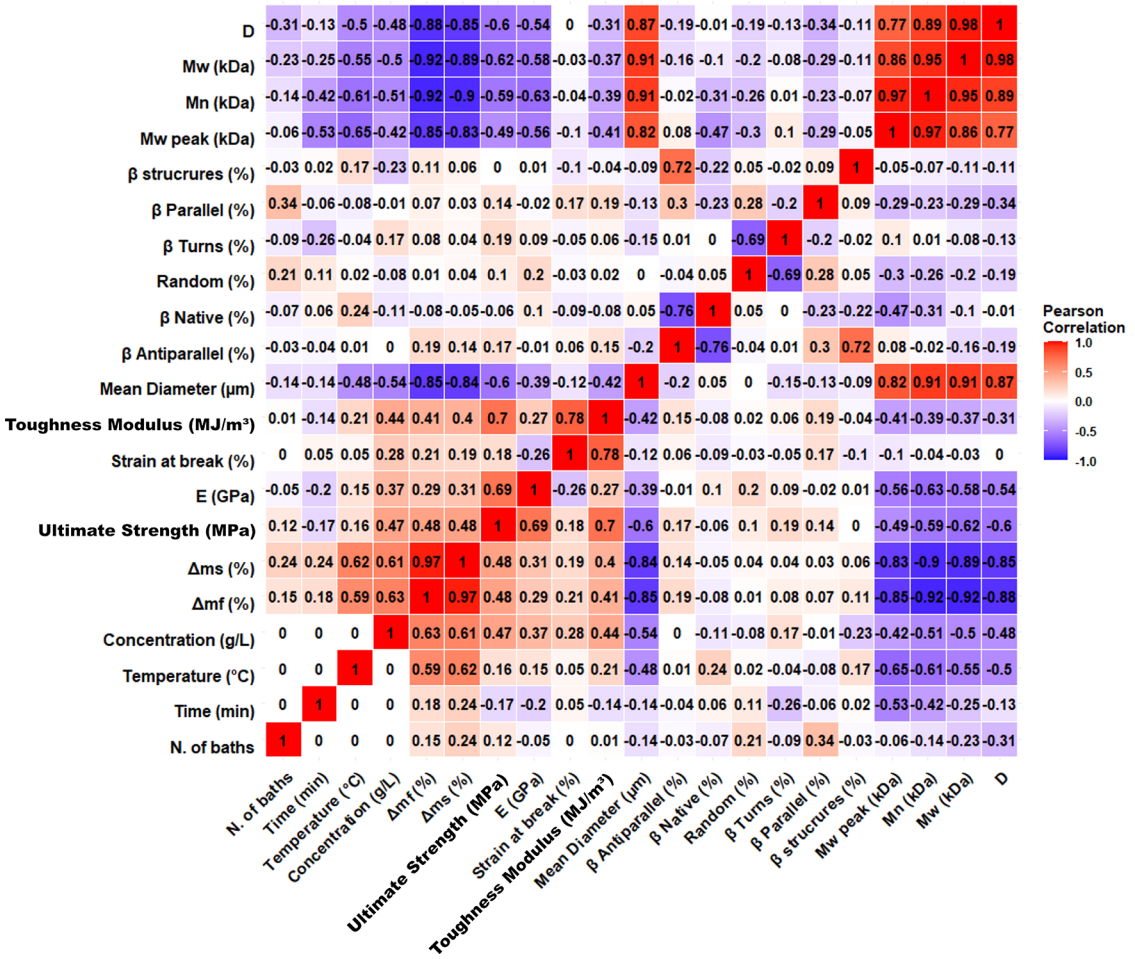

Figure 2. Correlation map between all the considered factors and yields. The matrix is symmetric, and it reports the same variables on the x and y axes. The color is associated with the Pearson correlation coefficient (r). A coefficient equal to +1 or −1 indicates a perfect correlation. Two variables are correlated if r is greater than 0.3 or lower than −0.3. As expected, the correlation on the diagonal is equal to 1 (each variable is perfectly correlated with itself). In addition, the chosen DOE factors are perfectly noncorrelated with each other (the right bottom corner of the matrix), and the different molecular weight parameters (M_w peak, M_w, M_n, and D) are strongly correlated with each other (the left top corner of the matrix). Interestingly, several patterns are recognizable; for example, the different molecular weight parameters are all inversely correlated with the process parameters, the weight loss, the percentage of removed sericin (blue area on the top left corner), and the ultimate strength, while they are directly correlated with the fiber diameter. This indicates that as soon as sericin was removed, the molecular weight decreases as well as the ultimate strength and the diameter.

calculated using eq 8, and the result was then used to build the empirical model.

$$\Delta m_f = \frac{m_i - m_f}{m_i} \times 100 \quad (5)$$

$$m_s(\text{mg}) = [\text{Ser}] \times 400 \quad (6)$$

$$m_s(\text{mg}) = [\text{Ser}]_{1\text{st bath}} \times 400 + [\text{Ser}]_{2\text{nd bath}} \times 400 \quad (7)$$

$$\Delta m_s = \frac{m_s}{m_i} \times 100 \quad (8)$$

Secondary Structure Analysis. The secondary structure changes on the fiber surface were evaluated using an ATR-FTIR spectrophotometer (PerkinElmer, Spectrum ONE) equipped with a ZnSe crystal. Only the degummed fibers were selected to avoid, as much as possible, the contribution of sericin to the signal. To maximize the signal-to-noise ratio, 16 spectra per sample were collected and averaged. The selected range was 4000−400 cm^{-1} and the resolution was 1 cm^{-1}. The secondary structures were quantitatively evaluated by analyzing the primary amide peak (1580−1720 cm^{-1}). The peak was smoothed with a 5-point adjacent averaging function followed by a Fourier self-deconvolution (FSD, with a smoothing factor of 0.3 and a gamma function of 30) to enhance the resolution and better shape the singular peaks. A second derivative of the deconvoluted peak was then performed to identify the peak positions, which were consequently used to fit them with a Gaussian function. The fitting routine was recursively applied until χ^2 was minimized. The ratio between each fitted peak area and the total area was calculated to determine the percentage of the specific structure assigned to the peak. In Table S1, the assigned secondary structure for different bandwidths of the FTIR spectrum is reported. The assignment of the peaks has been done following our previous works.[60,61]

Molecular Weight. The molecular weight was evaluated by gel permeation chromatography (GPC) using an SB-806MHQ Shodex column (8.0 × 300 mm exclusion limit (pullulan) 4000E3) mounted on the pumping system (SpectraSystem p4000 with a 20 μL loop and a vacuum membrane degasser thermo electron SCM1000) and using a UV detecting system (Jasco UV-1570) set on a 224 nm wavelength. The fibroin samples were dissolved in LiBr for 4 h at 60 °C, dialyzed in a tube (Sigma-Aldrich; cutting M_w, 3500 Da) against water for 3 days, and then double-filtered (50 μm glass fiber filter) to eliminate impurities. Subsequently, the resulting regenerated fibroin solution was diluted with the eluent (PBS, pH 7.4, Sigma P3813 plus 0.05 M

https://dx.doi.org/10.1021/acsbiomaterials.0c01657
ACS Biomater. Sci. Eng. 2021, 7, 1374−1393

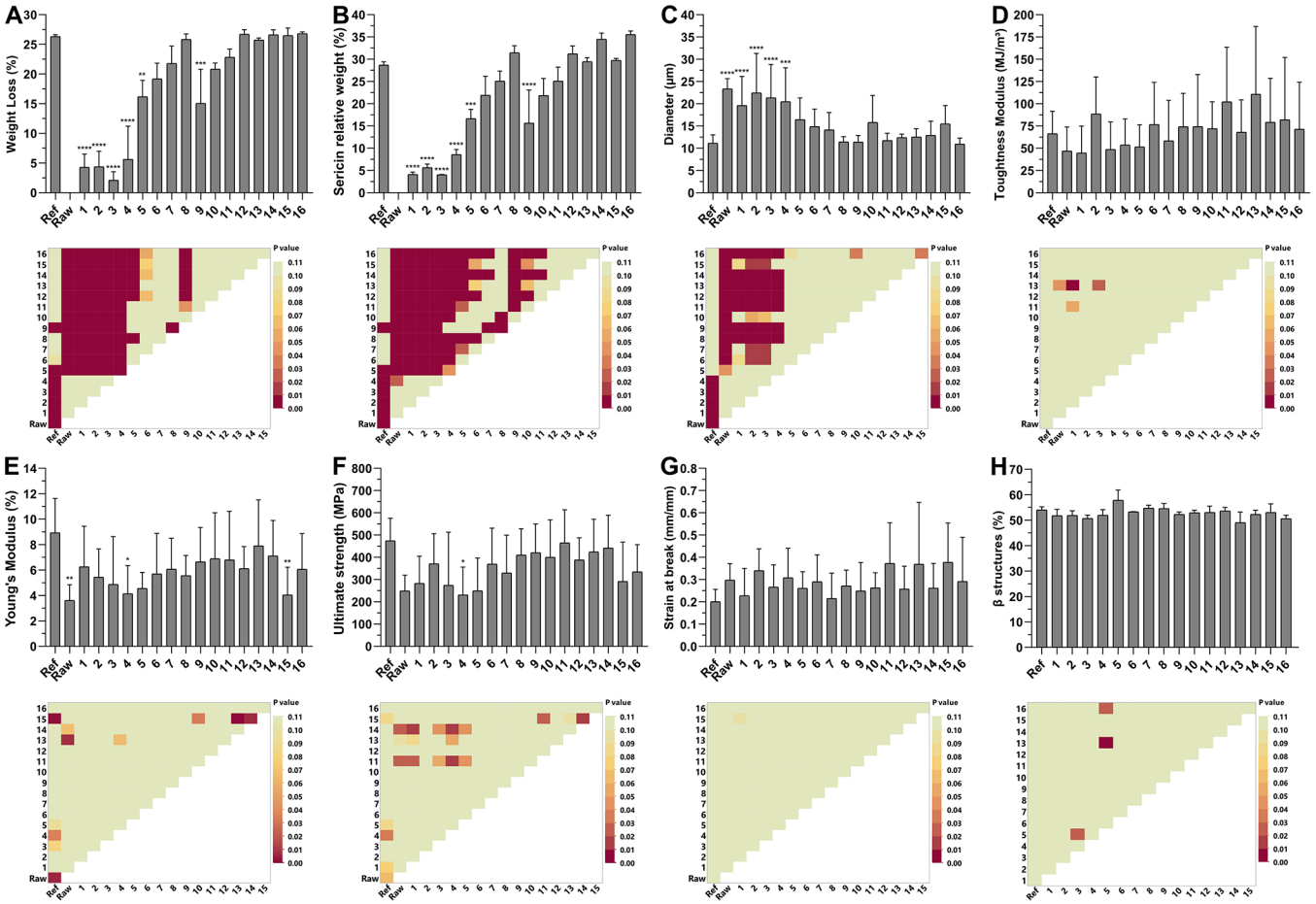

Figure 3. Comparison of the effect on the fiber's properties of the different degumming treatments. The bar charts show the mean values with the respective SD, and the significance refers to the comparison with the reference degumming procedure (Ref). The raw treatment indicates nondegummed fibers. The significance level was assigned as follows: $p \leq 0.1$ (.), $p \leq 0.05$ (*), $p \leq 0.01$ (**), $p \leq 0.001$ (***), and $p \leq 0.0001$ (****). The heat map reports the p value of the multiple-comparison Tukey test between all treatments; p values lower than 0.1 should be considered as significant (90% confidence interval). (A) For weight loss, in this case, if we consider the reference as completely degummed, treatments 1−5 and 9 could be considered as not completely degummed due to the significantly lower weight loss. All the other treatments should be considered as complete degumming. (B) The amount of sericin in the degumming baths (normalized on the cocoon weight) confirms the results obtained by the weight loss; treatments 1−5 and 9 removed a significant lower amount of sericin when compared with the reference. (C) Fibers coming from treatments 1−4 have a significantly larger diameter when compared to the reference. They were almost comparable with the nondegummed fiber (Raw). (D) No significant differences in terms of toughness could be found between the reference fibers and the fibers produced by other treatments, not even in the case of the nondegummed fibers. (E) Only treatments 4 and 15 were able to produce fibers with a significantly lower Young's modulus in comparison with the reference fiber. Also, the nondegummed fibers had a significantly lower Young's modulus than the reference fiber. (F) Only sample 4 had a significant lower ultimate strength compared to the reference. (G) No significant differences from the reference can be found in terms of strain at break. (H) The total amount of secondary structures can estimate the crystallinity of the fibers: as can be seen, no significant differences have been found, indicating that all the samples are crystalline as the reference fibers.

urea, filtered using a disposable filter with a 0.22 μm pore size) until a concentration of 0.6 mg/mL was obtained. This specific concentration was chosen to be in the 0.5−0.8 mg/L range, which is optimal to avoid the formation of protein aggregates due to the shear stress during the injection. The chromatography was conducted with a flow rate of 1 mL/min and a column temperature of 27 °C set using an oven. The specific temperature was set to compensate the environmental temperature variation. The calibration curve (Figure S2) was obtained with a Low/High Molecular Calibration Kit (Sigma-Aldrich). Prior to the measurement, both standards and samples were centrifuged at 1200 rpm for 15 min and filtered with a 0.22 μm filter to eliminate aggregates. The weight average molecular weight (M_w), the dispersion index (D), the number average molecular weight (M_n), and the molecular weight at the peak were evaluated starting from the chromatogram.

Tensile Test. Silk samples were glued, with double-sided tape, on a paper support (square window, 1 × 1 cm).[69] The fiber diameter was measured by image analysis (ImageJ[70]) on images obtained by optical microscopy.[71] The shape of the threads was approximated as a circular cylinder.[72] The samples were mounted on a nanotensile machine Agilent T150 UTM and the standard testing speed was 0.10 mm/s. The engineering strain was obtained by dividing the displacement for the gauge length and the engineering stress by dividing force for the cross-sectional area. Young's modulus was computed by the slope of the stress−strain curve in the initial linear elastic part. The toughness modulus was obtained by calculating the area under the stress−strain curve (by integration). Finally, the ultimate strength was obtained by taking the final engineering stress prior to fracture. For each of the 48 prepared samples, at least 3 fibers were tested, and the mean tensile modulus, mean ultimate strength, and mean toughness modulus with the corresponding standard deviations were calculated and used as input yields for the successive statistical analysis. All samples were tested at least 1 day after their preparation to stabilize the concentration of residual

https://dx.doi.org/10.1021/acsbiomaterials.0c01657
ACS Biomater. Sci. Eng. 2021, 7, 1374−1393

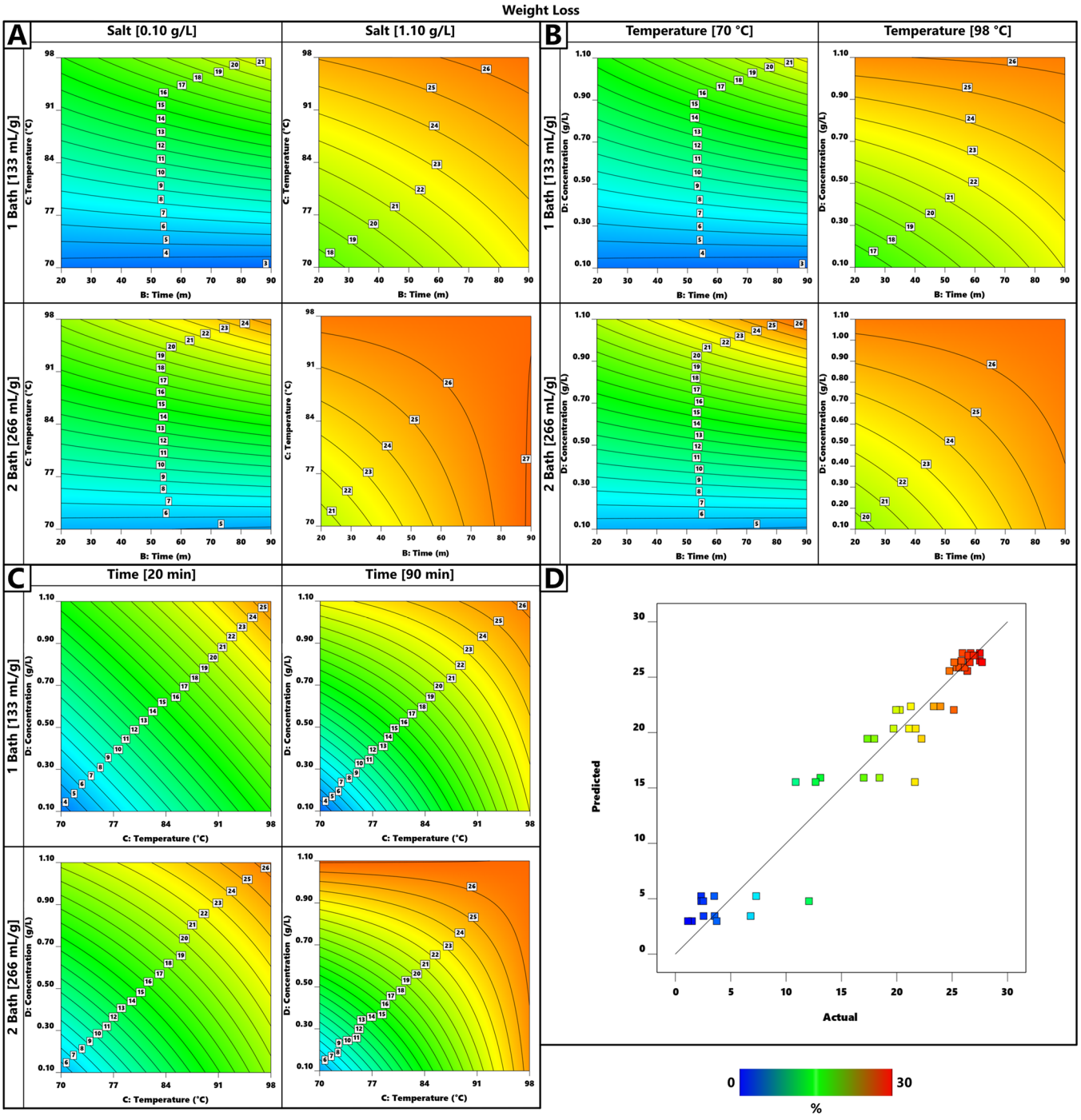

Figure 4. Contour plots of the modeled percentage mass loss on the degumming process. These data can be used to understand in which conditions the procedure is effective. In a complete degumming, when sericin is completely removed, the weight loss (Δm_f) is expected to be between 25 and 30% (taking the Rockwood protocol as a reference, the degumming is complete for a weight loss of >26%). Several terms were significant (ANOVA, Table S2) in order of importance: B (process time), C (process temperature), D (salt concentration), CD (process temperature × salt concentration), BCD (process time × process temperature × salt concentration), A (number of baths), and ACD (number of baths × process temperature × salt concentration). The model is reported as contour plots as follows: (A) weight loss vs temperature and time, (B) weight loss vs salt concentration and time, and (C) weight loss vs salt concentration and temperature. In all these cases, the number of baths is reported as an ordinal, and the missing variable is in its extreme values. These contours can be used to predict the weight loss inside the considered factors' space. It should be noted that several conditions allow one to obtain a complete degumming (Δm_f > 26%). (D) The actual vs predicted graph shows how the calculated points fit the collected data. As can be seen, all the points of the completely degummed (from 0 to 5%) and completely nondegummed (from 25 to 30%) samples are superimposed to the diagonal line, indicating a perfect fitting, and the intermediate points because of the variability of the process are slightly scattered in the line's proximity (this is expected due to the incomplete degumming).

stresses and thus to minimize its effects on the mechanical properties.[73−75] All samples were kept and tested in controlled conditions (20−21 °C and 39−42% RH).

Morphological Analysis. Secondary electron microscopy (FE-SEM, Carl-Zeiss Supra 40) was carried out to qualitatively evaluate the fiber morphology. The fibers were covered by sputtering with a

https://dx.doi.org/10.1021/acsbiomaterials.0c01657
ACS Biomater. Sci. Eng. 2021, 7, 1374−1393

layer of Pt/Pd. The images were used to verify the presence of residual sericin on the degummed fibers or any possible structural damaging of the internal fibroin filament.

RESULTS AND DISCUSSION

A design of experiment (DOE) method has been adopted to set up the experiment and elaborate the collected data statistically. Independent variables (the process parameters) in this method are called factors and the chosen values for each factor are called levels; from now on, in the text, factor and variable will be used interchangeably. The dependence between the different variables was verified by calculating the Pearson's r index to individuate the presence of linear relationships. The Pearson correlation index (r) was plotted in the correlation heat map of Figure 2. The closer the r value is to the extreme −1 or 1, the more the two considered variables become linearly correlated: as a general rule, two variables are considered to be significantly correlated if r is higher than 0.3 or lower than −0.3. Another simple comparison, shown in Figure 3, has been done by calculating the mean and the standard deviation of each studied yield and comparing them among the 16 treatments. The results are shown as asterisks on the bar plots for the direct comparisons with the reference and, since the overall number of comparison (between couples of treatments) is high and difficult to visualize by the conventional asterisk notation, all the missing comparisons are shown as a heat map under each bar plot. The heat map reports the p value of all the comparisons in a matrix, and values of p above 0.1 were not considered significant; consequently, they were reported with a lighter color. In Figure 3A−C, the weight loss, the sericin removal, and the fiber diameter are reported; as can be seen, samples from 1 to 5 all differ from the reference, confirming the results obtained by a visual comparison. Instead, sample 9 was significantly different in terms of weight loss and removed sericin but not in terms of diameter. However, the diameter of sample 9 was higher than those of the other samples and had a high standard deviation, indicating a higher variability between the fiber diameters. The toughness modulus, shown in Figure 3D, was poorly affected by the degumming procedure. None of the 16 treatments differed significantly from the reference. The same conclusions also applied to the ultimate strain and the percentage of β-structures (Figure 3G,H). Young's modulus obtained from treatments 4 and 15 was significantly lower than the reference (Figure 3E); interestingly, also the raw fiber was significantly less stiff, confirming the role of the presence of sericin on the decrease in modulus. Only sample 4 had a lower ultimate strength than the reference (Figure 3F). If we observe the heat maps, several differences are present among the different treatments for all the considered properties with the exclusion of the strain at break. For this reason, we could not model this last property, and the application of ANOVA, in fact, did not reveal any significant factor affecting it.

Weight Loss. The weight loss (referred also as a degumming ratio) is commonly accepted as a measure of the effectiveness of the process in removing sericin. With the universally accepted Rockwood protocol, the weight loss from the cocoons to the degummed fibers is in the range of 25−30%, depending on the quality and typology of used cocoons. Using our material, the medium weight loss was 26.3 ± 0.3, so we took 26% as a threshold, indicating a complete degumming (in which all sericin is removed). The effectiveness of the sericin removal was asserted by SEM (Figure 10), by the decrease in diameter (Figure 3C), and by the increase of sericin in the degumming bath (Figure 3B). In Figure 4, we report the contour plots related to the weight loss (empirical model in eq S1 of Table S24, 95% confidence intervals reported in Table S3). It should be noted that the multidimensionality of the equation does not allow us to plot a single graph. We chose two continuous factors, reporting them on the $x-y$ axes and then reporting the number of baths (discrete factor) as a row and the last continuous factor as a column, fixing it in its extreme values. With this method, we obtained four plots (with four contour plots each) for each choice of the two independent variables placed in the $x-y$ axes (Figure 4A−C). This procedure will be carried out also for all the other studied properties. Several portions of the contour plots reported in Figure 4 are above the threshold limit of 26%. As we can notice from the contour plot in Figure 4A, a single bath with a low amount of salt, even if conducted at the highest temperature (98 °C) and with the longest time (90 min), was not effective in removing sericin. Instead, when the double bath process was performed, using the same conditions as the single bath, we could eliminate almost all the present sericin, reaching a weight loss of almost 25%. With the increase in the amount of salt up to 1.10 g/L, the degumming process at 98 °C was effective regardless of the number of baths. With the same salt concentration, by choosing a double bath and prolonging the time to 80 min, even at 70 °C, it was possible to completely remove sericin; we can hypothesize that even a further decrement in temperature could be possible by improperly extrapolating data out of the experimental region analytically by using eq S1 or, graphically, by extending the contour lines. Analyzing the contour plots of Figure 4B, it is possible to conclude that in the low-temperature limits, the only way to obtain a complete degumming was by a double bath process with a higher salt concentration (1.1 g/L) and a longer process time (90 min). Instead, at a high temperature (98 °C), using a double bath, it was possible to obtain a complete degumming in 20 min if the salt concentration was higher than 1 g/L. However, it is possible to further decrease the amount of salt down to 0.5 g/L by increasing the degumming time above 80 min. Using the contour plot of Figure 4C, we can understand how the conventional protocol is far from being optimized. In fact, at a temperature close to the boiling point (98 °C) moving to the higher amounts of water and salt considered in our study (1.1 g and 260 mL/g, respectively), a double bath process was sufficient to remove 26% of sericin in 20 min, reducing almost one-half of the amount of salt and one-third of the volume of water compared to the standard degumming. Overall, the obtained surfaces suggest numerous numbers of different degumming setups to obtain a complete degumming. The contour plots can be also used to make some general observations about the process robustness. If we define the robustness as the ability of the process to maintain a determined yield (in this case, the weight loss) in a defined range of values even if the process factors slightly change, then we can relate the density of the contour lines directly to the robustness. Less dense contour lines indicate a more robust process. In this context, it is possible to conclude that a high amount of salt (Figure 4A, second column) and a high temperature (Figure 4B, second column) increased the robustness, and the use of a double bath process was also beneficial. The process robustness was more susceptible to the

https://dx.doi.org/10.1021/acsbiomaterials.0c01657
ACS Biomater. Sci. Eng. 2021, 7, 1374−1393

variation of the process time (this is further confirmed in the perturbation graph of Figure S3) with respect to the variation of the other factors. The accuracy of the model was evaluated by the graph reported in Figure 4D in which the weight loss obtained by the experiment was plot versus the value predicted by the model (eq S1) in the same condition. In a perfect matching model, all the points should be aligned to the diagonal line; in our case, the model well matches the experimental data. The results obtained by the weight loss have been double-checked using the amount of sericin collected in the degumming baths (Figures S4 and S5 and Tables S4 and S5) and the diameters of the fibroin after degumming (Figures S6 and S7 and Tables S6 and S7). Both models (eqs S2 and S3 of Table S24), even if built from a different set of collected data, showed the same trend of the weight loss model, confirming its reliability.

Secondary Structure Analysis. In the first analysis, the secondary structure determination conducted by the deconvolution of the I amide peak (1580−1720 cm^{-1}) in the FTIR spectrum (Figure S8) revealed that the influence of the degumming process is not statistically significant on the percentage amount of the different structural conformations of the protein. In fact, a trend in the variation of the relative amounts of the unique structures is not detectable, as can be seen in Figure 5A. A successive ANOVA test, followed by a Tukey multicomparison, conducted on each of secondary structures among the different treatments, revealed no statistical differences (Figure 5B). The heat map of Figure 2 further confirmed the lack of correlation between the secondary structure and the degumming factor; none of the secondary structures were correlated with any of the considered degumming factors ($|r| < 0.30$). However, considering the sum of all the β-structures (parallel, antiparallel, and native) as a measure of the fiber crystallinity and analyzing the data in depth using the design of experiment method, we could recognize the effect of several mixed terms. The effect of the degumming on the crystallinity was small but still detectable and statistically relevant (as proved by the ANOVA, Table S8). This effect probably occurred only on the fiber surface in direct contact with the alkaline bath. In Figure 6, the percentage amount of β-structures (empirical model reported in eq S4 of Table S24, 95% confidence intervals in Table S9) is presented as the previous case as a multiple set of contour plots. We reported the secondary structure as a function of temperature and time in Figure 6A, as a function of concentration and time in Figure 6B, and as a function of concentration and temperature in Figure 6C. In Figure 6D, the actual versus predicted plot shows that the model fitted the experimental values (the points are scattered around the diagonal). From the contour plots of Figure 6A, we can assert that in the case of a low salt concentration, regardless of the number of baths, an increase in the percentage of β-structures results from an increase in the temperature. The effect is inverted when the salt concentration was increased up to 1.1 g/L. A plausible explanation could be the presence of two competitive phenomena: the increase in the temperature that promotes the crystallization[76] and the salt that, in high quantity, breaks the H-bonds of the β-sheets, decreasing the amount of crystallinity.[77] Interestingly, none of the aforementioned effects were significant from the ANOVA analysis (Table S8); meanwhile, their mixed effect was significant, so they were mutually dependent (the significant term was temperature × concentration). In addition, the effect of the concentration was dependent on the number of baths and the time of the process (so the significant terms were salt concentration × time × number of baths). These interactions between different factors led to the complex trend in which the kinetics (time, temperature, and number of baths) plays an important role also influencing the effect of the salt. It should be noted that a double bath process was more effective in the removal of sericin, thus exposing the fibers directly to the salt. This did not have a strong effect when the concentration of salt was low. However, at a high concentration, we could hypothesize that the decrystallization promoted by the salt (especially at a high temperature) was stronger than the crystallization because of the temperature. It is worth noticing that the variation of the salt concentration strongly affected the secondary structure only in the case of

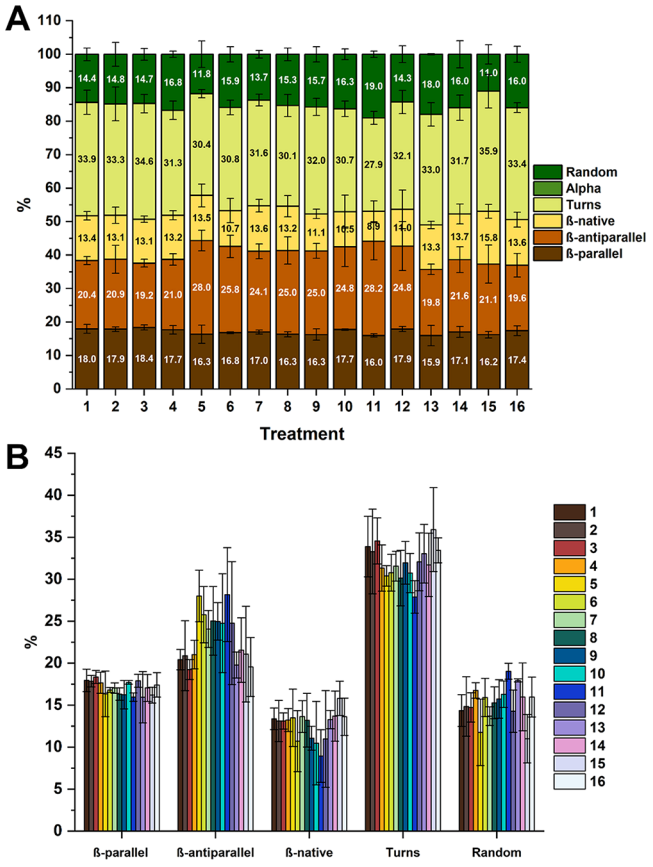

Figure 5. (A) Effect of the 16 treatments on the secondary structure, each bar representing a single treatment with the corresponding relative amounts of secondary structures (reported in different colors). The reported amount results from the mean of 3 replicas and 16 spectra collected for each of them. To determine the secondary structure, the I amide peak has been deconvoluted and, subsequently, a peak fitting has been applied to separate the components related to the different secondary structure conformations.[60,61] The standard deviation of each structure is reported as an error bar. It is not possible to recognize any trend due to the degumming procedure. (B) Different secondary structures divided into groups, each of them containing a bar relative to the specific degumming treatment. Also, in this case, the standard deviation is reported as an error bar. Inside each group, a Tukey test has been conducted. No significant differences have been found in each single group among the degumming treatments, indicating that the degumming process poorly influences the amount of the single secondary structures.

https://dx.doi.org/10.1021/acsbiomaterials.0c01657
ACS Biomater. Sci. Eng. 2021, 7, 1374−1393

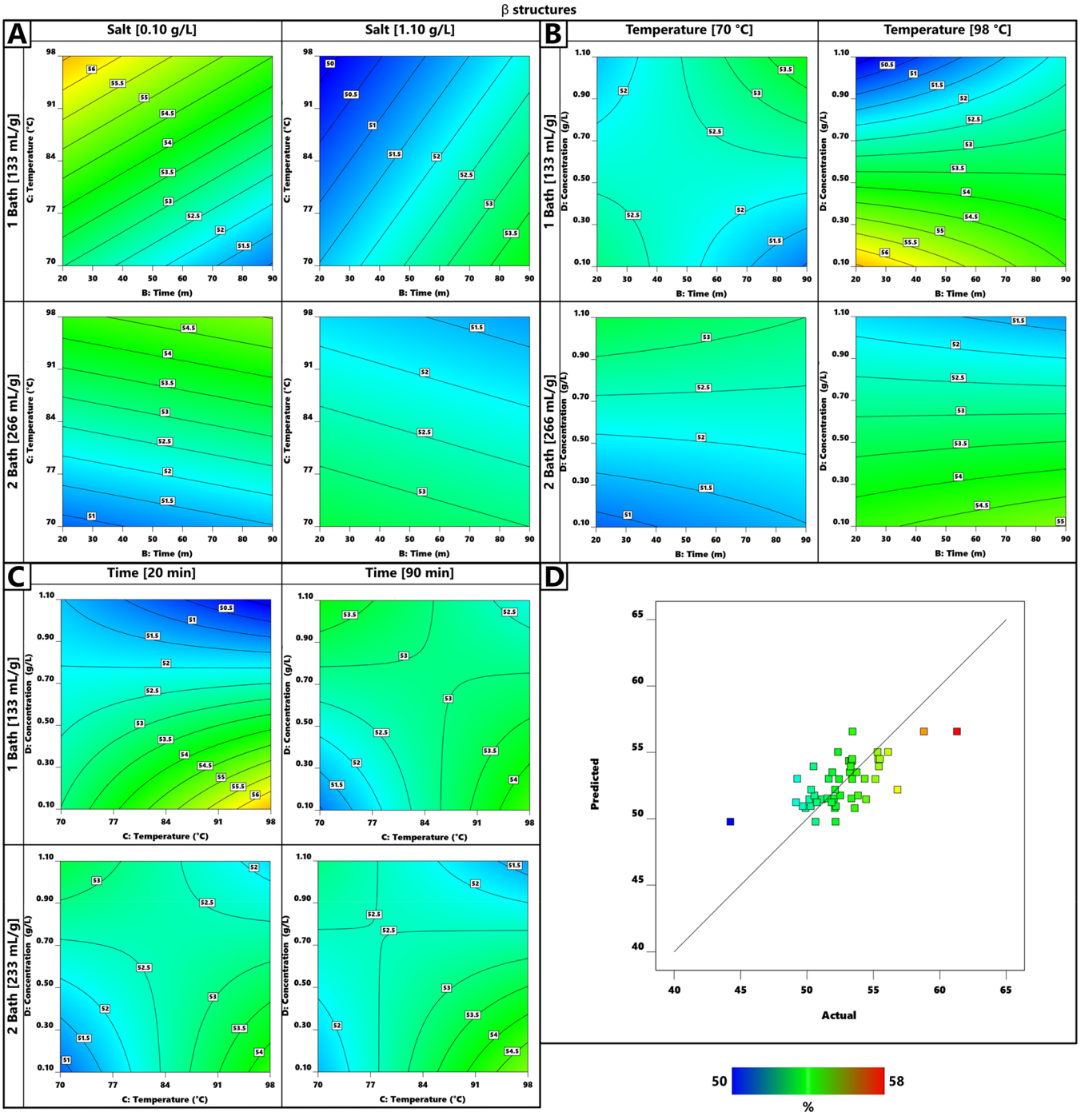

Figure 6. Contour plots of the modeled percentage amount of total β-structures (parallel, antiparallel, and native). These data can be used to understand how the degumming process influences the crystallinity on the fiber surface. The only first-order term that, from the ANOVA analysis (Table S8), was slightly significant was D (salt concentration). The other two significant terms in order of importance were C × D (temperature × salt concentration) and A × B × D (number of baths × degumming time × salt concentration). The model has been sliced in contour plots as follows: (A) β-structures vs temperature and time, (B) β-structures vs salt concentration and time, and (C) β-structures vs salt concentration and temperature. In all these cases, the number of baths is reported as an ordinal, and the missing variable is in its extreme values. These contours can be used to predict the percentage amount of β-structures inside the considered factors' space. (D) The actual vs predicted graph shows how the calculated point fits well the collected data. The points are concentrated on a small portion of the plot (roughly between 47 and 57%) with a few points out from this area. This indicates that the degumming process has only a small impact in terms of the fiber crystallinity but is still detectable.

high temperature (see comparison of the first and second columns of Figure 6B). In fact, at the lowest considered temperature, the β-structures only vary between 51 and 53% and the low density of the contour line indicates a robust region of the process. We could determine a saddle point for a 70 °C single bath at 45 min and 0.60 g/L. In Figure 6C, the mutual temperature−concentration dependence can be examined. Interestingly, we could determine a saddle point centered around 84 °C and 0.70 g/L for a 90 min single bath and for a 70 min double bath; meanwhile, for a 90 min double

https://dx.doi.org/10.1021/acsbiomaterials.0c01657
ACS Biomater. Sci. Eng. 2021, 7, 1374−1393

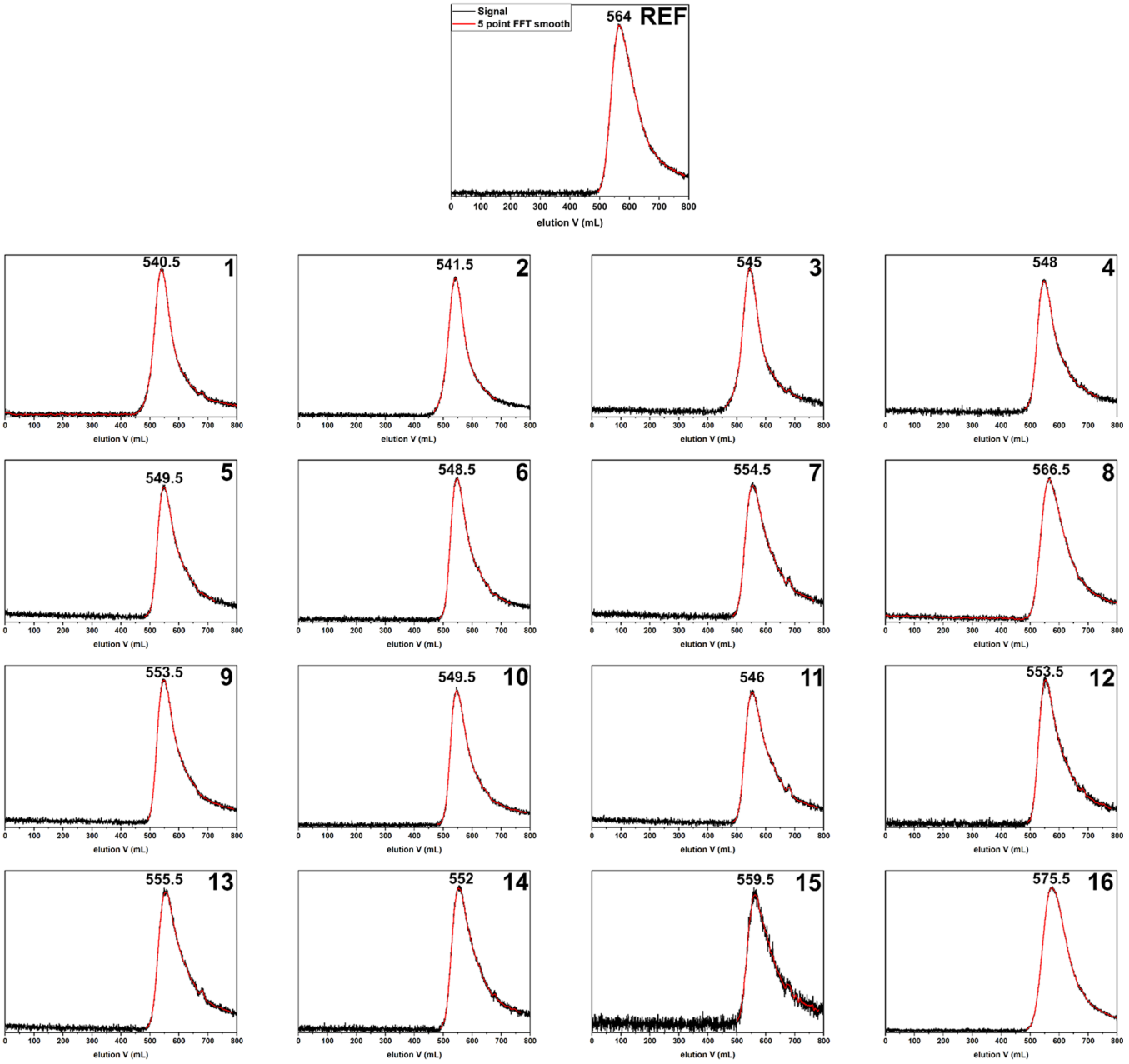

Figure 7. GPC curve from the reference and the 16 different degumming treatments. It should be noted that it is difficult to recognize a pattern; however, a difference in elution volume of 1/60 of mL (corresponding to an elution time of 1 s) in the higher range of the calibration corresponds to a difference in M_w of several tens of kDa.

bath, the saddle point was around 77 °C and 0.80 g/L. No saddle point was detected for a 20 min single bath.

Weight Average Molecular Weight and Polydispersity Index. To better understand the effect of the degumming on the molecular weight of silk fibroin it is necessary to know its structure. Structurally, silk fibroin is composed of a heavy chain (H-chain, with a molecular weight of approximately 390 kDa) and a light chain (L-chain with a molecular weight of 26 kDa) linked by a disulfide bond. Six of these H-L units are linked to the P-25 glycoprotein (25 kDa) to form a complex that is secreted to the fibroin brin.[2,3,78] The molecular weight of this complex was above 2000 kDa.[78] The molecular weight was analyzed on 16 samples (Figure 7, one for each of the 16 different degumming treatments); even if with a single sample per treatment, we could model the molecular weight accurately. In this section, we report the study of the weight average molecular weight (M_w) and the dispersion (D), leaving to the reader the possibility to consult the results of the number average molecular weight (M_n, Figures S11 and S12 and Tables S12 and S13) and the molecular weight of the peak of the chromatogram (M_p, Figures S13 and S14 and Tables S14 and S15) in the Supporting Information. The molecular weight was strongly correlated with the presence of sericin. In fact, during the degumming process, as soon as sericin was removed, the molecular weight suddenly decreased ($r = -0.92$ with Δm_f, $r = -0.89$ with Δm_s); this was further confirmed by the fact that the molecular weight increased with the increase in the fiber diameter ($r = 0.91$). This effect could be confounded with the subordinate effect of the hydrolisis of the protein chain.[79,80] In fact, we found also a modest

https://dx.doi.org/10.1021/acsbiomaterials.0c01657
ACS Biomater. Sci. Eng. 2021, 7, 1374−1393

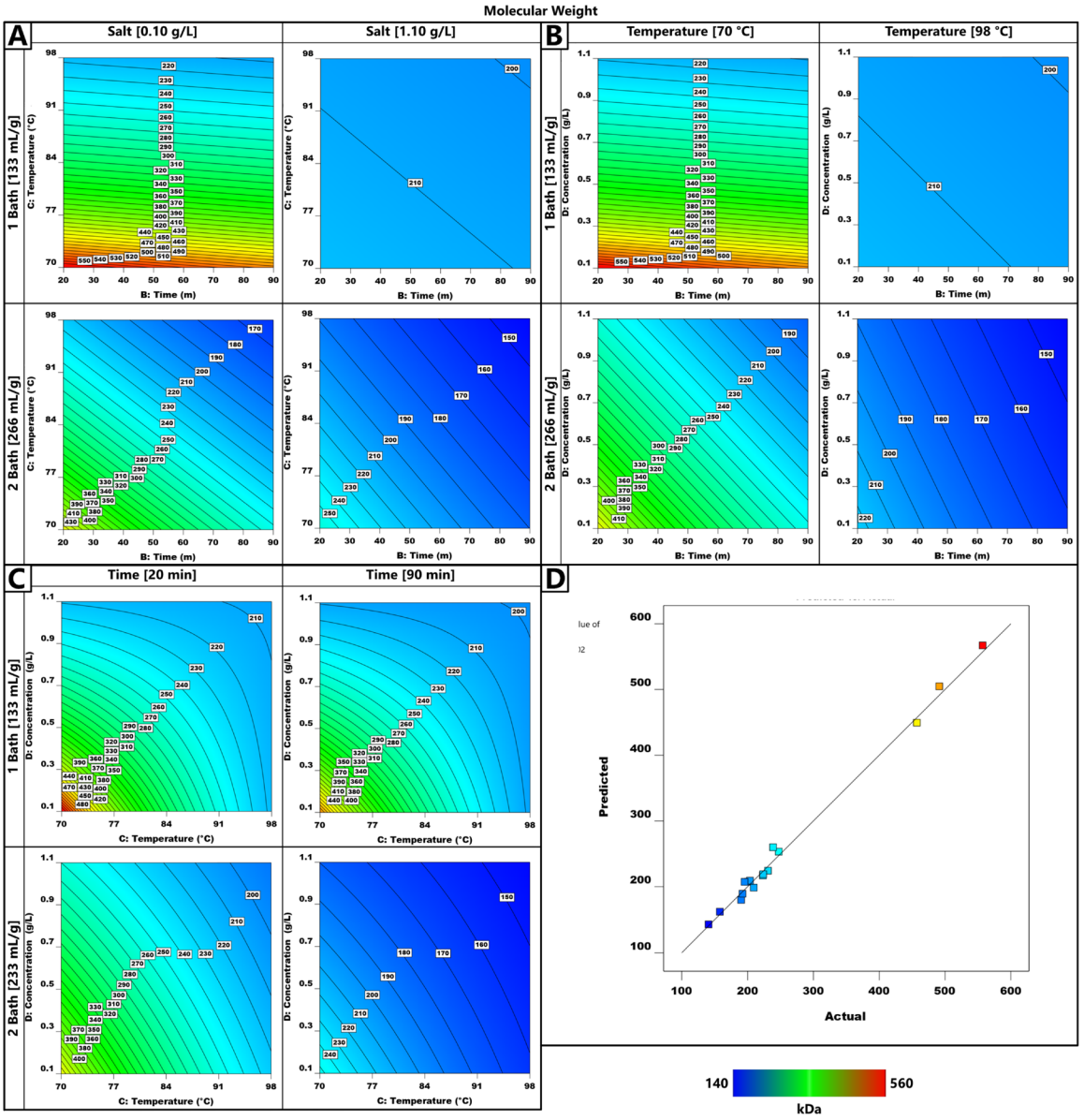

Figure 8. Contour plots of the modeled weight average molecular weight (M_w). The statistically significant terms (ANOVA, Table S10) are, in order of importance, as follows: C (process temperature), D (salt concentration), B (process time), CD (process temperature × salt concentration), A (number of baths), ACD (number of baths × process temperature × salt concentration). The model has been sliced in contour plots as follows: (A) M_w vs temperature and time, (B) M_w vs salt concentration and time, and (C) M_w vs salt concentration and temperature. In all these cases, the number of baths is reported as an ordinal, and the missing variable is in its extreme values. From the contour plots, we can observe that as soon as the process is able to remove the external sericin, the molecular weight of fibroin decreases. The molecular weight in the regions where we can consider the degumming almost complete ranges between 150 and 250 kDa. (D) The actual vs predicted graph shows that the data are divided into two groups: one with a molecular weight between 100 and 300 kDa and the other with a molecular weight between 400 and 600 kDa. The first group results from completely or partially degummed fibers, and the second group results from fibers in which the process was ineffective. As can be seen, the points follow the diagonal trend, indicating a good agreement of the model with the collected data.

correlation of M_w with both the salt concentration ($r = -0.55$) and the process temperature ($r = -0.5$). In Figure 8, the molecular weight M_w (reported in eq S5 of Table S24, 95% confidence intervals in Table S11) is presented as a multiple set of contour plots (four contour plots for each choice of the two independent variables). We reported the molecular weight as a function of temperature and time in Figure 8A, as a function of concentration and time in Figure 8B, and as a function of concentration and temperature in Figure 8C. In Figure 8D, the actual versus predicted plot shows an almost perfect agreement between the experimental values and the values obtained from the model. The higher molecular weight (around 550 kDa) was obtained with a single bath process conducted at a low temperature (70 °C) with a low salt concentration (0.1 g/L) and a lower process time (20 min). This molecular weight is slightly higher than that of the H-L complex of silk fibroin reported in the literature (400 kDa).[36,48,51,52,81−83] However, this high molecular weight corresponded to fibroin that is not completely degummed. We could hypothesize that the protein chain did not undergo degradation as long as a protective layer of sericin was present; when the alkaline solution suddenly reached the

https://dx.doi.org/10.1021/acsbiomaterials.0c01657
ACS Biomater. Sci. Eng. 2021, 7, 1374−1393

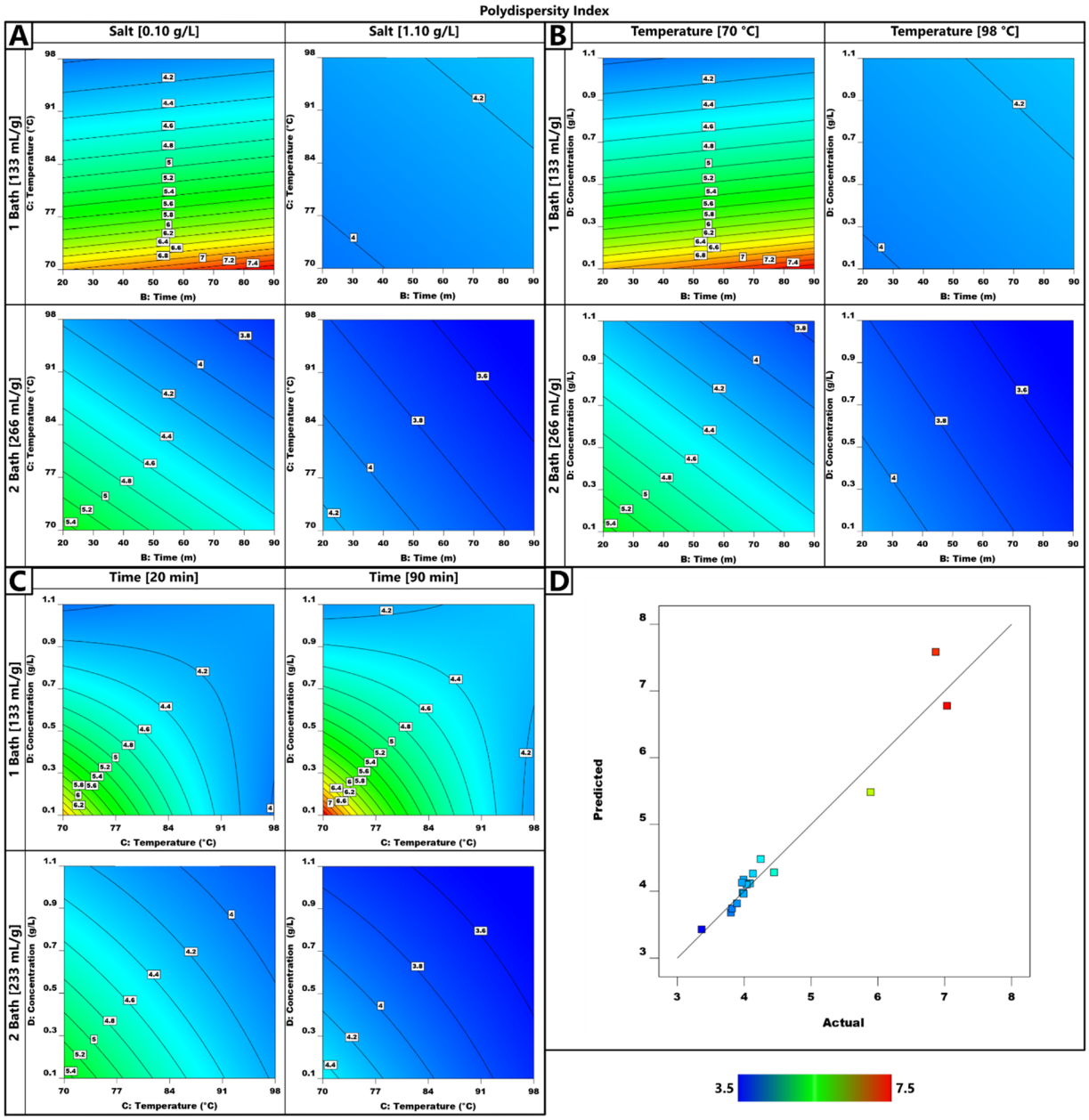

Figure 9. Contour plots of the modeled polydispersity index (PDI). The terms that were statistically significant from the ANOVA test (Table S10) were, in order of importance, as follows: D (salt concentration), C (process temperature), C × D (process temperature × salt concentration), A (number of baths), and A × C × D (number of baths × process temperature × salt concentration). The model has been sliced in contour plots as follows: (A) PDI vs temperature and time, (B) PDI vs salt concentration and time, and (C) PDI vs salt concentration and temperature. In all these cases, the number of baths is reported as an ordinal, and the missing variable is in its extreme values. A general statement can be made by this graph: a higher degumming rate lowers the dispersion index. As for the M_w, in (D) the actual vs predicted graph, the data are divided into two groups (the first between 3 and 5 and the second between 6 and 7) that can be related to a complete or partially complete degumming and an ineffective degumming. As can be seen, the points follow the diagonal trend, indicating a good agreement of the model with the collected data.

internal fibroin, its molecular weight decreased. This process could start before the complete removal of sericin on the exposed portions of the brin. In the process regions where the degumming could be considered complete, the molecular weight ranged between 150 and 250 kDa; moving to regions where the degumming rate was still acceptable but not complete (≥20%), it was possible to access molecular weights above 250 kDa and below 300 kDa. The molecular weight was particularly robust when the process was conducted in a single step and at a higher salt concentration (1.1 g/L) or higher temperature (98 °C), as can be seen in Figure 8A,B; in this condition, the change in the remaining two factors had only a slight effect on the molecular weight that remained around 200 kDa. It should be noted that the degumming time, almost universally used in the literature to tune the molecular weight,[48,51,52] is the factor that less influenced it (as can be seen from the perturbation plot of Figure S10). In fact, the molecular weight was more robust against the variation of the degumming time than the variation of the salt concentration and the process temperature. This can be understood also by

https://dx.doi.org/10.1021/acsbiomaterials.0c01657
ACS Biomater. Sci. Eng. 2021, 7, 1374−1393

observing the contour plots (Figure 9; the contour lines are slightly less dense toward the increase in the degumming time if compared with the direction of the increase in the other variables). An explanation of this effect resides in the fact that neither the higher molecular weights were obtained from partially or nondegummed fibers in which neither the temperature nor the salt concentration was sufficient to degrade the fibroin. In Figure 9, the model of the polydispersity index (PDI; empirical model reported in eq S6 of Table S24, 95% confidence intervals in Table S17) is presented as a multiple set of contour plots. As in the previous graph, PDI has been reported as a function of temperature and time in Figure 9A, as a function of concentration and time in Figure 9B, and as a function of concentration and temperature in Figure 9C. In Figure 9D, the actual versus predicted plot shows a good agreement for small values of PDI and a slightly worse prediction for the higher values. However, the predicted values follow the collected data and the model could be considered as predictive. The calculated dispersion index varied between 3.5 and 7.5, compatible to a chain growth polymerization mechanism[84] (in the case of synthetic polymers) and biopolymers coming from natural sources. The lower values of PDI was obtained in the areas where the degumming was complete and the molecular weight was low. This can be explained by the influence of the residual sericin; in fact, the amount of removed sericin was highly correlated with the PDI ($r = -0.85$), further confirmed by the correlation with the diameter ($r = 0.87$) and the weight loss ($r = -0.88$).

Microstructural Analysis. The SEM analysis of Figure 10 confirmed the results obtained from the weight loss and the removed sericin. Among the 16 treatments, numbers 1−5 present nondegummed fibers in which it was still possible to recognize the presence of two fibroin brines connected; this was coherent with the small weight loss from the cocoons during the process and the small amount of sericin present in the degumming bath. The fibers degummed by treatment 9 had a big spot of sericin still attached to the fibroin. All the other treatments were comparable with the reference sample in which some little spot of sericin was still present. We could conclude that a 20 min single bath process, regardless of the salt concentration and the process temperature, was not effective in the sericin removal. With a double bath process instead, 20 min could be sufficient to obtain an efficient degumming. In this case, only the process conducted at a lower temperature (70 °C) and a lower salt concentration (0.1 g/L) was inefficient. Interestingly, we could obtain an acceptable level of degumming (weight loss of 22%) even at 70 °C using the highest salt concentration (1.1 g /L) in a 90 min process. For the 90 min process, all the treatments were effective, with the exclusion of treatment 5 conducted with a single bath at a low temperature (70 °C) and a low salt concentration (0.1 g/L).

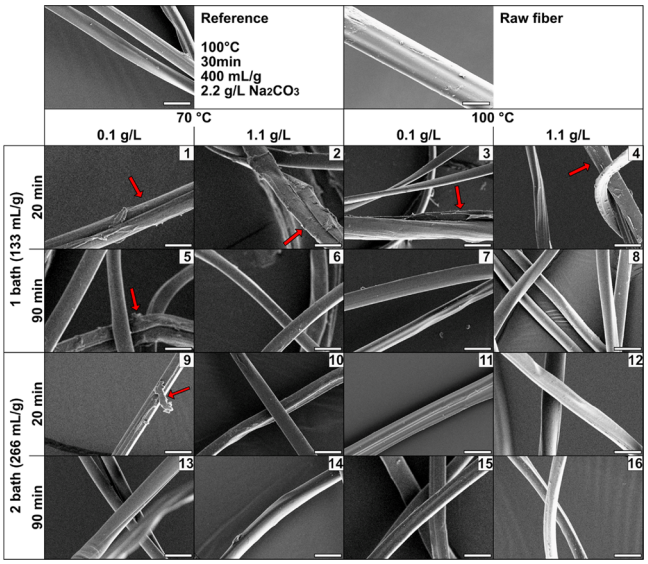

Figure 10. SEM micrographs of the fibers resulting from the 16 degumming treatments (from 1 to 16) and the reference degumming procedure (Ref). In the fibers produced by treatments 1−5 and 9, the presence of sericin is clear. It should be noted that in treatments 1−4, we could find several fibers with the fibroin brines not separated (highlighted by an arrow). Instead, in the fibers produced by treatment 9, sericin is present in large quantity (highlighted with an arrow). In all the other treatments, comprising the reference, small spots of sericin are visible on the surface of the degummed fibroin. Scale bars, 10 μm.

Mechanical Properties. On the degummed fibers, we conducted an extensive mechanical characterization by using a tensile test and analyzing the stress−strain curves (Figure 11) to calculate the ultimate strength, Young's modulus, and the toughness modulus. The only mechanical property that we could not study was the strain at break because it was statistically unaffected by the degumming (as shown in Figure 3G) and, even using the design of experiment method, it was not possible to recognize any significant mixed effect. We report here only the analysis conducted on the ultimate strength, leaving to the reader the possibility to consult the analysis of Young's modulus (Figures S17 and S18 and Tables S20 and S21) and the toughness modulus (Figures S19 and S20 and Tables S22 and S23) in the Supporting Information. The ultimate strength (empirical model in eq S9 of Table S24, 95% confidence intervals in Table S19) is reported as a function of temperature and time in Figure 12A, as a function of concentration and time in Figure 12B, and as a function of concentration and temperature in Figure 12C. In Figure 12D, the actual versus predicted plot shows that the model fitted the experimental values (the points are scattered around the diagonal). We could observe in Figure 12A that for a single bath process, when the salt concentration was at the minimum amount (0.1 g/L), a saddle point was present around 30 min and 83 °C and we could observe an increase in the ultimate strength with the increase in the process temperature. The same trend was present in the double bath process when conducted in the same condition (low salt concentration). When the concentration of salt was in its maximum, the ultimate strength increased with the decrease in the temperature and time process in the case of a single bath; instead, in the double bath process, above 60 min, the ultimate strength decreased with the increase in the temperature and time, whereas below 60 min, the ultimate strength increased with the increase in the temperature and the decrease in the time. Also, in this case, there was a saddle point at 70 °C and 65 min. From Figure 12B, we can see that at a low temperature (70 °C), the ultimate strength increased with the increase in the salt concentration and slightly decreased with the increase in the process time regardless of the number of baths. In the case of a high-temperature process (98 °C), we could detect a saddle point around 80 °C

https://dx.doi.org/10.1021/acsbiomaterials.0c01657
ACS Biomater. Sci. Eng. 2021, 7, 1374−1393

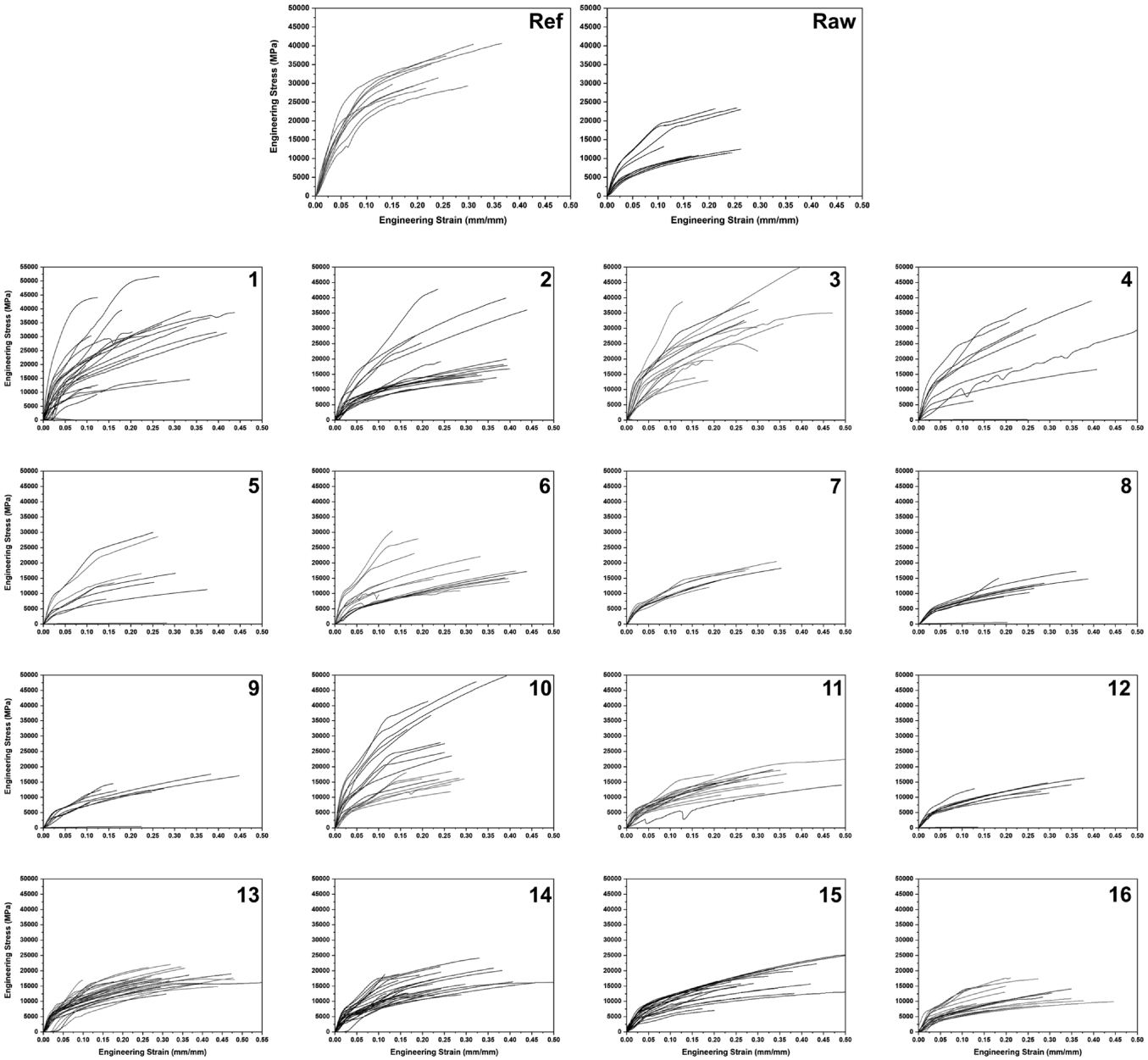

Figure 11. Stress−strain curves of the fibers after the degumming treatments. For the sake of clarity, not all curves were reported. From these curves, Young's modulus, the ultimate strength and strain at break, and the toughness modulus were obtained.

and 0.40 g/L for a single bath process and around 50 °C and 0.40 g/L for a double bath process. In Figure 12C, we can observe that in the case of a 20 min process, an increase in the salt concentration increased the ultimate strength, probably because of the higher removal of sericin. For a single bath, the increment in the ultimate strength is also in the same direction as the increment in the process time; meanwhile, in the case of a double bath, this trend is reversed. With a 90 min process, we could individuate a saddle point around 84 °C and 0.90 g/L for a single bath process and 95 °C and 0.50 g/L for a double bath process. The overall trend of the ultimate strength was difficult to explain because of its dependence on multiple factors and structural properties of the degummed fibers. In terms of robustness, it was also difficult to recognize areas in which the ultimate strength was less subjected to the process variation. However, around the saddle point, the process was more robust if compared to other areas. A more accurate analysis revealed that the salt concentration was critical in terms of robustness (Figure S20). Surprisingly, a moderate inverse correlation (Figure 2) was found between the ultimate strength and the molecular weight (r = −0.62), indicating that the increase in the molecular weight may decrease such property. This unexpected effect, which is not reported in the literature,[51,52] can be explained here, considering the effect of a lurking variable. This hypothesis is also supported by a previous work[85] that compared the mechanical properties of the silk bave and brin, proving the beneficial effect of the degumming. However, the comparison was less general than the one provided here. In particular, we proved the effect also on partially degummed fibers, which can be seen in Figure 3D−F by comparing the raw column with the other 16 processes. In fact, the removal of sericin affects the ultimate strength,[86] as proved by its correlation with the weight loss (r = 0.48), the removed

https://dx.doi.org/10.1021/acsbiomaterials.0c01657
ACS Biomater. Sci. Eng. 2021, 7, 1374−1393

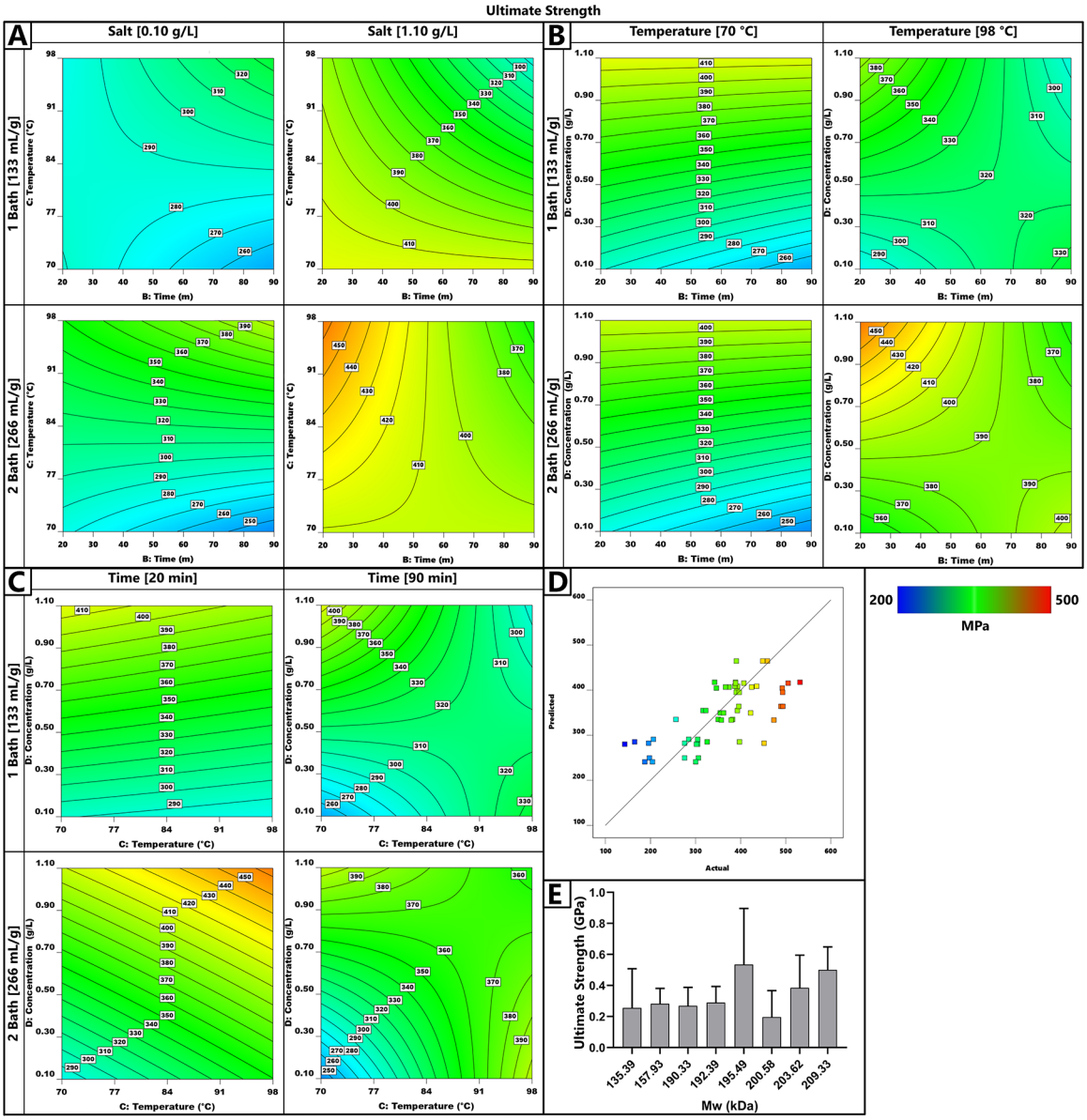

Figure 12. Contour plots of the modeled mean ultimate strength (σ_{ult}) from the fibers of the degummed fibroin. The statistically significant terms of the model (ANOVA, Table S18) were, in order of importance, as follows: D (salt concentration), CD (process temperature × salt concentration), and BCD (process time × process temperature × salt concentration). The contour plots are reported as follows: (A) weight loss vs temperature and time, (B) weight loss vs salt concentration and time, and (C) weight loss vs salt concentration and temperature. In all these cases, the number of baths is reported as an ordinal, and the missing variable is in its extreme values. The trend of the ultimate strength is complex and difficult to attribute to one specific property (like the molecular weight or the secondary structure), although the removal of sericin is beneficial in terms of the increase in the ultimate strength. (D) The actual versus predicted plot shows that even if the points are scattered (as expected from a mechanical test), they are following a diagonal trend, indicating an agreement between the model and the collected values. (E) Mean ultimate strength vs molecular weight in the cases of complete degumming; the tendency is the increase in σ_{ult} with the increase in M_w. However, no statistical differences could be found.

sericin (r = 0.48), and the mean diameter (r = −0.6). We could then hypothesize that the sericin removal had a greater impact on the fiber's ultimate strength than the molecular weight, and as soon as sericin was removed, the effect of the molecular weight was no longer detectable. However, reducing the data only to samples with a high degumming ratio (>25%) and plotting their ultimate strength versus the molecular weight, a trend of the ultimate strength within the increase in the molecular weight is recognizable, even if we could not find any significant difference among the different samples, as shown in Figure 12E. This was probably due to the fact that the number of tested fibers was not sufficiently large to detect the effect of the molecular weight on the mechanical properties; it was enough to detect the influence of the process variables. To better clarify this point, in Figure S21A, the ultimate strength was plotted against M_w and Δm_f; the white part of the plot shows inaccessible regions of the $M_w - \Delta m_f$ space. Analyzing the plot, it was clear that it was not possible to eliminate sericin without decreasing the molecular weight. As a consequence, with the fact that the sericin removal was widely more important than the increment in the molecular weight in terms of improvement of the mechanical

https://dx.doi.org/10.1021/acsbiomaterials.0c01657
ACS Biomater. Sci. Eng. 2021, 7, 1374−1393

Table 4. Numerical Optimization Based on the Desirability Approach inside Our Factors' Space[a]

minimize	maximize	d_{tot}	no. of baths	t (min)	T (°C)	[Na_2CO_3] (g/L)	Δm_f (%)	M_w (kDa)	D	σ_{ult} (MPa)
	Δm_f	0.98	2	90	70	1.1	27.2	182.0	3.7	406.8
increment (%)							3.4	30.9	5.4	−0.3
	M_w	1	1	23	70	0.1	3.6	558.0	7.2	289.4
increment (%)							−86.3	301.4	105.1	−29.1
D		0.985	2	90	98	1.1	26.9	150.0	3.4	354.8
increment (%)							2.3	7.9	−3.2	−13.0
	σ_{ult}	0.827	2	20	98	1.1	26.5	184.0	3.8	464.6
increment (%)							0.7	32.4	8.3	13.9
	M_w, Δm_f	0.503	1	90	84	0.7	19.0	269.0	4.8	325.8
increment (%)							−27.7	93.5	36.7	−20.1
D	M_w, Δm_f	0.752	2	20	83	0.9	21.0	245.0	4.2	410.4
increment (%)							−20.1	82.7	19.6	0.6
	σ_{ult}, Δm_f	0.748	2	20	98	1.1	26.5	184.0	3.8	464.6
increment (%)							0.7	32.4	8.3	13.9

[a]Within the maximization of the single properties (the weight loss (Δm_f), the molecular weight (M_w), the dispersion index (D), and the ultimate strength (σ_{ult})), a set of multivariable optimizations has been conducted. The increment row provides the difference in percentage in comparison with the reference protocol.

properties, we could conclude that, macroscopically, the effect of the sericin removal dominates against the effect increasing the M_w. No significant correlation between the ultimate strength and any of the analyzed secondary structure could be found (Figure 2) as could be expected due to the small impact of the degumming process on the fiber crystallinity.

Optimization. Using the desirability function approach and the combined results obtained in the previous paragraphs, Table 4 has been built with a series of ready-to-use processes to optimize the different material properties. Besides the obvious solutions of the maximization or minimization of the single parameters (easily obtainable from the graphs reported in the other paragraph), a set of three nontrivial problems has been solved: the maximization of both the weight loss and the molecular weight, the same problem within the minimization of the dispersion index, and the maximization of the mechanical properties and the weight loss. It should be noted that as previously discussed, the maximization of the molecular weight is against the maximization of the weight loss, which is the result when a numerical optimization is conducted, maximizing both; the best results predict a weight loss of 19% and a molecular weight of 269 kDa. The maximization of the mechanical properties is instead in the same direction as the maximization of the weight loss.

CONCLUSIONS

Natural biopolymers are subjected for their own nature to variations of their properties. The impact of the degumming process further increases these variations, making it sometimes difficult to have a control on the final material properties. The degumming process is at the base of fibroin materials' preparation. Although this process significantly affects—as we have demonstrated here—the properties of the outcoming fibroin and those of the obtained biomaterial, the degumming procedure is often not considered in the modulation of the material properties. In fact, a conventional and universal protocol based on the use of a boiling bath of Na_2CO_3 with well-fixed variables (salt concentration, process time and temperature, and volume of water) is currently used. Statistical methods can effectively control the relation between the process factors and the outcoming property of the material, considering also the natural variability. We applied a statistical method, namely, design of experiment, to the alkali Na_2CO_3 degumming process of silk. We could determine the empirical equations relating the studied properties (weight loss, removed sericin, fiber diameter, crystallinity, molecular weight, polydispersity, ultimate strength, Young's modulus, and toughness modulus) to the process parameters (number of baths, salt concentration, and process temperature and time). These equations, provided with the 95% confidence bands, can be used both to tune the fibers properties precisely and to find areas where the considered properties were robust in terms of the variation of the process parameters. We proved that the degumming can be regarded as a complex system,[87] which is sensitive not only to the single process parameters but also to their mixed effects. It was possible to complete a degumming with less amount of salt and water and using a lower-temperature process compared with the commonly used alkali Na_2CO_3 degumming, moving toward a greener approach. Interestingly, as soon as the external layer was removed, the molecular weight and the polydispersity decreased. However, in the region of complete degumming, the molecular weight could be tuned between 150 and 300 kDa. Only a small variation on the fiber secondary structures was found (between 50 and 53%) and only in the case in which the β-structures were taken as a whole to measure the total crystallinity. We found an inverse relationship between the mechanical properties and the fiber molecular weight. This result, which seems to be in contrast to the previous study on the subject, was justified by the effect of the sericin removal that acted as a lurking variable. In fact, the major improvement of the mechanical properties was due to the

https://dx.doi.org/10.1021/acsbiomaterials.0c01657
ACS Biomater. Sci. Eng. 2021, 7, 1374−1393

removal of sericin that implied the decrease in the molecular weight, probably due to the protein degradation. Whenever only the completely degummed samples were considered, the trend was reversed; an increase in the molecular weight gave an increase in the mechanical properties. No significant effect on the mechanical properties could be related to the fiber crystallinity. The final optimization with the desirability method allowed us to solve some nontrivial question on how to contemporarily maximize properties in which the singular optimization goes in opposite directions (i.e. maximization of the molecular weight and the amount of removed sericin and maximization of all the mechanical properties). This set of degumming procedures can be applied effectively on the conventional *B. mori* cocoons; however, to extend its use on cocoons from different species, a further study will be necessary.

■ ASSOCIATED CONTENT

Supporting Information

The Supporting Information is available free of charge at https://pubs.acs.org/doi/10.1021/acsbiomaterials.0c01657.

Calibration curves, FTIR, and statistical analysis (ANOVA tables, perturbation plots, empirical models, and confidence intervals) (PDF)

■ AUTHOR INFORMATION

Corresponding Author

Alessio Bucciarelli − *Microsystem Technology Group, Center for Materials and Microsystems, Fondazione Bruno Kessler, Trento 38123, Italy;* orcid.org/0000-0001-5719-4617; Email: bucciarelli@fbk.eu

Authors

Gabriele Greco − *Laboratory of Bio-inspired, Bionic, Nano, Meta Materials and Mechanics, Department of Civil, Environmental and Mechanical Engineering, University of Trento, Trento 38123, Italy*

Ilaria Corridori − *Laboratory of Bio-inspired, Bionic, Nano, Meta Materials and Mechanics, Department of Civil, Environmental and Mechanical Engineering, University of Trento, Trento 38123, Italy;* orcid.org/0000-0002-7348-9578

Nicola M. Pugno − *Laboratory of Bio-inspired, Bionic, Nano, Meta Materials and Mechanics, Department of Civil, Environmental and Mechanical Engineering, University of Trento, Trento 38123, Italy; School of Engineering and Materials Science, Queen Mary University of London, E14NS London, United Kingdom;* orcid.org/0000-0003-2136-2396

Antonella Motta − *Department of Industrial Engieneering, University of Trento, Trento 38123, Italy; BIOTech Research Center and European Institute of Excellence on Tissue Engineering and Regenerative Medicine, Trento 38123, Italy;* orcid.org/0000-0003-4893-6863

Complete contact information is available at: https://pubs.acs.org/10.1021/acsbiomaterials.0c01657

Author Contributions

A.B. conceived the idea, performed part of the experiments (degumming of the silk fibroin), analyzed the data to obtain the empirical models, and wrote the manuscript. G.G. and I.C. performed all the mechanical measurements and analyzed the mechanical curves. N.M.P. and A.M. edited the manuscript and supervised the work in all its stages, from the conceived idea to the experimental planning. All authors contributed to the final editing of the manuscript prior to its submission.

Notes

The authors declare no competing financial interest.

■ ACKNOWLEDGMENTS

N.M.P. is supported by the European Commission under the FET Proactive ("Neurofibers") grant no. 732344, as well as by the Italian Ministry of Education, University and Research (MIUR), under the "Departments of Excellence" grant L. 232/2016 and the ARS01-01384-PROSCAN and PRIN-20177TTP3S grants. I.C. is supported by FET Proactive ("Neurofibers") grant no. 732344. The project leading this application has received funding from the European Union's Horizon 2020 Research and Innovation Staff Exchange Programme (RISE) under the Marie Sklodowska-Curie grant agreement MSCA-RISE 778078 (Remix project).

■ REFERENCES

(1) Xiang, H.; Liu, X.; Li, M.; Zhu, Y.; Wang, L.; Cui, Y.; Liu, L.; Fang, G.; Qian, H.; Xu, A.; Wang, W.; Zhan, S. The Evolutionary Road from Wild Moth to Domestic Silkworm. *Nat. Ecol. Evol.* **2018**, 1268−1279.

(2) Koh, L.-D.; Cheng, Y.; Teng, C.-P.; Khin, Y.-W.; Loh, X.-J.; Tee, S.-Y.; Low, M.; Ye, E.; Yu, H.-D.; Zhang, Y.-W.; Han, M.-Y. Structures, Mechanical Properties and Applications of Silk Fibroin Materials. *Prog. Polym. Sci.* **2015**, *46*, 86−110.

(3) Qi, Y.; Wang, H.; Wei, K.; Yang, Y.; Zheng, R. Y.; Kim, I.; Zhang, K. Q. A Review of Structure Construction of Silk Fibroin Biomaterials from Single Structures to Multi-Level Structures. *Int. J. Mol. Sci.* **2017**, 237.

(4) Vepari, C.; Kaplan, D. L. Silk as a Biomaterial. *Prog. Polym. Sci.* **2007**, *32*, 991−1007.

(5) Kasoju, N.; Bora, U. Silk Fibroin in Tissue Engineering. *Adv. Healthcare Mater.* **2012**, *1*, 393−412.

(6) Johansson, S. G. O.; Wüthrich, B.; Zortea-Caflisch, C. Nightly Asthma Caused by Allergens in Silkfilled Bed Quilts: Clinical and Immunologic Studies. *J. Allergy Clin. Immunol.* **1985**, 452.

(7) Vlachou, C.; Thomas, K. S.; Williams, H. C. A Case Report and Critical Appraisal of the Literature on the Use of DermaSilk ® in Children with Atopic Dermatitis. *Clin. Exp. Dermatol.* **2009**, e901.

(8) Cosmi, F.; Schiatti, R.; Ignesti, C. Diagnostic Study of 5 Cases of Allergic Asthma Due to Sensitization to Silk Allergens in Textile Workers from the Prato Area. *Quad. Sclavo Diagn. Clin. Lab.* **1986**, *22*, 433−440.

(9) Yang, Y. J.; Ganbat, D.; Aramwit, P.; Bucciarelli, A.; Chen, J.; Migliaresi, C.; Motta, A. Processing Keratin from Camel Hair and Cashmere with Ionic Liquids. *eXPRESS Polym. Lett.* **2019**, *13*, 97−108.

(10) Mandal, B. B.; Grinberg, A.; Seok Gil, E.; Panilaitis, B.; Kaplan, D. L. High-Strength Silk Protein Scaffolds for Bone Repair. *Proc. Natl. Acad. Sci.* **2012**, 7699.

(11) Raggio, R.; Bonani, W.; Callone, E.; Dirè, S.; Gambari, L.; Grassi, F.; Motta, A. Silk Fibroin Porous Scaffolds Loaded with a Slow-Releasing Hydrogen Sulfide Agent (GYY4137) for Applications of Tissue Engineering. *ACS Biomater. Sci. Eng.* **2018**, 2956.

(12) Gambari, L.; Amore, E.; Raggio, R.; Bonani, W.; Barone, M.; Lisignoli, G.; Grigolo, B.; Motta, A.; Grassi, F. Hydrogen Sulfide-Releasing Silk Fibroin Scaffold for Bone Tissue Engineering. *Mater. Sci. Eng. C* **2019**, 471.

(13) Cho, H.; Bucciarelli, A.; Kim, W.; Jeong, Y.; Kim, N.; Jung, J.; Yoon, S.; Khang, G. Natural Sources and Applications of Demineralized Bone Matrix in the Field of Bone and Cartilage Tissue Engineering. In *Bioinspired Biomaterials. Advances in*

Experimental Medicine and Biology; Chun, H. J.; Reis, R. L. A. M.; Khang, G., Eds.; Springer, Singapore, 2020; pp. 3−14, DOI: 10.1007/978-981-15-3258-0_1.
(14) Cho, H. H.; Been, S. Y.; Kim, W. Y.; Choi, J. M.; Choi, J. H.; Song, C. U.; Song, J. E.; Bucciarelli, A.; Khang, G. Comparative Study on the Effect of the Different Harvesting Sources of Demineralized Bone Particles on the Bone Regeneration of a Composite Gellan Gum Scaffold for Bone Tissue Engineering Applications. *ACS Appl. Bio Mater.*. 2021, *0* (), DOI: 10.1021/acsabm.0c01549.
(15) Ribeiro, V. P.; da Silva Morais, A.; Maia, F. R.; Canadas, R. F.; Costa, J. B.; Oliveira, A. L.; Oliveira, J. M.; Reis, R. L. Combinatory Approach for Developing Silk Fibroin Scaffolds for Cartilage Regeneration. *Acta Biomater.* **2018**, 167.
(16) Cheng, G.; Davoudi, Z.; Xing, X.; Yu, X.; Cheng, X.; Li, Z.; Deng, H.; Wang, Q. Advanced Silk Fibroin Biomaterials for Cartilage Regeneration. *ACS Biomater. Sci. Eng.* **2018**, 2704−2715.
(17) Farokhi, M.; Mottaghitalab, F.; Fatahi, Y.; Saeb, M. R.; Zarrintaj, P.; Kundu, S. C.; Khademhosseini, A. Silk Fibroin Scaffolds for Common Cartilage Injuries: Possibilities for Future Clinical Applications. *Eur. Polym. J.* **2019**, 251.
(18) Font Tellado, S.; Bonani, W.; Balmayor, E. R.; Foehr, P.; Motta, A.; Migliaresi, C.; Van Griensven, M. Fabrication and Characterization of Biphasic Silk Fibroin Scaffolds for Tendon/Ligament-to-Bone Tissue Engineering. *Tissue Eng. - Part A* **2017**, 859.
(19) Fang, Q.; Chen, D.; Yang, Z.; Li, M. In Vitro and in Vivo Research on Using Antheraea Pernyi Silk Fibroin as Tissue Engineering Tendon Scaffolds. *Mater. Sci. Eng. C* **2009**, 1527.
(20) Naghashzargar, E.; Farè, S.; Catto, V.; Bertoldi, S.; Semnani, D.; Karbasi, S.; Tanzi, M. C. Nano/Micro Hybrid Scaffold of PCL or P3Hb Nanofibers Combined with Silk Fibroin for Tendon and Ligament Tissue Engineering. *J. Appl. Biomater. Funct. Mater.* **2015**, 0.
(21) Gholipourmalekabadi, M.; Sapru, S.; Samadikuchaksaraei, A.; Reis, R. L.; Kaplan, D. L.; Kundu, S. C. Silk Fibroin for Skin Injury Repair: Where Do Things Stand? *Adv. Drug Delivery Rev.* **2019**, 28.
(22) Min, S.; Gao, X.; Han, C.; Chen, Y.; Yang, M.; Zhu, L.; Zhang, H.; Liu, L.; Yao, J. Preparation of a Silk Fibroin Spongy Wound Dressing and Its Therapeutic Efficiency in Skin Defects. *J. Biomater. Sci. Polym. Ed.* **2012**, 97.
(23) Farokhi, M.; Mottaghitalab, F.; Fatahi, Y.; Khademhosseini, A.; Kaplan, D. L. Overview of Silk Fibroin Use in Wound Dressings. *Trends Biotechnol.* **2018**, 907.
(24) Tran, S. H.; Wilson, C. G.; Seib, F. P. A Review of the Emerging Role of Silk for the Treatment of the Eye. *Pharm. Res.* **2018**, 248.
(25) Madden, P. W.; Lai, J. N. X.; George, K. A.; Giovenco, T.; Harkin, D. G.; Chirila, T. V. Human Corneal Endothelial Cell Growth on a Silk Fibroin Membrane. *Biomaterials* **2011**, 4076.
(26) Applegate, M. B.; Partlow, B. P.; Coburn, J.; Marelli, B.; Pirie, C.; Pineda, R.; Kaplan, D. L.; Omenetto, F. G. Photocrosslinking of Silk Fibroin Using Riboflavin for Ocular Prostheses. *Adv. Mater.* **2016**, *28*, 2417−2420.
(27) Mitropoulos, A. N.; Marelli, B.; Ghezzi, C. E.; Applegate, M. B.; Partlow, B. P.; Kaplan, D. L.; Omenetto, F. G. Transparent, Nanostructured Silk Fibroin Hydrogels with Tunable Mechanical Properties. *ACS Biomater. Sci. Eng.* **2015**, *1*, 964−970.
(28) Shi, C.; Wang, J.; Sushko, M. L.; Qiu, W.; Yan, X.; Liu, X. Y. Silk Flexible Electronics: From Bombyx Mori Silk Ag Nanoclusters Hybrid Materials to Mesoscopic Memristors and Synaptic Emulators. *Adv. Funct. Mater.* **2019**, 1904777.
(29) Zhu, B.; Wang, H.; Leow, W. R.; Cai, Y.; Loh, X. J.; Han, M. Y.; Chen, X. Silk Fibroin for Flexible Electronic Devices. *Adv. Mater.* **2016**, *28*, 4250−4265.
(30) Wang, C.; Xia, K.; Zhang, Y.; Kaplan, D. L. Silk-Based Advanced Materials for Soft Electronics. *Acc. Chem. Res.* **2019**, 2916.
(31) Bucciarelli, A.; Pal, R. K.; Maniglio, D.; Quaranta, A.; Mulloni, V.; Motta, A.; Yadavalli, V. K. Fabrication of Nanoscale Patternable Films of Silk Fibroin Using Benign Solvents. *Macromol. Mater. Eng.* **2017**, *302*, 1−9.
(32) Bucciarelli, A.; Mulloni, V.; Maniglio, D.; Pal, R. K.; Yadavalli, V. K.; Motta, A.; Quaranta, A. A Comparative Study of the Refractive Index of Silk Protein Thin Films towards Biomaterial Based Optical Devices. *Opt. Mater. (Amst).* **2018**, *78*, 407−414.
(33) Tao, H.; Kainerstorfer, J. M.; Siebert, S. M.; Pritchard, E. M.; Sassaroli, A.; Panilaitis, B. J. B.; Brenckle, M. A.; Amsden, J. J.; Levitt, J.; Fantini, S.; Kaplan, D. L.; Omenetto, F. G. Implantable, Multifunctional, Bioresorbable Optics. *Proc. Natl. Acad. Sci. U. S. A.* **2012**, 19584.
(34) Applegate, M. B.; Perotto, G.; Kaplan, D. L.; Omenetto, F. G. Biocompatible Silk Step-Index Optical Waveguides. *Biomed. Opt. Express* **2015**, *6*, 4221.
(35) Rockwood, D. N.; Preda, R. C.; Yücel, T.; Wang, X.; Lovett, M. L.; Kaplan, D. L. Materials Fabrication from Bombyx Mori Silk Fibroin. *Nat. Protoc.* **2011**, *6*, 1612−1631.
(36) Kim, H. J.; Kim, M. K.; Lee, K. H.; Nho, S. K.; Han, M. S.; Um, I. C. Effect of Degumming Methods on Structural Characteristics and Properties of Regenerated Silk. *Int. J. Biol. Macromol.* **2017**, *104*, 294−302.
(37) Allardyce, B. J.; Rajkhowa, R.; Dilley, R. J.; Atlas, M. D.; Kaur, J.; Wang, X. The Impact of Degumming Conditions on the Properties of Silk Films for Biomedical Applications. *Text. Res. J.* **2016**, *86*, 275−287.
(38) Wang, Z.; Yang, H.; Li, W.; Li, C. Effect of Silk Degumming on the Structure and Properties of Silk Fibroin. *J. Text. Inst.* **2019**, *110*, 134−140.
(39) Reddy, N. New Developments in Degumming Silk. *Silk Mater. Process. Appl.* **2020**, 49−71.
(40) Wang, X. R.; Fan, P. K.; Zhang, Y. Application Performances of Gemini Surfactant as Silk Degumming Auxiliaries. *Adv. Mater. Res.* **2011**, *233-235*, 147−150.
(41) Freddi, G.; Allera, G.; Candiani, G. Degumming of Silk Fabrics with Tartaric Acid. *J. Soc. Dyers Colour.* **1996**, *112*, 191−195.
(42) Vyas, S. K.; Shukla, S. R. Degumming of Tasar Silk Using Imidazolium-Based Ionic Liquids. *J. Text. Inst.* **2020**, *111*, 1364−1370.
(43) Zhang, H.; Li, H.; Liu, H.; Lang, D. A.; Xu, H.; Zhu, H. Degumming Raw Silk by a Halotolerant Metalloprotease Isolated from Metabolites of Vibrio Sp. LA-05. *Int. Biodeterior. Biodegrad.* **2019**, *142*, 124−130.
(44) More, S. V.; Khandelwal, H. B.; Joseph, M. A.; Laxman, R. S. Enzymatic Degumming of Silk with Microbial Proteases. *J. Nat. Fibers* **2013**, *10*, 98−111.
(45) More, S. V.; Chavan, S.; Prabhune, A. A. Silk Degumming and Utilization of Silk Sericin by Hydrolysis Using Alkaline Protease from Beauveria Sp. (MTCC 5184): A Green Approach. *J. Nat. Fibers* **2018**, *15*, 373−383.
(46) Wang, W.; Pan, Y.; Gong, K.; Zhou, Q.; Zhang, T.; Li, Q. A Comparative Study of Ultrasonic Degumming of Silk Sericin Using Citric AcidSodium Carbonate and Papain. *Color. Technol.* **2019**, *135*, 195−201.
(47) Gulrajani, M. L.; Sinha, S. Studies in Degumming of Silk with Aliphatic Amines. *J. Soc. Dyers Colour.* **1993**, *109*, 256−260.
(48) Rastogi, S.; Kandasubramanian, B. Processing Trends of Silk Fibers: Silk Degumming, Regeneration and Physical Functionalization. *J. Text. Inst.* **2020**, *111*, 1794−1810.
(49) Wang, R.; Zhu, Y.; Shi, Z.; Jiang, W.; Liu, X.; Ni, Q. Q. Degumming of Raw Silk via Steam Treatment. *J. Cleaner Prod.* **2018**, *203*, 492−497.
(50) Wang, L.; Luo, Z.; Zhang, Q.; Guan, Y.; Cai, J.; You, R.; Li, X. Effect of Degumming Methods on the Degradation Behavior of Silk Fibroin Biomaterials. *Fibers Polym.* **2019**, *20*, 45−50.
(51) Nultsch, K.; Bast, L. K.; Näf, M.; El Yakhlfi, S.; Bruns, N.; Germershaus, O. Effects of Silk Degumming Process on Physicochemical, Tensile, and Optical Properties of Regenerated Silk Fibroin. *Macromol. Mater. Eng.* **2018**, *303*, 1−10.

(52) Pérez-Rigueiro, J.; Elices, M.; Llorca, J.; Viney, C. Effect of Degumming on the Tensile Properties of Silkworm (Bombyx Mori) Silk Fiber. *J. Appl. Polym. Sci.* **2002**, *84*, 1431−1437.
(53) Zhang, H.; Li, L. L.; Dai, F. Y.; Zhang, H. H.; Ni, B.; Zhou, W.; Wu, Z. Preparation and Characterization of Silk Fibroin as a Biomaterial with Potential for Drug Delivery. *J. Transl. Med.* **2012**, *10*, 1−9.
(54) Partlow, B. P.; Tabatabai, A. P.; Leisk, G. G.; Cebe, P.; Blair, D. L.; Kaplan, D. L. Silk Fibroin Degradation Related to Rheological and Mechanical Properties. *Macromol. Biosci.* **2016**, *16*, 666−675.
(55) Wang, H.-Y.; Zhang, Y.-Q. Effect of Regeneration of Liquid Silk Fibroin on Its Structure and Characterization. *Soft Matter* **2013**, *9*, 138−145.
(56) Rnjak-Kovacina, J.; Wray, L. S.; Burke, K. A.; Torregrosa, T.; Golinski, J. M.; Huang, W.; Kaplan, D. L. Lyophilized Silk Sponges: A Versatile Biomaterial Platform for Soft Tissue Engineering. *ACS Biomater. Sci. Eng.* **2015**, 260.
(57) Yao, Y.; Allardyce, B. J.; Rajkhowa, R.; Hegh, D.; Sutti, A.; Subianto, S.; Gupta, S.; Rana, S.; Greenhill, S.; Venkatesh, S.; Wang, X.; Razal, J. M. Improving the Tensile Properties of Wet Spun Silk Fibers Using Rapid Bayesian Algorithm. *ACS Biomater. Sci. Eng.* **2020**, *6*, 3197−3207.
(58) Pham, D. T.; Saelim, N.; Tiyaboonchai, W. Design of Experiments Model for the Optimization of Silk Fibroin Based Nanoparticles. *Int. J. Appl. Pharm* **2018**, *10*, 195.
(59) Perucca Orfei, C.; Talò, G.; Viganò, M.; Perteghella, S.; Lugano, G.; Fabro Fontana, F.; Ragni, E.; Colombini, A.; De Luca, P.; Moretti, M.; Torre, M.; de Girolamo, L. Silk/Fibroin Microcarriers for Mesenchymal Stem Cell Delivery: Optimization of Cell Seeding by the Design of Experiment. *Pharmaceutics* **2018**, *10*, 200.
(60) Bucciarelli, A.; Muthukumar, T.; Kim, J. S.; Kim, W. K.; Quaranta, A.; Maniglio, D.; Khang, G.; Motta, A. Preparation and Statistical Characterization of Tunable Porous Sponge Scaffolds Using UV Cross-Linking of Methacrylate-Modified Silk Fibroin. *ACS Biomater. Sci. Eng.* **2019**, 6374.
(61) Bucciarelli, A.; Chiera, S.; Quaranta, A.; Yadavalli, V. K.; Motta, A.; Maniglio, D. A Thermal-Reflow-Based Low-Temperature, High-Pressure Sintering of Lyophilized Silk Fibroin for the Fast Fabrication of Biosubstrates. *Adv. Funct. Mater.* **2019**, *29*, 1901134.
(62) Montgomery, D. C. *Design and Analysis of Experiments*; Eighth Ed.; Wiley: 2012.
(63) Bucciarelli, A.; Reddy Chandraiahgari, C.; Adami, A.; Mulloni, V.; Lorenzelli, L. Precise Dot Inkjet Printing Thought Multifactorial Statistical Optimization of the Piezoelectric Actuator Waveform. *Flex. Print. Electron.* **2020**, *5*, No. 045002.
(64) Bucciarelli, A.; Adami, A.; Chandaiahgari, C. R.; Lorenzelli, L. Multivariable Optimization of Inkjet Printing Process of Ag Nanoparticle Ink on Kapton. In *2020 IEEE International Conference on Flexible and Printable Sensors and Systems (FLEPS)*; IEEE: 2020; pp. 1−4, DOI: 10.1109/FLEPS49123.2020.9239474.
(65) Gaiardo, A.; Novel, D.; Scattolo, E.; Crivellari, M.; Picciotto, A.; Ficorella, F.; Iacob, E.; Bucciarelli, A.; Petti, L.; Lugli, P.; Bagolini, A. Optimization of a Low-Power Chemoresistive Gas Sensor: Predictive Thermal Modelling and Mechanical Failure Analysis. *Sensors* **2021**, *21*, 783.
(66) Jeong, I. J.; Kim, K. J. An Interactive Desirability Function Method to Multiresponse Optimization. *Eur. J. Oper. Res.* **2009**, 412.
(67) Ardakani, M. K.; Wulff, S. S. An Overview of Optimization Formulations for Multiresponse Surface Problems. *Qual. Reliab. Eng. Int.* **2013**, 3.
(68) Aznar-Cervantes, S. D.; Pagan, A.; Monteagudo Santesteban, B.; Cenis, J. L. Effect of Different Cocoon Stifling Methods on the Properties of Silk Fibroin Biomaterials. *Sci. Rep.* **2019**, *9*, 1−11.
(69) Blackledge, T. A. Quasistatic and Continuous Dynamic Characterization of the Mechanical Properties of Silk from the Cobweb of the Black Widow Spider Latrodectus Hesperus. *J. Exp. Biol.* **2005**, *208*, 1937−1949.
(70) Schneider, C. A.; Rasband, W. S.; Elceiri, K. W. NIH Image to ImageJ: 25 Years of Image Analysis. *Nat. Methods* **2012**, *9*, 671−675.
(71) Blackledge, T. A.; Cardullo, R. A.; Hayashi, C. Y. Polarized Light Microscopy, Variability in Spider Silk Diameters, and the Mechanical Characterization of Spider Silk. *Invertebr. Biol.* **2005**, *124*, 165−173.
(72) Greco, G.; Pantano, M. F.; Mazzolai, B.; Pugno, N. M. Imaging and Mechanical Characterization of Different Junctions in Spider Orb Webs. *Sci. Rep.* **2019**, *9*, 5776.
(73) Pasquet, A.; Toscani, C.; Anotaux, M. Influence of Aging on Brain and Web Characteristics of an Orb Web Spider. *J. Ethol.* **2018**, *36*, 85−91.
(74) Work, R.; Dimensions, W. Birefringences, and Force-Elongation Behavior of Major and Minor Ampullate Silk Fibers from Orb-Web-Spinning Spiders—The Effects of Wetting on These Properties. *Text. Res. J.* **1977**, *47*, 650−662.
(75) Edmonds, D. T.; Vollrath, F. The Contribution of Atmospheric Water Vapour to the Formation and Efficiency of a Spider's Capture Web. *Proc. R. Soc. B Biol. Sci.* **1992**, *248*, 145−148.
(76) Motta, A.; Fambri, L.; Migliaresi, C. Regenerated Silk Fibroin Films: Thermal and Dynamic Mechanical Analysis. *Macromol. Chem. Phys.* **2002**, *203*, 1658e−1665e.
(77) Sashina, E. S.; Bochek, A. M.; Novoselov, N. P.; Kirichenko, D. A. Structure and Solubility of Natural Silk Fibroin. *Russ. J. Appl. Chem. Khimii* **2006**, *79*, 1070−1876.
(78) Inoue, S.; Tanaka, K.; Arisaka, F.; Kimura, S.; Ohtomo, K.; Mizuno, S. Silk Fibroin of Bombyx Mori Is Secreted, Assembling a High Molecular Mass Elementary Unit Consisting of H-Chain, L-Chain, and P25, with a 6:6:1 Molar Ratio. *J. Biol. Chem.* **2000**, *275*, 40517−40528.
(79) Nultsch, K.; Germershaus, O. Silk Fibroin Degumming Affects Scaffold Structure and Release of Macromolecular Drugs. *Eur. J. Pharm. Sci.* **2017**, *106*, 254−261.
(80) Dou, H.; Zuo, B. Effect of Sodium Carbonate Concentrations on the Degumming and Regeneration Process of Silk Fibroin. *J. Text. Inst.* **2015**, *106*, 311−319.
(81) Wray, L. S.; Hu, X.; Gallego, J.; Georgakoudi, I.; Omenetto, F. G.; Schmidt, D.; Kaplan, D. L. Effect of Processing on Silk-Based Biomaterials: Reproducibility and Biocompatibility. *J. Biomed. Mater. Res., Part B* **2011**, *99B*, 89−101.
(82) Gulrajani, M. L. Degumming of Silk. *Rev. Prog. Color. Relat. Top.* **1992**, *22*, 79−89.
(83) Rajkhowa, R.; Wang, L.; Kanwar, J. R.; Wang, X. Molecular Weight and Secondary Structure Change in Eri Silk during Alkali Degumming and Powdering. *J. Appl. Polym. Sci.* **2011**, 1339.
(84) Shrivastava, A. Polymerization. In *Introduction to Plastics Engineering*; Plastics Design Library; William Andrew Publishing: 2018; pp. 17−48, DOI: 10.1016/B978-0-323-39500-7.00002-2.
(85) Chen, S.; Liu, M.; Huang, H.; Cheng, L.; Zhao, H. P. Mechanical Properties of Bombyx Mori Silkworm Silk Fibre and Its Corresponding Silk Fibroin Filament: A Comparative Study. *Mater. Des.* **2019**, *181*, 108077.
(86) Yang, Y.; Greco, G.; Maniglio, D.; Mazzolai, B.; Migliaresi, C.; Pugno, N.; Motta, A. Spider (Linothele Megatheloides) and Silkworm (Bombyx Mori) Silks: Comparative Physical and Biological Evaluation. *Mater. Sci. Eng. C* **2020**, 110197.
(87) Thurner, S.; Klimek, P.; Hanel, R. *Introduction to the Theory of Complex Systems*; Oxford University Press: 2018; Vol. *1*, DOI: 10.1093/oso/9780198821939.001.0001.

A design of experiment rational optimization of the degumming process and its impact on the silk fibroin properties.

Alessio Bucciarelli[1*], Gabriele Greco[4], Ilaria Corridori[4], Nicola M. Pugno[4,5], Antonella Motta[2,3]

[1]Microsystem Technology Group, Center for materials and microsystems, Fondazione Bruno Kessler, Via Sommarive 9, 38123 Trento (TN), Italy

[2] Department of Industrial Engieneering, University of Trento, via Delle Regole 101, Trento 38123, Italy

[3]BIOTech Research Center and European Institute of Excellence on Tissue Engineering and Regenerative Medicine, Via delle Regole 101, Trento 38123, Italy

[4]Laboratory of Bio-inspired, Bionic, Nano, Meta Materials and Mechanics, Department of Civil, Environmental and Mechanical Engineering, University of Trento, Via Mesiano 77, 38123 Trento (TN), Italy

[5]School of Engineering and Materials Science, Queen Mary University of London, Mile End Road, E14NS London, United Kingdom

Calibration Curves

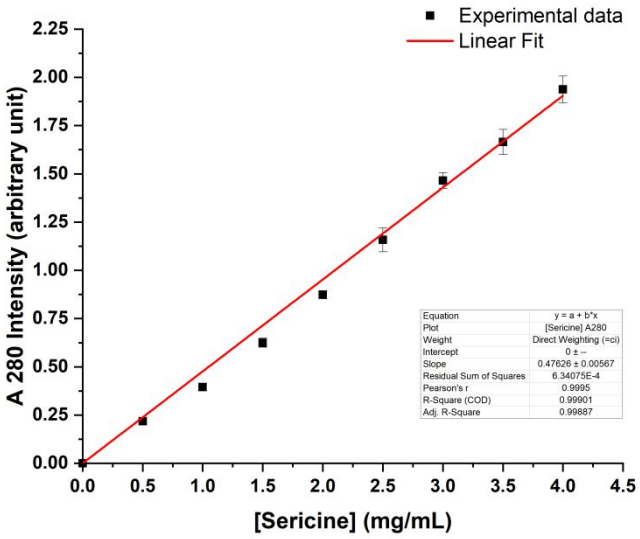

Figure S 1: Calibration curve used to determine the concentration of sericin in the degumming baths. The curve was prepared by standard solutions with a known concentration of sericin versus the intensity at 280 nm of their UV/VIS spectra. This curve was used to determine the unknown concentration of sericin the degumming bath by evaluating the UV intensity at 280 nm and interpolating the corresponding sericin concentration.

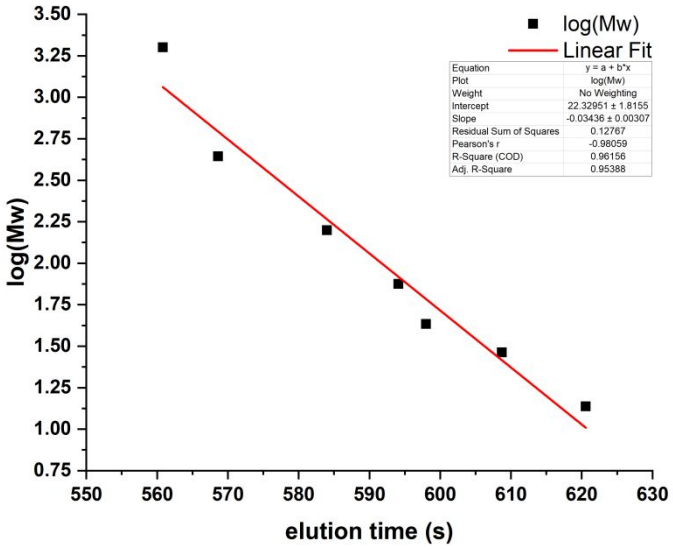

Figure S 2: Calibration curve of the molecular weight analysis conducted by Gel Permeation Chromatography (GPC). The curve was produced by using reference proteins with a known molecular weight.

FTIR Assignment

Assignment	Peak position cm^{-1}	Reference
Side chain	1597-1609	[1–4]
Antiparallel β – sheet	1610-1625	[1–3,5–12]
Native β – sheet	1626-1636	[1,4,6–11]
Random coil	1637-1655	[1,4,6,10,12,13]
α – helix	1656-1662	[1,4,6,10]
B – turns	1663-1696	[1,3,5,6,10,11,14]
Parallel β – sheet	1697-1703	[1,10,11,15]

Table S 1: Peaks position for the assignment of the peaks after the Self-Fourier Deconvolution of the I Amide peak in the FTIR structural analysis. When the peak center is inside the bandwidth of a specific structure, that structure is assigned to the peak.

Weight Loss

Source	Sum of Squares	df	Mean Square	F-value	p-value	
Model	3760.21	11	341.84	53.73	< 0.0001	significant
A-Number of baths	86.70	1	86.70	13.63	0.0007	***
B-Time	126.23	1	126.23	19.84	< 0.0001	***
C-Temperature	1411.00	1	1411.00	221.79	< 0.0001	***
D-Concentration	1575.78	1	1575.78	247.70	< 0.0001	***
AC	4.65	1	4.65	0.7309	0.3982	
AD	0.0079	1	0.0079	0.0012	0.9721	
BC	0.0395	1	0.0395	0.0062	0.9377	
BD	2.01	1	2.01	0.3152	0.5780	
CD	402.11	1	402.11	63.21	< 0.0001	***
ACD	26.34	1	26.34	4.14	0.0493	*
BCD	125.34	1	125.34	19.70	< 0.0001	***
Residual	229.02	36	6.36			
Lack of Fit	12.69	4	3.17	0.4694	0.7577	not significant
Pure Error	216.33	32	6.76			
Cor Total	3989.23	47				

Table S 2: ANOVA table for the model of the weight loss. The significance level was assigned as follow: p≤0.1 (.), p≤0.05 (*), p≤0.01 (**), p≤0.001 (***). All the first order terms, and several second and third order terms resulted to be significant. In order of importance the significant terms were: A, B, C, D, CD, BCD and ACD. It should be noticed that all the other terms were insert in the model to maintain the overall hierarchy.

Factor	Model coefficients	95% CI Low	95% CI High
Intercept	18.16	17.42	18.90
A-Number of baths	1.34	0.6056	2.08
B-Time	1.62	0.8834	2.36
C-Temperature	5.42	4.68	6.16
D-Concentration	5.73	4.99	6.47
AC	-0.3113	-1.05	0.4271
AD	0.0128	-0.7255	0.7512
BC	0.0287	-0.7097	0.7670
BD	0.2044	-0.5339	0.9427
CD	-2.89	-3.63	-2.16
ACD	-0.7408	-1.48	-0.0025
BCD	-1.62	-2.35	-0.8776
Transformation	None		

Table S 3: Coefficients of the coded equations of the weight loss model and of the 95% confidence intervals. In this case the factors are normalized in the range [-1,1] to allow a direct comparison between the coefficients of the different terms. No transforming function was applied to the data.

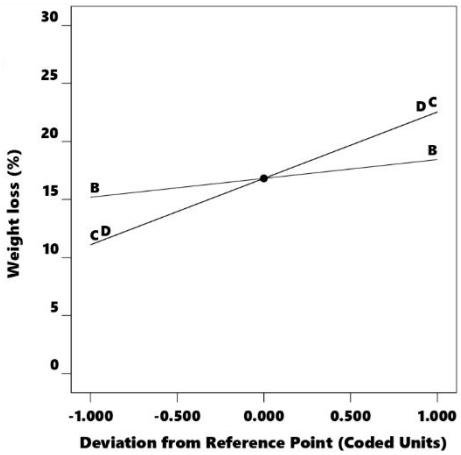

Figure S 3: Perturbation graph in coded terms of the weight loss. The variation of the terms D and C have a greater impact in terms of variation in the weight loss respect to a variation of the term B. In term of robustness, we can state that the process is more robust to a variation of B if compared to the other terms.

Removed Sericin

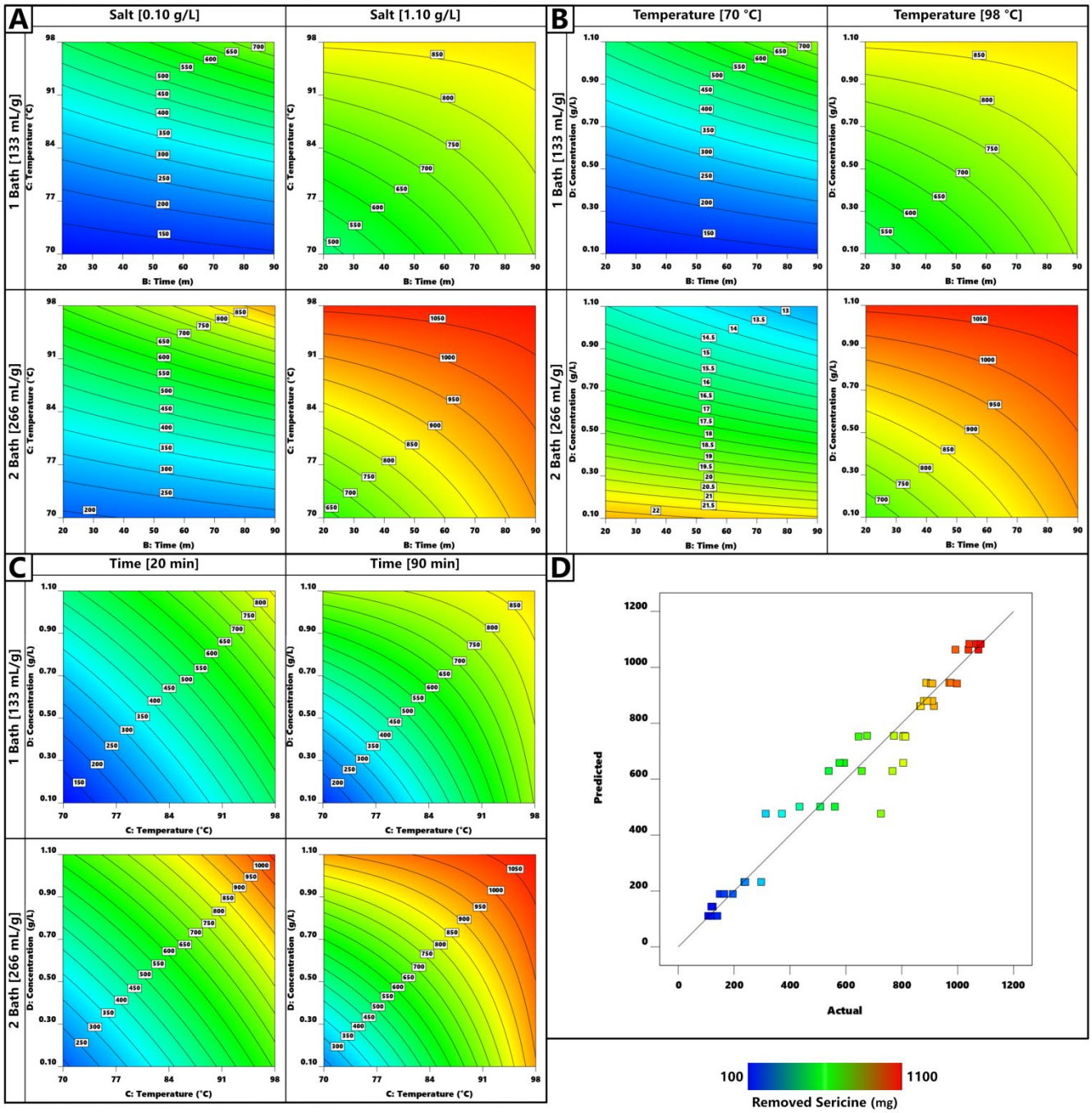

Figure S 4: Contour plots of the modelled amount of removed sericine (sericine present in the degumming bath). Due to the significance of all factors the model is 4 dimensional, so the contour plots are reported as follow: (A)removed sericine vs temperature and time, (B)removed sericine vs salt concentration and time, and (C) removed sericine vs salt concentration and temperature. In all these cases the number of baths is reported as an ordinal, and the missing variable in its extreme values. The actual versus predicted plot (D) shows that the model seems to fit better the data collected for the not successful degumming (in which there was only a small removal of the sericine) and the successful degumming (with a large amount or sericine solubilized) the data in between results to be scattered around the diagonal.

Source	Sum of Squares	df	Mean Square	F-value	p-value	
Model	2556.45	8	319.56	120.56	< 0.0001	significant
A-Number of baths	127.76	1	127.76	48.20	< 0.0001	***
B-Time	117.23	1	117.23	44.23	< 0.0001	***
C-Temperature	1040.66	1	1040.66	392.61	< 0.0001	***
D-Concentration	973.49	1	973.49	367.27	< 0.0001	***
BC	2.15	1	2.15	0.8098	0.3737	
BD	0.3131	1	0.3131	0.1181	0.7329	
CD	235.29	1	235.29	88.77	< 0.0001	***
BCD	59.56	1	59.56	22.47	< 0.0001	***
Residual	103.37	39	2.65			
Lack of Fit	10.10	7	1.44	0.4949	0.8312	not significant
Pure Error	93.28	32	2.91			
Cor Total	2659.82	47				

Table S 4: ANOVA table for the model of the removed sericine. The significance level was assigned as follow: p≤0.1 (.), p≤0.05 (*), p≤0.01 (**), p≤0.001 (***). All the first order terms, and several second and third order terms resulted to be significant. In order of importance the significant terms were: A, B, C, D, CD, BCD, all the other terms were insert in the model to maintain the overall hierarchy. As could be expected, the significant terms are the same found in the analysis of the weight loss if we exclude the term ACD that in this case is not significant and in the previous one was slightly significant. This result confirms the correctness of the weight loss model.

Factor	Model coefficients	95% CI Low	95% CI High
Intercept	24.15	23.67	24.62
A-Number of baths	1.63	1.16	2.11
B-Time	1.56	1.09	2.04
C-Temperature	4.66	4.18	5.13
D-Concentration	4.50	4.03	4.98
BC	-0.2115	-0.6868	0.2638
BD	-0.0808	-0.5561	0.3945
CD	-2.21	-2.69	-1.74
BCD	-1.11	-1.59	-0.6387
Transformation	Square root		

Table S 5: Coefficients of the coded equations of the removed sericine model and of the 95% confidence intervals. In this case the factors are normalized in the range [-1,1] to allow a direct comparison between the coefficients of the different terms. In this case the square root function was applied to the data in order to make the residues normal distributed.

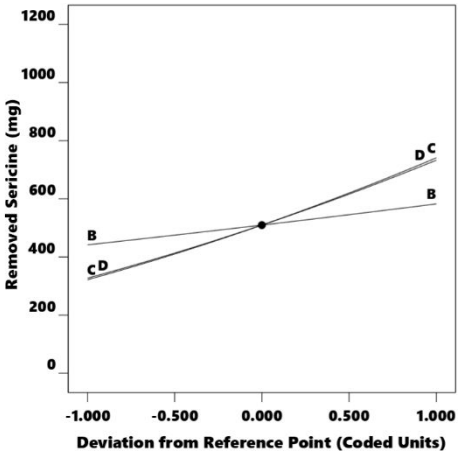

Figure S 5: Perturbation graph in coded terms of the removed sericine. As in the case of the weight loss the variation of the terms D and C have a greater impact in terms of sericine removal respect to a variation of the term B. In term of robustness, we can state that the process is more robust to a variation of B if compared to the other terms.

Fibers diameter

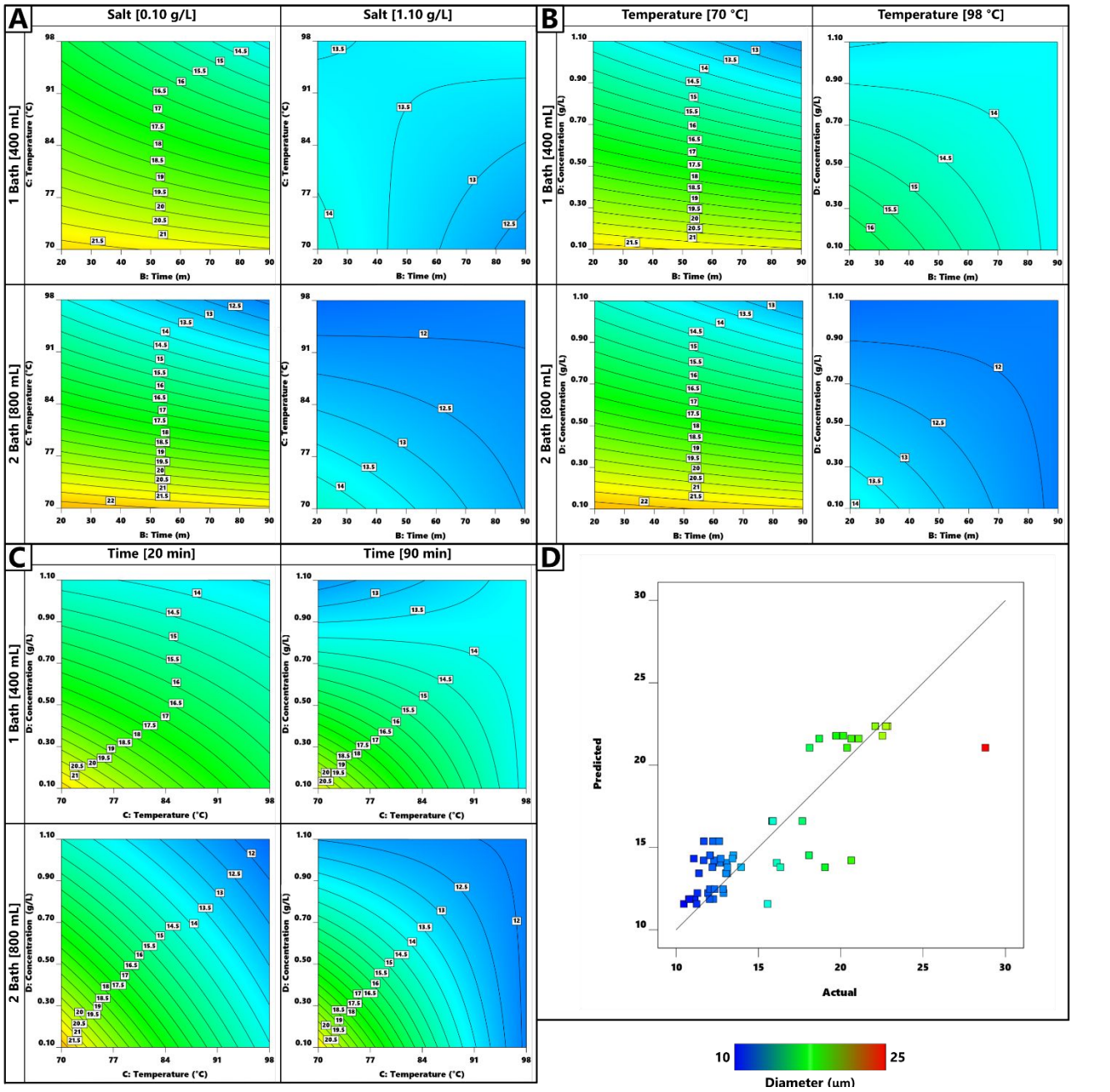

Figure S 6: Contour plots of the modelled fiber diameter (sericine present in the degumming bath). Due to the significance of all factors the model is 4 dimensional, so the contour plots are reported as follow: (A) diameter vs temperature and time, (B) diameter vs salt concentration and time, and (C) diameter vs salt concentration and temperature. In all these cases the number of baths is reported as an ordinal, and the missing variable in its extreme values. The actual versus predicted plot (D) shows that the model seems to fit better the data collected for the successful degumming in which the diameter resulted to be lower.

Source	Sum of Squares	df	Mean Square	F-value	p-value	
Model	0.0100	9	0.0011	12.90	< 0.0001	significant
A-Number of baths	0.0003	1	0.0003	3.79	0.0582	.
B-Time	0.0004	1	0.0004	4.82	0.0335	*
C-Temperature	0.0027	1	0.0027	31.56	< 0.0001	***
D-Concentration	0.0041	1	0.0041	47.95	< 0.0001	***
AC	0.0005	1	0.0005	6.23	0.0165	*
BC	1.363E-06	1	1.363E-06	0.0159	0.9003	
BD	0.0000	1	0.0000	0.2823	0.5979	
CD	0.0014	1	0.0014	16.68	0.0002	***
BCD	0.0004	1	0.0004	4.80	0.0340	*
Residual	0.0037	43	0.0001			
Lack of Fit	0.0003	7	0.0000	0.5191	0.8141	not significant
Pure Error	0.0034	36	0.0001			
Cor Total	0.0145	53				

Table S 6: ANOVA table for the model of the fiber diameter. The significance level was assigned as follow: p≤0.1 (.), p≤0.05 (*), p≤0.01 (**), p≤0.001 (***). All the first order terms, and several second and third order terms resulted to be significant. In order of importance the significant terms were: B, C, D, CD, BCD, all the other terms were insert in the model to maintain the overall hierarchy. As could be expected, the significant terms are the same found in the analysis of the weight loss and the removed sericine if we exclude the term A (present in both the others model) and ACD (only present in the weight loss model). This result confirms the correctness of the previous two models.

Factor	Model coefficients	95% CI Low	95% CI High
Intercept	0.0694	0.0667	0.0721
A-Number of baths	0.0025	-0.0001	0.0050
B-Time	0.0029	0.0002	0.0056
C-Temperature	0.0075	0.0048	0.0102
D-Concentration	0.0093	0.0066	0.0120
AC	0.0033	0.0006	0.0060
BC	-0.0002	-0.0029	0.0025
BD	-0.0007	-0.0034	0.0020
CD	-0.0055	-0.0082	-0.0028
BCD	-0.0029	-0.0056	-0.0002
Transformation	Inverse		

Table S 7: Coefficients of the coded equations of the fiber diameter model and of the 95% confidence intervals. In this case the factors are normalized in the range [-1,1] to allow a direct comparison between the coefficients of the different terms. In this case the inverse transformation was applied to the data in order to make the residues normal distributed.

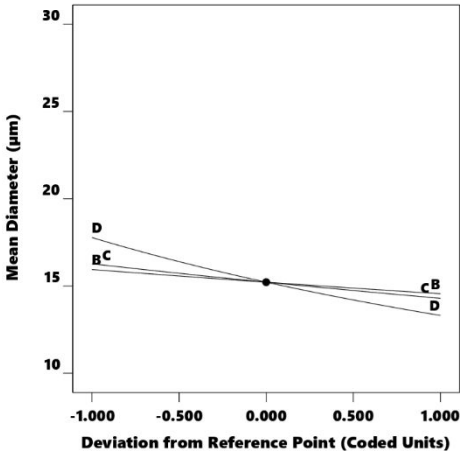

Figure S 7: Perturbation graph in coded terms of the removed sericine. As in the case of the weight loss and sericin removal the variation of the terms D and C have a greater impact in terms of diameter variation respect to a variation of the term B. In term of robustness, we can state that the process is more robust to a variation of B if compared to the other terms.

Secondary structure

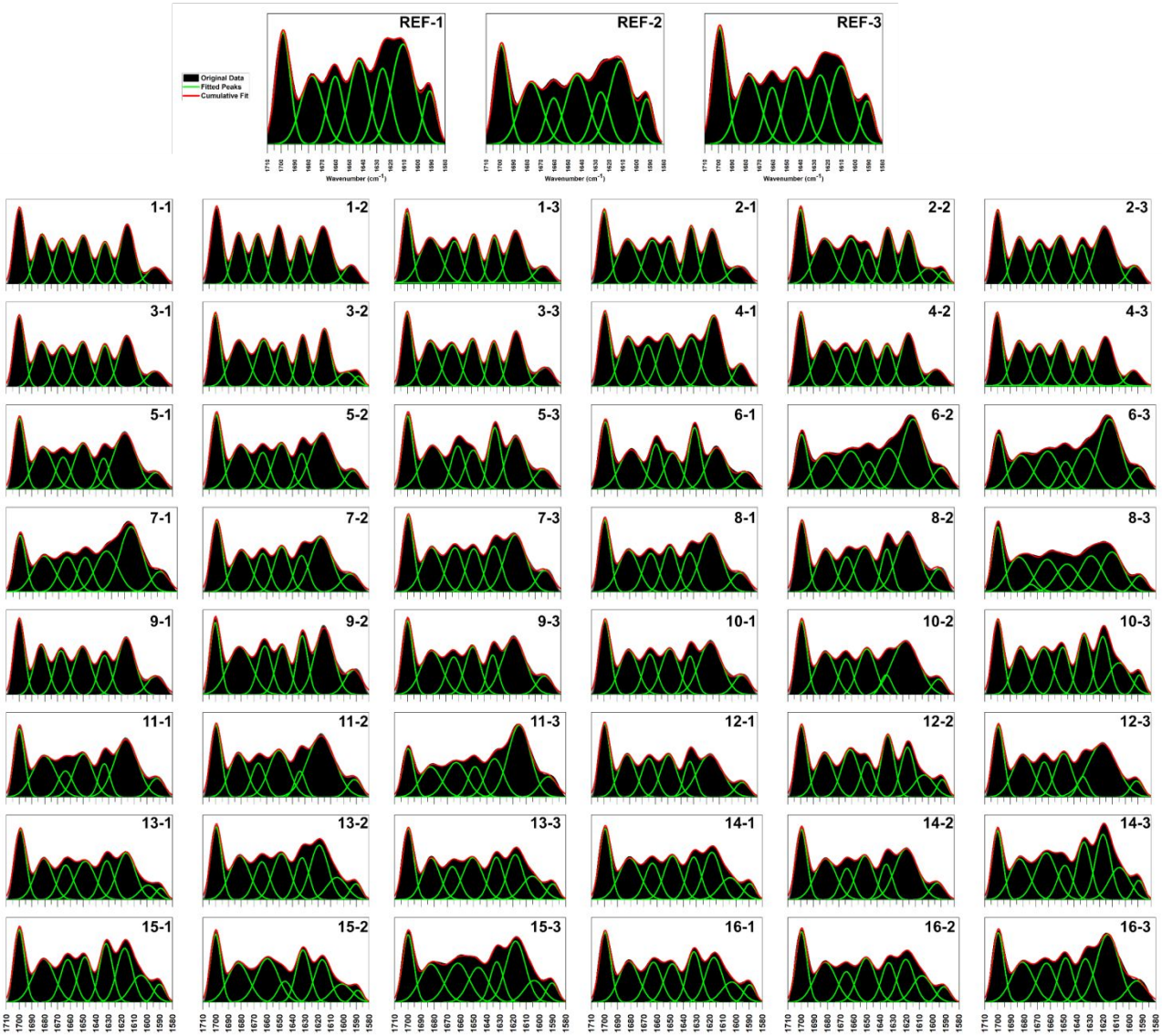

Figure S 8: Deconvolution and peak fitting of the 48 samples (3 trial for each of the 16 degumming procedure) and the three replicates of the reference procedure. The Amide I peak (1710-1580 cm^{-1}) was deconvolved by a Fourier Self -Deconvolution (FSD) the peaks were then identified by the second derivative. For each peak a secondary structure was assigned based on the assignment table (Table 4) and finally fitted with a Gaussian function. The area under each peak was taken as a measure of the amount of the specific secondary structure. It should be noticed that we didn't make any assumption in the number and position of the peaks before the deconvolution, and we always found 7 peaks for each sample, proving the robustness of this method.

Source	Sum of Squares	df	Mean Square	F-value	p-value	
Model	150.55	9	16.73	3.29	0.0047	significant
A-Number of baths	0.3385	1	0.3385	0.0666	0.7978	
B-Time	0.1983	1	0.1983	0.0390	0.8445	
C-Temperature	9.86	1	9.86	1.94	0.1719	
D-Concentration	17.86	1	17.86	3.51	0.0686	.
AB	0.0268	1	0.0268	0.0053	0.9425	
AD	5.55	1	5.55	1.09	0.3030	
BD	8.20	1	8.20	1.61	0.2117	
CD	84.52	1	84.52	16.62	0.0002	***
ABD	23.99	1	23.99	4.72	0.0362	*
Residual	193.24	38	5.09			
Lack of Fit	30.48	6	5.08	0.9987	0.4432	not significant
Pure Error	162.76	32	5.09			
Cor Total	343.79	47				

Table S 8: ANOVA table for the model of the β structure percentage. The significance level was assigned as follow: p≤0.1 (.), p≤0.05 (*), p≤0.01 (**), p≤0.001 (***). Only one first order term, and one second and one third order terms resulted to be significant. In order of importance the significant terms were: CD, ABD and D, all the other terms were insert in the model to maintain the overall hierarchy. Interestingly the amount of β-structures resulted to be mainly influenced by "high-order" terms that cannot be properly studied by the one-factor-at-time method.

Factor	Model coefficient	95% CI Low	95% CI High
Intercept	52.73	52.07	53.39
A-Number of baths	-0.0840	-0.7429	0.5749
B-Time	0.0643	-0.5946	0.7232
C-Temperature	0.4532	-0.2057	1.11
D-Concentration	-0.6100	-1.27	0.0489
AB	-0.0236	-0.6825	0.6353
AD	0.3399	-0.3190	0.9988
BD	0.4134	-0.2455	1.07
CD	-1.33	-1.99	-0.6680
ABD	-0.7070	-1.37	-0.0481
Transformation	none		

Table S 9: Coefficients of the coded equations of the percentage of β structures model and of the 95% confidence intervals. The factors are normalized in the range [-1,1] to allow a direct comparison between the coefficients of the different terms. In this case no transformation to the data was applied.

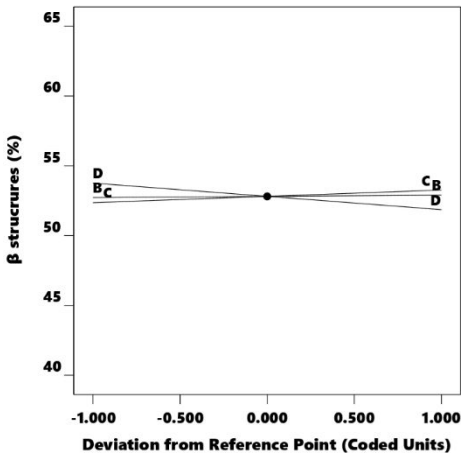

Figure S 9: Perturbation graph in coded terms of the percentage amount of β structures. The variation of the terms D and C have a greater impact in terms of amount of β structures respect to a variation of the term B. In term of robustness, we can state that the process is more robust to a variation of B if compared to the other terms, even though only a slight there is only a slight difference between the three terms.

Weight average molecular weight (M_w)

Source	Sum of Squares	df	Mean Square	F-value	p-value	
Model	0.0000	9	3.399E-06	40.61	0.0001	significant
A-Number of baths	2.300E-06	1	2.300E-06	27.48	0.0019	**
B-Time	3.690E-06	1	3.690E-06	44.09	0.0006	***
C-Temperature	0.0000	1	0.0000	134.74	< 0.0001	***
D-Concentration	7.338E-06	1	7.338E-06	87.67	< 0.0001	***
AB	2.234E-06	1	2.234E-06	26.69	0.0021	**
AC	8.209E-08	1	8.209E-08	0.9808	0.3603	
AD	7.939E-08	1	7.939E-08	0.9486	0.3677	
CD	2.799E-06	1	2.799E-06	33.44	0.0012	**
ACD	7.878E-07	1	7.878E-07	9.41	0.0220	*
Residual	5.022E-07	6	8.370E-08			
Cor Total	0.0000	15				

Table S 10: ANOVA table for the model of M_w. The significance level was assigned as follow: p≤0.1 (.), p≤0.05 (*), p≤0.01 (**), p≤0.001 (***).All the first order terms were significant , as well as two second order terms and the one third order term. In order of importance the significant terms were: C, D, B, A, CD, AB and ACD, all the other terms were insert in the model to maintain the overall hierarchy. As can be clearly observed M_w is influenced by several factors and several mixed terms, difficult to observe with other methodologies.

Factor	Coefficient Estimate	95% CI Low	95% CI High
Intercept	0.0044	0.0043	0.0046
A-Number of baths	0.0004	0.0002	0.0006
B-Time	0.0005	0.0003	0.0007
C-Temperature	0.0008	0.0007	0.0010
D-Concentration	0.0007	0.0005	0.0009
AB	0.0004	0.0002	0.0006
AC	0.0001	-0.0001	0.0002
AD	-0.0001	-0.0002	0.0001
CD	-0.0004	-0.0006	-0.0002
ACD	0.0002	0.0000	0.0004
Transformation	Inverse		

Table S 11: Coefficients of the coded equations of the M_w model and of the 95% confidence intervals. The factors are normalized in the range [-1,1] to allow a direct comparison between the coefficients of the different terms. In this case no transformation to the data was applied.

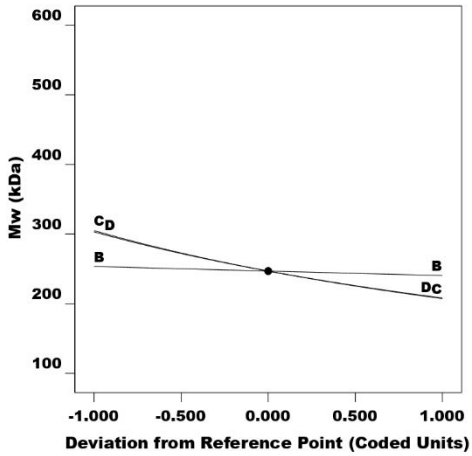

Figure S 10: Perturbation graph in coded terms of M_w. The variation of the terms D and C have a greater impact respect to a variation of the term B. In term of robustness, we can state that the process is more robust to a variation of B if compared to the other terms, even though only a slight there is only a slight difference between the three terms.

Number average molecular weight (Mn)

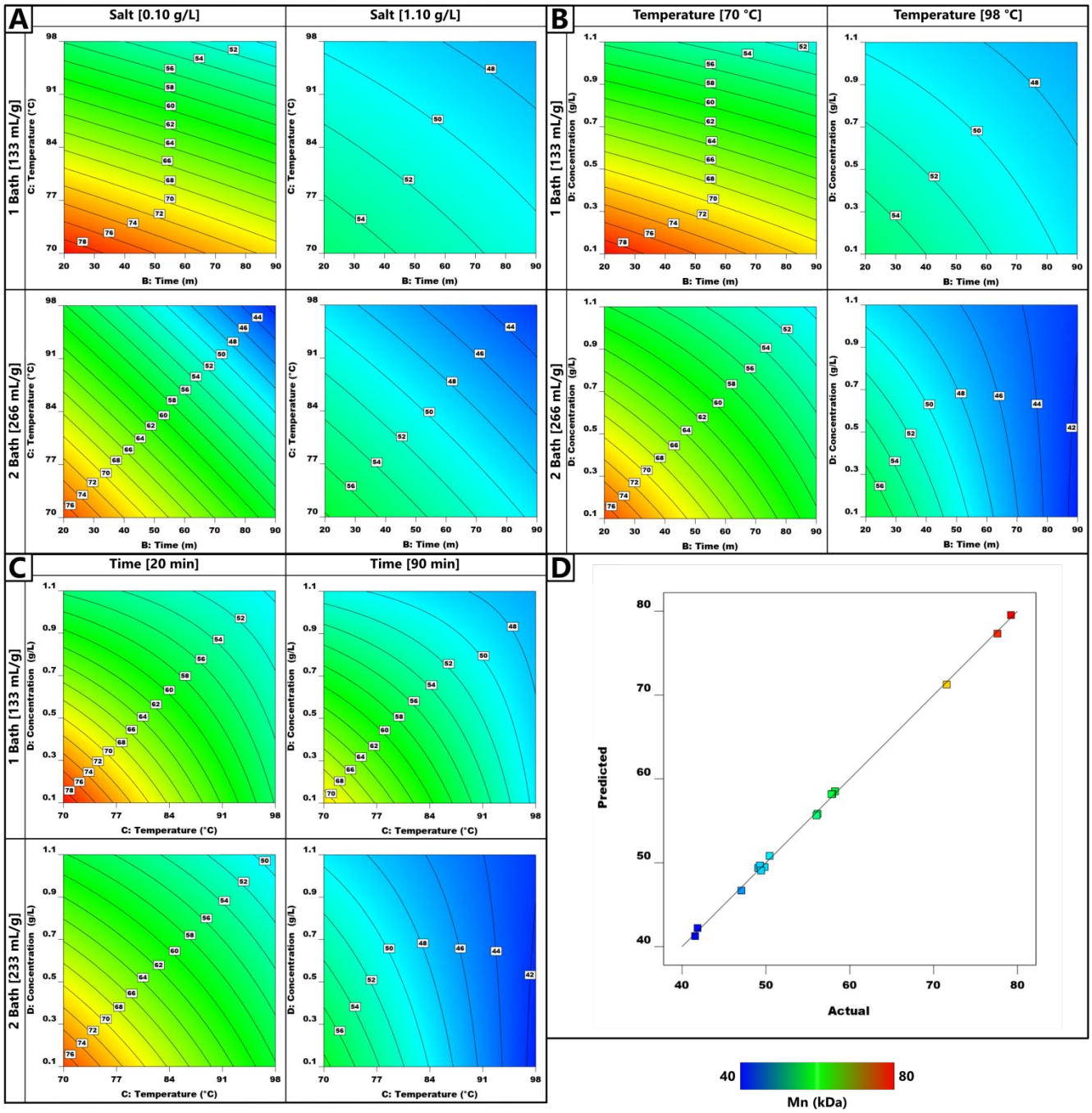

Figure S 11: Contour plots of the modelled M_n. Due to the significance of all factors the model is 4 dimensional, so the contour plots are reported as follow: (A) M_n vs temperature and time, (B) M_n vs salt concentration and time, and (C) M_n vs salt concentration and temperature. In all these cases the number of baths is reported as an ordinal, and the missing variable in its extreme values. The actual versus predicted plot (D) shows that the model accurately fit the experimental data.

Source	Sum of Squares	df	Mean Square	F-value	p-value	
Model	1952.77	12	162.73	264.65	0.0003	significant
A-Number of baths	37.76	1	37.76	61.41	0.0043	**
B-Time	340.82	1	340.82	554.27	0.0002	***
C-Temperature	735.00	1	735.00	1195.33	< 0.0001	***
D-Concentration	501.79	1	501.79	816.07	< 0.0001	***
AB	51.61	1	51.61	83.93	0.0027	**
AC	0.5230	1	0.5230	0.8505	0.4244	
AD	17.67	1	17.67	28.74	0.0127	*
BC	3.38	1	3.38	5.49	0.1009	
BD	46.08	1	46.08	74.94	0.0032	**
CD	192.26	1	192.26	312.68	0.0004	***
ABD	10.97	1	10.97	17.84	0.0243	*
ACD	14.91	1	14.91	24.25	0.0161	**
Residual	1.84	3	0.6149			
Cor Total	1954.61	15				

Table S 12: ANOVA table for the model of M_n. The significance level was assigned as follow: p≤0.1 (.), p≤0.05 (*), p≤0.01 (**), p≤0.001 (***).All the first order terms were significant , as well as four second order terms and the two third order term. In order of importance the significant terms were: C, D, B, CD, AB, BD, A, ACD, AD and ABD all the other terms were insert in the model to maintain the overall hierarchy. M_n is influenced by several factors and several mixed terms, difficult to observe with other methodologies.

Factor	Coefficient Estimate	95% CI Low	95% CI High
Intercept	55.82	55.20	56.44
A-Number of baths	-1.54	-2.16	-0.9123
B-Time	-4.62	-5.24	-3.99
C-Temperature	-6.78	-7.40	-6.15
D-Concentration	-5.60	-6.22	-4.98
AB	-1.80	-2.42	-1.17
AC	0.1808	-0.4431	0.8047
AD	1.05	0.4271	1.67
BC	0.4594	-0.1644	1.08
BD	1.70	1.07	2.32
CD	3.47	2.84	4.09
ABD	0.8280	0.2042	1.45
ACD	-0.9653	-1.59	-0.3414
Transformation	None		

Table S 13: Coefficients of the coded equations of the M_n model and of the 95% confidence intervals. The factors are normalized in the range [-1,1] to allow a direct comparison between the coefficients of the different terms. In this case no transformation to the data was applied.

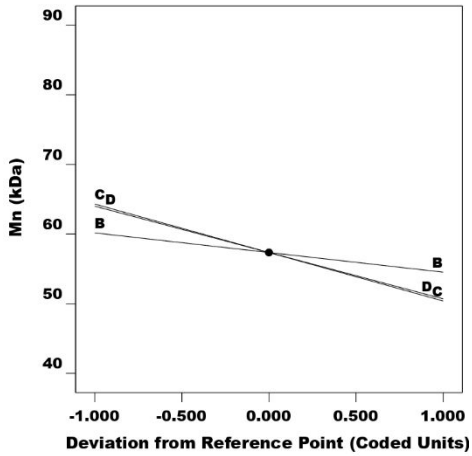

Figure S 12: Perturbation graph in coded terms of M_n. As could be expected this graph follows the trend of M_w, the variation of the terms D and C have a greater impact respect to a variation of the term B. In term of robustness, we can state that the process is more robust to a variation of B if compared to the other terms, even though only a slight there is only a slight difference between the three terms.

Peak molecular weight (M_p)

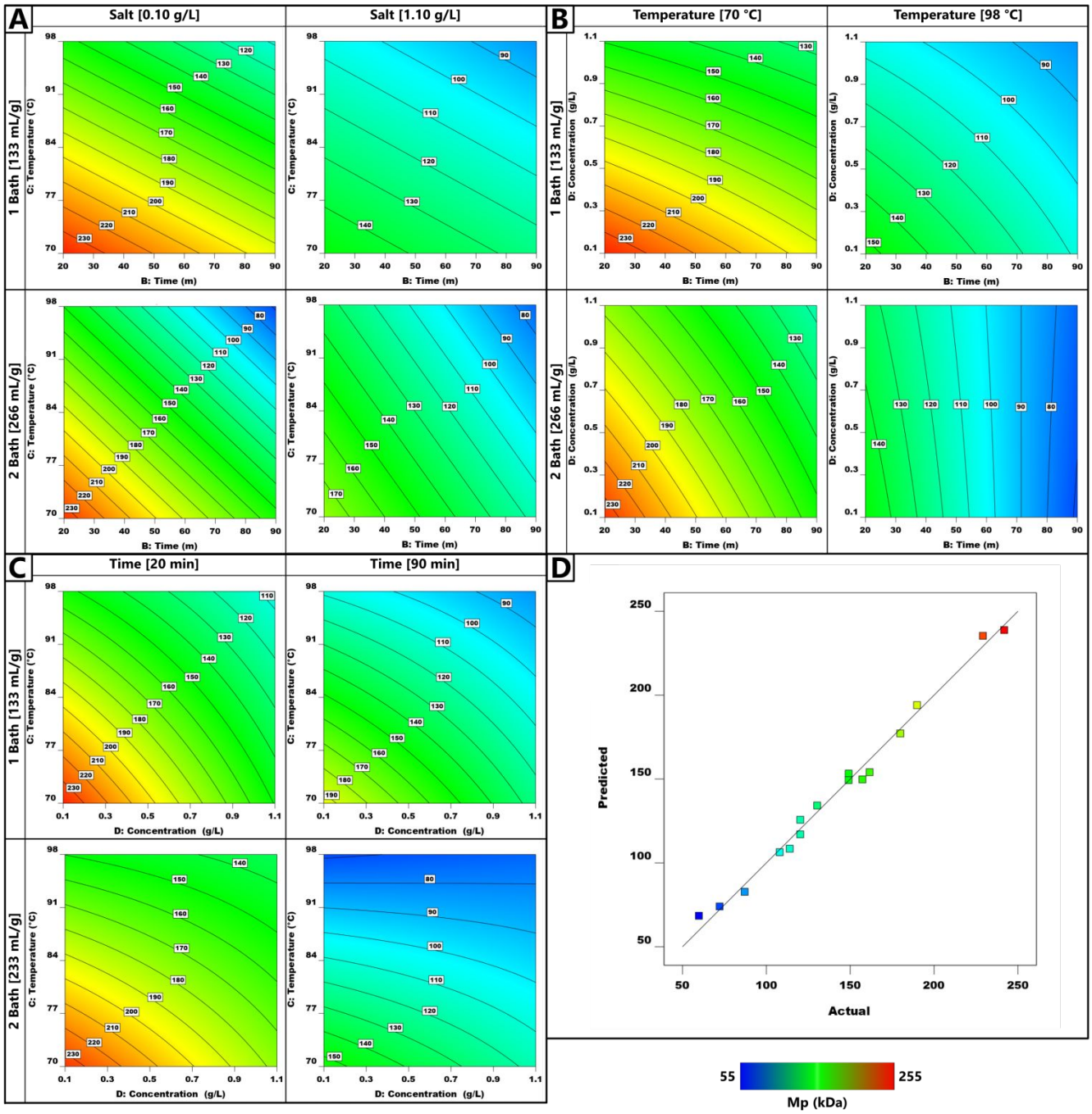

Figure S 13: Contour plots of the modelled M_p. Due to the significance of all factors the model is 4 dimensional, so the contour plots are reported as follow: (A) M_w vs temperature and time, (B) M_p vs salt concentration and time, and (C) M_p vs salt concentration and temperature. In all these cases the number of baths is reported as an ordinal, and the missing variable in its extreme values. The actual versus predicted plot (D) shows that the model accurately fit the experimental data.

Source	Sum of Squares	df	Mean Square	F-value	p-value	
Model	39305.97	8	4913.25	88.38	< 0.0001	significant
A-Number of baths	147.52	1	147.52	2.65	0.1473	
B-Time	11014.49	1	11014.49	198.13	< 0.0001	***
C-Temperature	16530.25	1	16530.25	297.34	< 0.0001	***
D-Concentration	7037.03	1	7037.03	126.58	< 0.0001	***
AB	1335.01	1	1335.01	24.01	0.0018	**
AD	978.66	1	978.66	17.60	0.0041	**
BD	447.32	1	447.32	8.05	0.0252	*
CD	1815.70	1	1815.70	32.66	0.0007	***
Residual	389.15	7	55.59			
Cor Total	39695.13	15				

Table S 14: ANOVA table for the model of M_p. The significance level was assigned as follow: p≤0.1 (.), p≤0.05 (*), p≤0.01 (**), p≤0.001 (***). All the first order terms were significant with the exclusion of the term A that was inserted to maintain the model hierarchy. Also, four second order resulted to be significant. In order of importance the significant terms were: B, C, D, CD, AB, AD and BD. M_p is influenced by several factors and several mixed terms, difficult to observe with other methodologies.

Factor	Coefficient Estimate	95% CI Low	95% CI High
Intercept	141.82	137.41	146.22
A-Number of baths	-3.04	-7.44	1.37
B-Time	-26.24	-30.65	-21.83
C-Temperature	-32.14	-36.55	-27.73
D-Concentration	-20.97	-25.38	-16.56
AB	-9.13	-13.54	-4.73
AD	7.82	3.41	12.23
BD	5.29	0.8798	9.70
CD	10.65	6.25	15.06
Transformation	None		

Table S 15: Coefficients of the coded equations of the M_n model and of the 95% confidence intervals. The factors are normalized in the range [-1,1] to allow a direct comparison between the coefficients of the different terms. In this case no transformation to the data was applied.

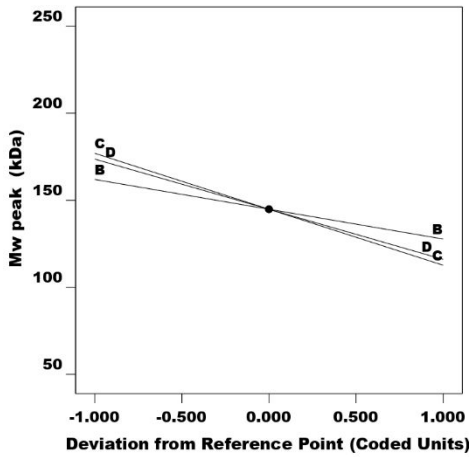

Figure S 14: Perturbation graph in coded terms of M_p. As could be expected this graph follows the trend of M_p, the variation of the terms D and C have a greater impact respect to a variation of the term B. In term of robustness, we can state that the process is more robust to a variation of B if compared to the other terms, even though only a slight there is only a slight difference between the three terms.

Dispersion index (PDI)

Source	Sum of Squares	df	Mean Square	F-value	p-value	
Model	0.0048	9	0.0005	16.19	0.0015	significant
A-Number of baths	0.0006	1	0.0006	17.22	0.0060	**
B-Time	0.0001	1	0.0001	4.49	0.0783	.
C-Temperature	0.0013	1	0.0013	40.86	0.0007	***
D-Concentration	0.0012	1	0.0012	36.71	0.0009	***
AB	0.0004	1	0.0004	12.79	0.0117	.
AC	6.744E-07	1	6.744E-07	0.0205	0.8908	
AD	4.409E-06	1	4.409E-06	0.1340	0.7268	
CD	0.0008	1	0.0008	23.93	0.0027	**
ACD	0.0003	1	0.0003	9.57	0.0213	*
Residual	0.0002	6	0.0000			
Cor Total	0.0050	15				

Table S 16: ANOVA table for the model of D. The significance level was assigned as follow: p≤0.1 (.), p≤0.05 (*), p≤0.01 (**), p≤0.001 (***). All the first order terms resulted to be significant. Also, two second order and one third order term were significant. In order of importance the significant terms were: C, D, CD, A, ACD and B. D is influenced by several factors and several mixed terms, difficult to observe with other methodologies.

Factor	Coefficient Estimate	95% CI Low	95% CI High
Intercept	0.0563	0.0528	0.0598
A-Number of baths	0.0059	0.0024	0.0095
B-Time	0.0030	-0.0005	0.0065
C-Temperature	0.0092	0.0057	0.0127
D-Concentration	0.0087	0.0052	0.0122
AB	0.0051	0.0016	0.0086
AC	0.0002	-0.0033	0.0037
AD	-0.0005	-0.0040	0.0030
CD	-0.0070	-0.0105	-0.0035
ACD	0.0044	0.0009	0.0079
Transformation	-Square		

Table S 17: Coefficients of the coded equations of the D model and of the 95% confidence intervals. The factors are normalized in the range [-1,1] to allow a direct comparison between the coefficients of the different terms. In this case no transformation to the data was applied.

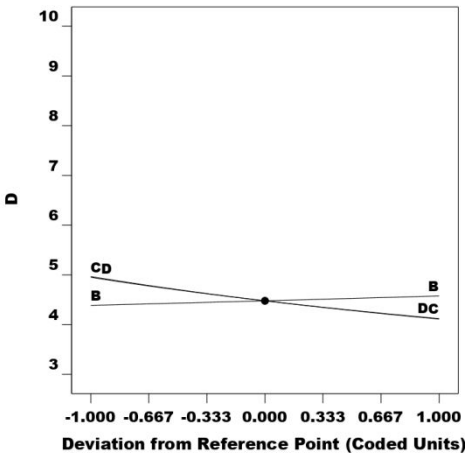

Figure S 15: Perturbation graph in coded terms of D. The variation of the terms D and C have a greater impact respect to a variation of the term B. In term of robustness, we can state that the process is more robust to a variation of B if compared to the other terms, even though only a slight there is only a slight difference between the three terms.

Mechanical properties

Ultimate strength

Source	Sum of Squares	df	Mean Square	F-value	p-value	
Model	2.203E+05	9	24482.07	5.29	< 0.0001	significant
A-Number of baths	12453.47	1	12453.47	2.69	0.1081	
B-Time	7198.83	1	7198.83	1.56	0.2190	
C-Temperature	4607.92	1	4607.92	0.9961	0.3238	
D-Concentration	95941.93	1	95941.93	20.74	< 0.0001	***
AC	18274.41	1	18274.41	3.95	0.0532	.
BC	99.56	1	99.56	0.0215	0.8841	
BD	11824.72	1	11824.72	2.56	0.1172	
CD	38634.74	1	38634.74	8.35	0.0060	**
BCD	31303.02	1	31303.02	6.77	0.0127	*
Residual	1.989E+05	43	4625.85			
Lack of Fit	20007.26	7	2858.18	0.5751	0.7712	not significant
Pure Error	1.789E+05	36	4969.57			
Cor Total	4.557E+05	53				

Table S 18: ANOVA table for the model of the ultimate strength. The significance level was assigned as follow: p≤0.1 (.), p≤0.05 (*), p≤0.01 (**), p≤0.001 (***). Only one first order term, two second and one third order terms resulted to be significant. In order of importance the significant terms were: D, CD, BCD and AC all the other terms were insert in the model to maintain the overall hierarchy.

Factor	Model coefficients	95% CI Low	95% CI High
Intercept	348.84	329.04	368.63
A-Number of baths	15.19	-3.48	33.85
B-Time	-12.25	-32.04	7.55
C-Temperature	9.80	-10.00	29.60
D-Concentration	44.71	24.91	64.51
AC	19.51	-0.2857	39.31
BC	-1.44	-21.24	18.36
BD	-15.70	-35.49	4.10
CD	-28.37	-48.17	-8.57
BCD	-25.54	-45.33	-5.74
Transformations	none		

Table S 19: Coefficients of the coded equations of the ultimate strength model and of the 95% confidence intervals. The factors are normalized in the range [-1,1] to allow a direct comparison between the coefficients of the different terms. In this case no transformation to the data was applied.

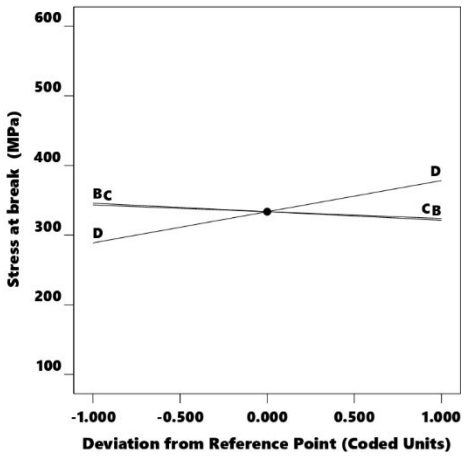

Figure S 16: Perturbation graph in coded terms of the stress at break. The variation of the terms D has a greater impact in terms of amount of β structures respect to a variation of the other terms. In term of robustness, we can state that the process is more robust to a variation of C and B if compared to the term D.

Young's Modulus

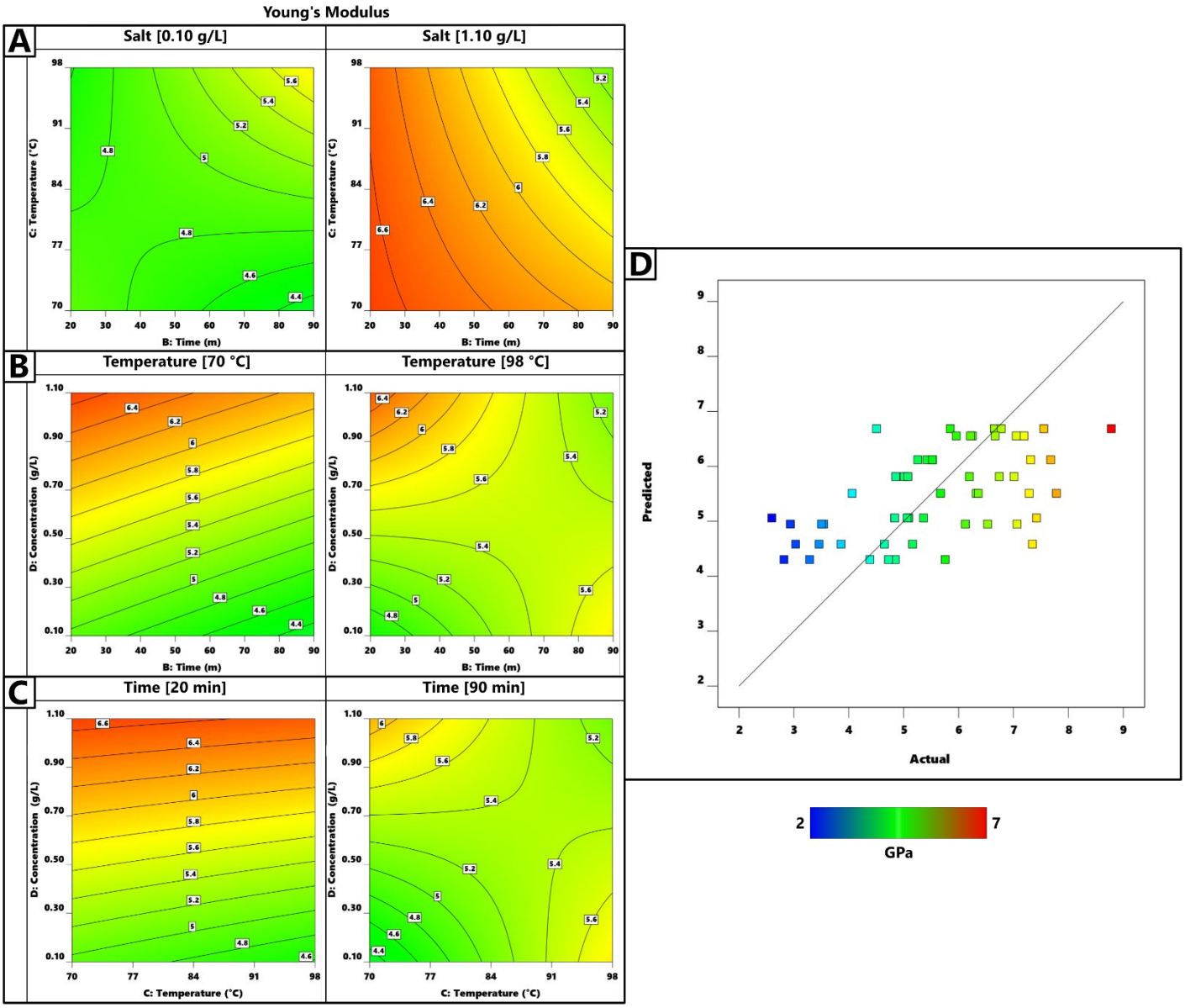

*Figure S 17: Contour plot of the modelled Young's modulus (E) of the degummed silk fibers. In his case the number of baths term was not significant, all the other terms were instead significant, making the model dependent on 3 variables. In order of importance the significative terms were (ANOVA **Table S20**): D (salt concentration), BCD (process time*process temperature*salt concentration), and BD (process time*salt concentration) The contour plots are reported as follows: (**A**) E vs temperature and time, (**B**) E vs salt concentration and time, and (**C**) E vs salt concentration and temperature. In all these cases the number of baths is reported as an ordinal, and the missing variable in its extreme values. As in the previous case, is extremely difficult to relate the Young's modulus to a specific property. The actual versus predicted plot (**D**) shows scattered point following a diagonal trend, this indicates a general agreement between the model and the collected values trends.*

Source	Sum of Squares	df	Mean Square	F-value	p-value	
Model	34.60	7	4.94	2.89	0.0139	significant
B-Time	1.64	1	1.64	0.9565	0.3333	
C-Temperature	0.0014	1	0.0014	0.0008	0.9772	
D-Concentration	17.07	1	17.07	9.98	0.0028	**
BC	0.6750	1	0.6750	0.3948	0.5330	
BD	5.24	1	5.24	3.06	0.0870	.
CD	4.09	1	4.09	2.39	0.1291	
BCD	5.90	1	5.90	3.45	0.0699	.
Residual	76.94	45	1.71			
Lack of Fit	7.63	9	0.8479	0.4404	0.9038	not significant
Pure Error	69.31	36	1.93			
Cor Total	114.44	53				

Table S 20: ANOVA table for the model of the tensile modulus (E). The significance level was assigned as follow: p≤0.1 (.), p≤0.05 (*), p≤0.01 (**), p≤0.001 (***). Only one first order term, one second and one third order terms resulted to be significant. In order of importance the significant terms were: D, BCD, and BD all the other terms were insert in the model to maintain the overall hierarchy.

Factor	Model coefficients	95% CI Low	95% CI High
Intercept	5.51	5.13	5.89
B-Time	-0.1846	-0.5647	0.1956
C-Temperature	-0.0054	-0.3856	0.3747
D-Concentration	0.5963	0.2162	0.9764
BC	0.1186	-0.2616	0.4987
BD	-0.3303	-0.7104	0.0499
CD	-0.2918	-0.6719	0.0884
BCD	-0.3505	-0.7306	0.0296
Treatments	none		

Table S 21: Coefficients of the coded equations of the tensile modulus model and of the 95% confidence intervals. The factors are normalized in the range [-1,1] to allow a direct comparison between the coefficients of the different terms. In this case no transformation to the data was applied.

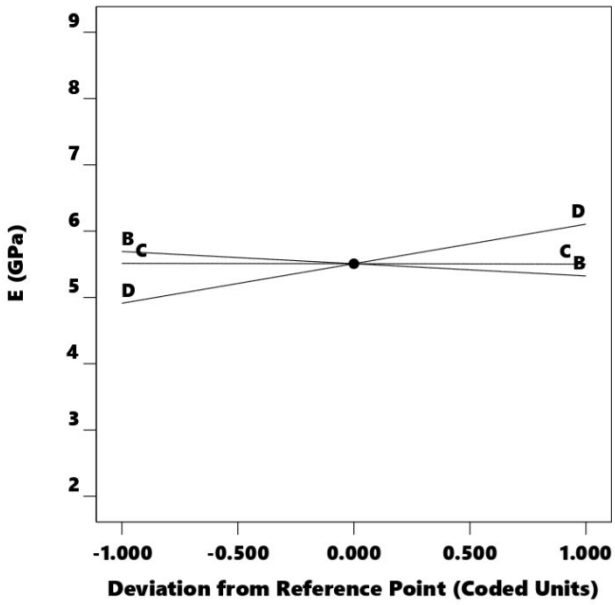

Figure S 18: Perturbation graph in coded terms of the tensile modulus. The variation of the terms D has a greater impact in terms of amount of β structures respect to a variation of the other terms. In term of robustness, we can state that the process is more robust to a variation of C and B if compared to the term D.

Toughness

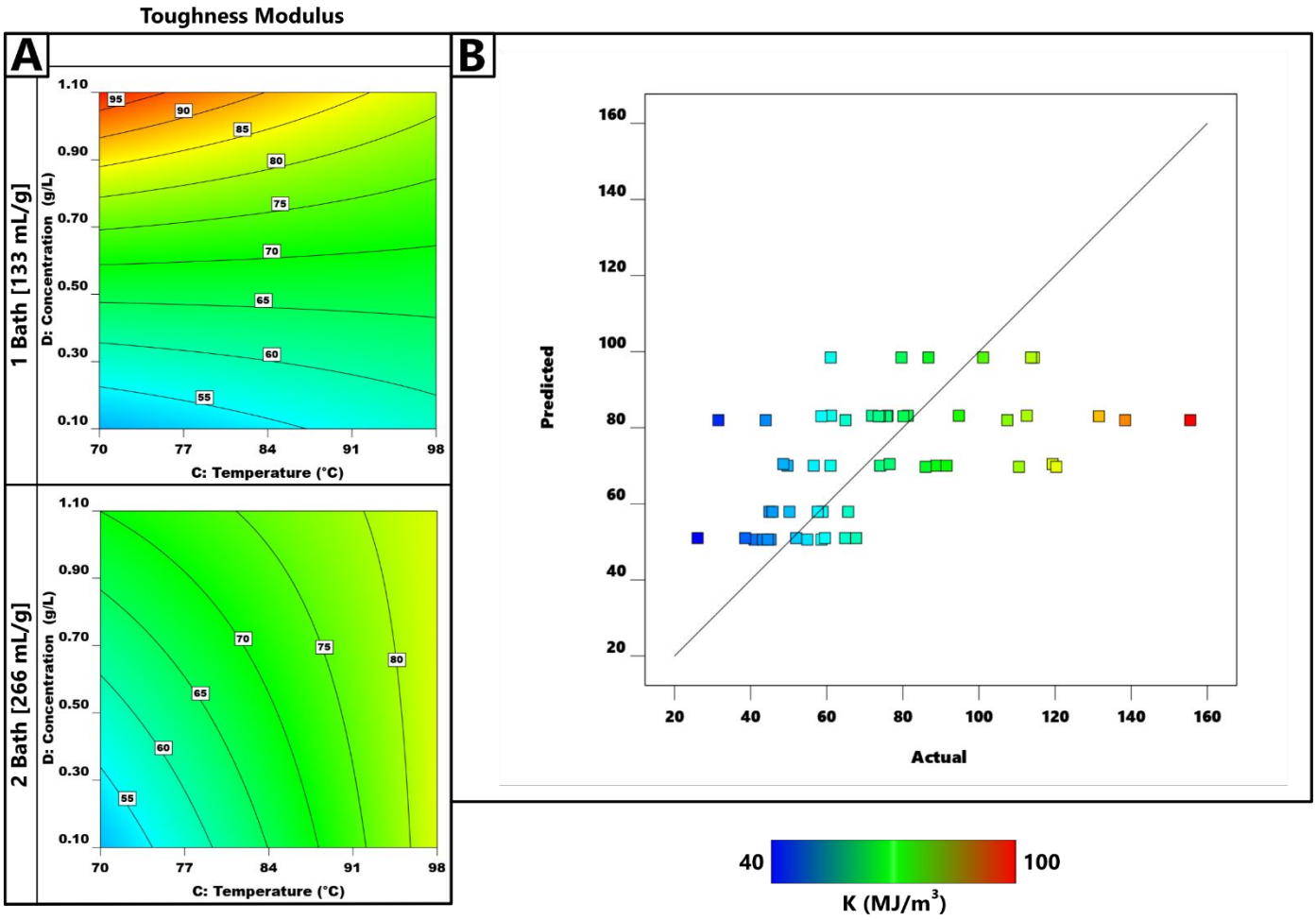

*Figure S 19: Contour plot of the modelled toughness modulus (K) of the degummed silk fibres. The statistically significant terms (ANOVA **Table S21**), in order of importance, were: D (salt concentration), AC (number of baths*process temperature), AD (number of baths*salt concentration), and CD (process temperature*salt concentration). (**A**) K vs salt concentration and temperature, the number of baths is reported as an ordinal, and the missing variable in its extreme values. The actual versus predicted plot (**B**) shows scattered point following a diagonal trend, this indicates a general agreement between the model and the collected values trends. However, in this case the model was less precise than in all the previous cases because of the high variability on the obtained values.*

Source	Sum of Squares	df	Mean Square	F-value	p-value	
Model	2.65	6	0.4417	4.21	0.0019	significant
A-Number of baths	0.0014	1	0.0014	0.0137	0.9074	
C-Temperature	0.2807	1	0.2807	2.68	0.1087	
D-Concentration	1.32	1	1.32	12.61	0.0009	***
AC	0.3747	1	0.3747	3.57	0.0651	.
AD	0.3650	1	0.3650	3.48	0.0686	.
CD	0.3046	1	0.3046	2.90	0.0952	.
Curvature	0.4628	1	0.4628	4.41	0.0412	*
Residual	4.83	46	0.1049			
Lack of Fit	0.8647	10	0.0865	0.7856	0.6422	not significant
Pure Error	3.96	36	0.1101			
Cor Total	7.94	53				

Table S 22: ANOVA table for the model of the toughness. The significance level was assigned as follow: p≤0.1 (.), p≤0.05 (*), p≤0.01 (**), p≤0.001 (***). Only one first order term, one second and one third order terms resulted to be significant. In order of importance the significant terms were: D, AC, AD, and CD. All the other terms were insert in the model to maintain the overall hierarchy.

Factor	Model coefficients	95% CI Low	95% CI High
Intercept	1.82	1.78	1.86
A-Number of baths	0.0226	-0.0171	0.0623
D-Concentration	0.0583	0.0162	0.1005
AD	-0.0395	-0.0816	0.0027
Transformation	Logarithmic		

Table S 23: Coefficients of the coded equations of the Young Modulus model and of the 95% confidence intervals. The factors are normalized in the range [-1,1] to allow a direct comparison between the coefficients of the different terms. In this case a logarithmic transformation was applied to the data to make the residues normally distributed.

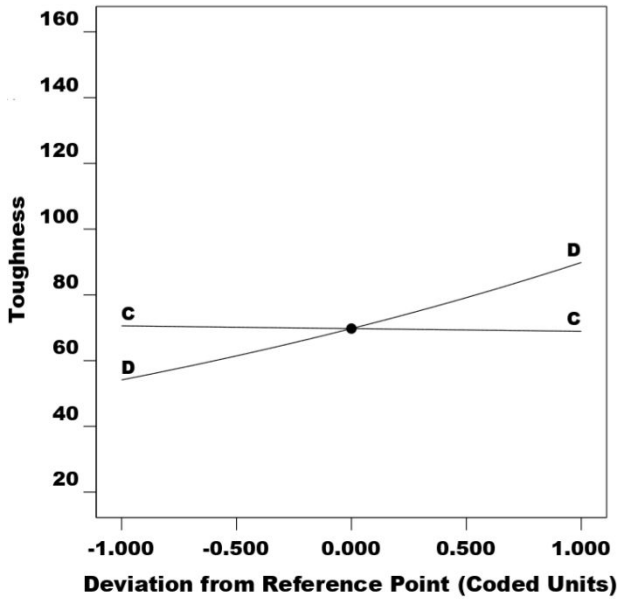

Figure S 20: Perturbation graph in coded terms of the toughness modulus. The variation of the terms D has a greater impact in terms of K respect to a variation of the other term. In term of robustness, we can state that the process is more robust to a variation of C if compared to the term D.

Mechanical properties vs molecular weight

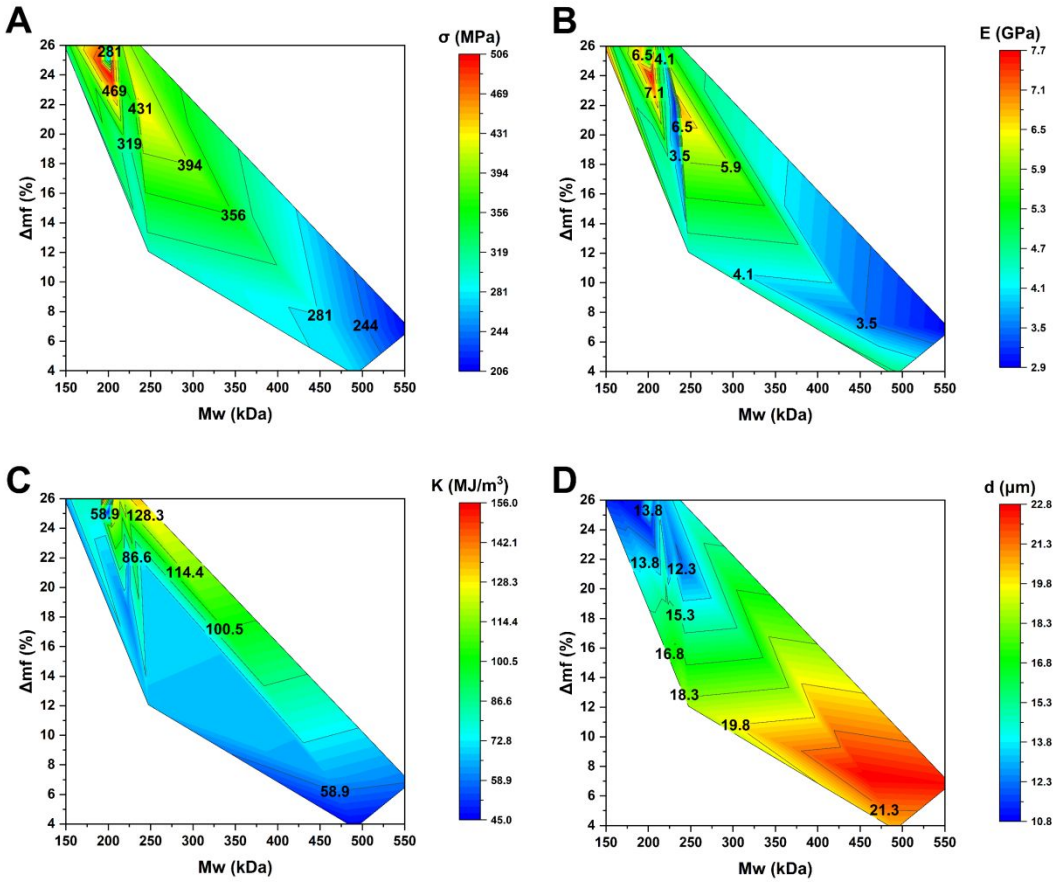

*Figure S 21: Trends of (**A**) the ultimate strength, (**B**) the Young's modulus (**D**) the toughness index, and (**D**) the fibers mean diameter vs. the molecular weight and the weight loss. The blank area in the graph represents area not accessible with the current range choose for the process variables. These graphs have not to be intended as refined model punctual model (which is indeed the case of the empirical models that link the process variables to the material property) but as visualization of the general trend. In each of the reported graph is not possible to increase the mass loss (thus the amount of removed sericine) without decreasing the molecular weight. This explains why the decreasing of the molecular weight seems to improve the mechanical properties while instead is the decreasing of the sericine content that improv them. However, the two effects cannot be effectively separated if not extending the range of process variables or, by changing typology of degumming process. The conclusions on the mechanical property are further confirm from (**D**) in fact the lower part of the graph with the higher molecular weight results also in the higher diameter, implying fibers surrounded by sericin.*

Empirical Models

$\Delta m_{f(1bath)}(\%) = -23.56037 - 0.298006B + 0.373219C + 6.16206D + 0.00401586BC + 0.565710\,BD + 0.05 \quad - 0.00659$ $\Delta m_{f(2baths)}(\%) = -27.83598 - 0.298006B + 0.455753\,C + 23.99304D + 0.00401586BC + 0.565710BD - 0.1565 \quad - 0.00659$	(1)
$m_{s(1bath)}(\%) = -3.40712 - 0.026723B + 0.0720592C + 2.70125D + 0.000421437BC + 0.0686623BD - 0.0119812CD - 0.000828($ $m_{s(2baths)}(\%) = -2.80993 - 0.026723B + 0.0720592C + 2.70125\,D + 0.000421437BC + 0.0686623BD - 0.0119819CD + - 0.000828047BCD$	(2)
$1/d_{(1bath)}(\mu m) = 0.0170618 - 0.000465366B + 0.000390867C + 0.031071D + 0.00000682933BC + 0.000963647BD \quad - 0.0001227 - 0.0000119554BCD$ $1/d_{(2baths)}(\mu m) = -0.0180805 - 0.000465366\,B + 0.000867654C + 0.031071D + 0.00000682933BC + 0.000963647BD - 0.0001227 - 0.0000119554BCD$	(3)
$\beta tot_{(1bath)}(\%) = 43.65546 - 0.035903B + 0.146111C + 10.50220\,D + 0.0640237BD - 0.189564CD$ $\beta tot_{(2baths)}(\%) = 40.07968 + 0.0112263B + 0.146111C + 16.30562D - 0.0167738BBD - 0.189564CD$	(4)
$1/M_{w(1baths)}(kDa) = -0.006211 + 3.044E(-6)B + 0.000110C + 0.009177D - 0.000091CD$ $1/M_{w(2baths)}(kDa) = -0.004122 + 0.000024B + 0.000082C + 0.03570D - 0.000028C_{\mathrm{D}}$	(5)
$1/D_{(1baths)}(kDa) = -0.0936274 - 0.000059641B + 0.00162134C + 0.155811D - 0.00163555CD$ $1/D_{(2baths)}(kDa) = -0.0351749 + 0.000233335B + 0.000890282C + 0.047258D - 0.000368248CD$	(6)
$M_p(kDa) = 485.80643 - 0.669943\,B + - 3.20899\,C - 202.03613\,D + 0.302142\,BC + 1.52182\,CD$ $M_p(kDa) = 489.67177 - 1.19191\,B - 3.20899\,C - 170.75261D + 0.302142BC + 1.52182CD$	(7)
$M_n = 149.39843 - 0.189110B - 0.928469C - 69.21448D + 0.000937635BC + 0.0496594BD + 0.633106CD$ $M_n = 136.50153 - 0.348516B - 0.737167C - 47.04875D + 0.000937635BC + 0.144292BD + 0.357313\,CD$	(8)

$\sigma_{Break(1bath)}(MPa) = 399.02078 - 4.81823\ B - 1.54014\ C - 2.36632D + 0.0596008BC + 7.85871BD + 1.67989CD - 0.104233ABC$ $\sigma_{Break(2baths)}(MPa) = 195.24952 - 4.81823B + 1.24728C - 2.36632D + 0.0596008BC + 7.85871BD + 1.67989CD - 0.104233BCD$	(9)
$\ln(E(GPa)) = 1.90252 - 0.0176811B - 0.00520623C - 0.644751D + 0.000224341BC + 0.0260522BD + 0.0134485CD - 0.0003635$	(10)
$\ln(K_{(1baths)}(MJ/m^3)) = 3.38615 + 0.00598015C + 1.46248D - 0.0113804CD$ $\ln(K_{(2baths)}(MJ/m^3)) = 2.54554 + 0.0186014C + 1.11369D - 0.0113804CD$	(11)

Table S 24: Empirical models of the considered yields.

References

(1) Hu, X.; Kaplan, D.; Cebe, P. Determining Beta-Sheet Crystallinity in Fibrous Proteins by Thermal Analysis and Infrared Spectroscopy. *Macromolecules* **2006**, *39* (18), 6161–6170. https://doi.org/10.1021/ma0610109.

(2) Jung, C. Insight into Protein Structure and Protein-Ligand Recognition by Fourier Transform Infrared Spectroscopy. *Journal of Molecular Recognition*. 2000. https://doi.org/10.1002/1099-1352(200011/12)13:6<325::AID-JMR507>3.0.CO;2-C.

(3) Mouro, C.; Jung, C.; Bondon, A.; Simonneaux, G. Comparative Fourier Transform Infrared Studies of the Secondary Structure and the CO Heme Ligand Environment in Cytochrome P-450cam and Cytochrome P-420cam. *Biochemistry* **1997**. https://doi.org/10.1021/bi9700173.

(4) Teramoto, H.; Miyazawa, M. Molecular Orientation Behavior of Silk Sericin Film as Revealed by ATR Infrared Spectroscopy. *Biomacromolecules* **2005**. https://doi.org/10.1021/bm0500547.

(5) Dong, A.; Huang, P.; Caughey, W. S. Protein Secondary Structures in Water from Second-Derivative Amide I Infrared Spectra. *Biochemistry* **1990**. https://doi.org/10.1021/bi00465a022.

(6) Shimanovich, U.; Ruggeri, F. S.; De Genst, E.; Adamcik, J.; Barros, T. P.; Porter, D.; Müller, T.; Mezzenga, R.; Dobson, C. M.; Vollrath, F.; Holland, C.; Knowles, T. P. J. Silk Micrococoons for Protein Stabilisation and Molecular Encapsulation. *Nat. Commun.* **2017**, *8* (May), 1–9. https://doi.org/10.1038/ncomms15902.

(7) Shivu, B.; Seshadri, S.; Li, J.; Oberg, K. A.; Uversky, V. N.; Fink, A. L. Distinct β-Sheet Structure in Protein Aggregates Determined by ATR-FTIR Spectroscopy. *Biochemistry* **2013**. https://doi.org/10.1021/bi400625v.

(8) Ruggeri, F. S.; Longo, G.; Faggiano, S.; Lipiec, E.; Pastore, A.; Dietler, G. Infrared Nanospectroscopy Characterization of Oligomeric and Fibrillar Aggregates during Amyloid Formation. *Nat. Commun.* **2015**. https://doi.org/10.1038/ncomms8831.

(9) Zandomeneghi, G.; Krebs, M. R. H.; McCammon, M. G.; Fändrich, M. FTIR Reveals Structural Differences between Native β-Sheet Proteins and Amyloid Fibrils. *Protein Sci.* **2009**, *13* (12), 3314–3321. https://doi.org/10.1110/ps.041024904.

(10) Tretinnikov, O. N.; Tamada, Y. Influence of Casting Temperature on the Near-Surface Structure and Wettability of Cast Silk Fibroin Films. *Langmuir* **2001**. https://doi.org/10.1021/la010791y.

(11) Taddei, P.; Monti, P. Vibrational Infrared Conformational Studies of Model Peptides Representing the Semicrystalline Domains of Bombyx Mori Silk Fibroin. *Biopolymers* **2005**. https://doi.org/10.1002/bip.20275.

(12) Goormaghtigh, E.; Cabiaux, V.; Ruysschaert, J. -M. Secondary Structure and Dosage of Soluble and Membrane Proteins by Attenuated Total Reflection Fourier-transform Infrared Spectroscopy on Hydrated Films. *Eur. J. Biochem.* **1990**. https://doi.org/10.1111/j.1432-1033.1990.tb19354.x.

(13) Monti, P.; Freddi, G. Raman Spectroscopic Studies of Silk Fibroin from Bombyx Mori. *J. Raman Spectrosc.* **1998**, *29* (January), 297–304. https://doi.org/10.1002/(SICI)1097-4555(199804)29:4<297::AID-JRS240>3.0.CO;2-G.

(14) Wilson, D.; Valluzzi, R.; Kaplan, D. Conformational Transitions Model Silk Peptides. *Biophys. J.* **2000**. https://doi.org/10.1016/S0006-3495(00)76813-5.

(15) Chen, X.; Shao, Z.; Marinkovic, N. S.; Miller, L. M.; Zhou, P.; Chance, M. R. Conformation Transition Kinetics of Regenerated Bombyx Mori Silk Fibroin Membrane Monitored by Time-Resolved FTIR Spectroscopy. *Biophys. Chem.* **2001**, *89* (1), 25–34. https://doi.org/10.1016/S0301-4622(00)00213-1.